

# Microjoining of Flexible Materials using Nanoheaters

A thesis  
submitted by

Alexander Pallas Dienst

In partial fulfillment of the requirements  
for the degree of

Master of Science

In

Mechanical Engineering

TUFTS UNIVERSITY

August, 2013

ADVISER:

Prof. Peter Y. Wong

## **Abstract**

With the continuing integration of electronics and humans, microelectronics need to become smaller, lighter, and now flexible for wearability. This thesis reports on the feasibility of using nanoheaters, exothermic alloy structures, for joining flexible polymer parts for batteries. While flexible displays have come into production there are few reliable flexible power sources for flexible electronics. The main difficulty with flexible batteries is that it is difficult to find a flexible packaging material that can either keep the electrolytic solution inside the battery or keep water and other possible contaminants out of the battery. Rigid metals such as aluminum have been the norm for this task as they are impervious to nearly anything and use some plastic parts as seals. Liquid Crystal Polymers have potential to be used in flexible packaging since they are resistant to electrolytic solutions and are impervious to water and contaminants. The concern with using LCP to package flexible batteries is sealing the LCP. With smaller cells and more complex configurations of integrated electronics and batteries the need for a smaller and more localized joining method such as a localized heat source is needed. Nanoheaters have been identified to provide a very short and local heat source that limits the heat affected zone considerably when compared to other joining methods. In this thesis, methods for using nanoheaters to join and seal flexible batteries are explored using numerical models with COMSOL and experiments with commercial and laboratory grade nanoheaters.

## **Acknowledgements**

I would like to thank the National Science Foundation (Grant # CMI 1029567) for funding my research and I would like to thank Prof. Wong for his encouragement and support in my research. I would also like to thank Prof. Zimmerman for his instruction in ME 0129 Finite Elements and for his supply of novel LCP material which I used in my research. I would like to thank the lead research collaborators from Northeastern University and UMass Lowell . Prof. Ando, Prof. Gu, Prof. Chen. I would also like to thank Somayeh Gheybi for providing me with materials. I would like to thank Prof. Cebe for testing the LCP in the Differential Scanning Calorimeter in such short notice. I would like to thank James Collins for helping me out in the lab with all my experiments. Lastly I would like to thank my parents for their encouragement and support.

## Table of Contents

Abstract.....	ii
Acknowledgements.....	iii
List of Figures .....	v
List of Tables .....	viii
1 Introduction .....	1
1.1 Significance .....	1
1.2 State of Knowledge in Joining .....	2
2 Research Goals.....	5
3 Nanofoil.....	6
4 Numerical Model .....	7
4.1 Finite Element Analysis in COMSOL.....	7
4.2 Geometry & Boundary Conditions.....	7
4.2.1 Mesh .....	11
4.3 Thermomechanical Settings.....	18
4.4 Nanoheater Simulation Approximation.....	18
4.5 Study Parameters.....	18
4.6 Solver .....	19
4.7 Generalized Numerical Analysis and Pi Numbers .....	19
4.7.1 Design of Experiments Using Pi Numbers.....	22
5 Experimental Models .....	22
5.1 General Welding of LCP .....	23
5.2 Taco Joining Method.....	24
5.2.1 Taco Peel Tests.....	26
5.2.2 Taco Leak Test.....	28
5.3 Sandwich Joining Method .....	30
5.4 Sandwich Joining & Leak Test .....	32
5.3 LCP Battery Prototype.....	35

6 Results .....	37
6.1 Taco Results .....	37
6.2 Numerical Model results .....	38
6.2.1 Sample of Temperature and Stress Distributions .....	38
6.2.2 Pi Group Results .....	44
6.2.3 Micro-Model Results .....	58
6.3 Sandwich Joining Results .....	66
6.4 Sandwich Method Leak Test Results .....	67
6.5 LCP Battery .....	68
7 Discussion .....	69
7.1 Discussion of General Welding .....	69
7.2 Discussion of Numerical Analysis .....	70
7.2.1 Physical Size Model .....	70
7.2.1 Comparison with micro model .....	77
7.4 Discussion of Taco Method .....	78
7.5 Discussion of Sandwich Method .....	79
7.5.1 Discussion of Inside Out Sandwich Method .....	79
7.6 Discussion of Leak Test and Battery .....	80
8 Conclusion .....	82
9 Future Work .....	85
Appendix A .....	86
Heat Capacity/Latent Heat of Fusion of LCP .....	86
Works Cited .....	87

## List of Figures

Figure 1: Concept of microscale joining on flexible (or curved) substrates using nanoheater structures. Colored squares indicate different types of functional components (such as electronics or sensors elements). On the right side (cross-section view) it shows the joining of components using thin nanoheater layers (different shades of red indicate nanoheaters designed for different heat output) with non-contact (i.e., IR or lase) ignition .....	1
Figure 2: Nanofoil composition (NanoFoil®) .....	6

<i>Figure 3: The full COMSOL model (a) and a close up of the layers in the model (b) featuring Nanofoil as the top layer, Al and Cu as the middle layer and LCP as the bottom layer. The thickness of the nanofoil was 60 microns but since symmetry was imposed the nanofoil was represented as 30microns when one nanofoil was used and 60microns when two nanofoils were used. The thickness of the heat spreaders when either Al or Cu were used was 0.1016mm and the LCP was .11mm when one LCP was needed and .22 when two were needed.....</i>	<i>8</i>
<i>Figure 4: The microscale COMSOL model (a) and a close up of the layers in the model (b) featuring Nanofoil as the top layer, Al and Cu as the middle layer and LCP as the bottom layer. The thickness of the nanofoil was 0.6 microns but since symmetry was imposed the nanofoil was represented as 0.3 micros when one nanofoil was used and 0.3 microns when two nanofoils were used. The thickness of the heat spreaders when either Al or Cu are used was 1.016 microns and the LCP was 1.1 microns when one LCP was needed and 2.2 microns when two were needed.....</i>	<i>9</i>
<i>Figure 5: The blue colored faces are all of the areas where a symmetry boundary condition was applied. ....</i>	<i>10</i>
<i>Figure 6: The blue colored domain is the domain which represents the nanofoil and which the heat source is specified. ....</i>	<i>10</i>
<i>Figure 7: The blue colored faces indicate an area where a convective cooling parameter of 5W/m<sup>2</sup> are placed. ....</i>	<i>11</i>
<i>Figure 8: The blue colored face indicates an area where a convective cooling parameter of 10,000W/m<sup>2</sup> is placed. ....</i>	<i>11</i>
<i>Figure 9: Final Mesh Configuration .....</i>	<i>12</i>
<i>Figure 10: The final mesh (a) with an enlargement of the area where there are many elements through the through the thickness of the model (b).....</i>	<i>13</i>
<i>Figure 11: The percent difference in stress and temperature compared to the mesh with the most elements which has 27846 elements. ....</i>	<i>14</i>
<i>Figure 12: Measured heat capacity curve in relation to temperature of LCP from differential scanning calorimeter with the increase in heat capacity to account for latent heat of fusion for melting. The X axis is temperature and the Y axis is k/kg-K.....</i>	<i>16</i>
<i>Figure 13: Specific heat capacity curve in relation to Temperature obtained by COMSOL Model Library for Al 1145 which incorporates a spike in LCP needed to represent the latent heat of fusion. The X axis is temperature and the Y axis is J/kg-K.....</i>	<i>17</i>
<i>Figure 14: Testing of optimal temperature for joining LCP with a soldering iron. The top left specimen was joined when 280C (553K) was applied and the temperature was increased by 10 degrees C for each subsequent piece until 440C (713K) was reached which is the bottom right specimen. ....</i>	<i>24</i>
<i>Figure 15: A cross section of a joining specimen using the taco method. The area where the pressure is applied is where the joining LCP to LCP bond is formed. ....</i>	<i>25</i>
<i>Figure 16: Joining set up of taco method. The taco and LCP are clamped down with clamps to a glass slide while a second glass slide is used to apply pressure where the Taco ends and the two pieces of LCP meet. The piece of metal on the left of the LCP is an ignition antenna used to ignite the Nanofoil using an induction heater. This method of ignition was later dropped in favor of spark ignition.....</i>	<i>26</i>
<i>Figure 17: Custom pull-testpull-test machine used for conducting pull tests.....</i>	<i>27</i>
<i>Figure 18: LCP specimens are glued onto a glass slide and a golf tee is glued to the LCP. These test specimens have the aluminum and nanofoil taco not cut out.....</i>	<i>27</i>

<i>Figure 19:</i> LCP specimens are glued onto a glass slide and a golf tee is glued to the LCP. A hole is drilled into the top of the golf tee and an eye hook was screwed into the hole. These test specimens have the aluminum and nanofoil taco cut out.....	28
<i>Figure 20:</i> Leak test specimen using a soldering iron to seal the LCP.....	29
<i>Figure 21:</i> Leak test specimen using nanofoil to seal the LCP.....	29
<i>Figure 22:</i> The pieces used in the sandwich joining tests. The two outside tan colored pieces are LCP, the two copper colored pieces are copper and the shiny metallic piece in the center is nanofoil. The antenna used for igniting the nanofoil is no shown in this picture .....	31
<i>Figure 23:</i> A partially completed sandwich test before the final piece of LCP is placed on top. The metallic protrusion on the right side of the specimen is the antenna. ....	31
<i>Figure 24:</i> Test specimen before ignition. The sandwich specimen is in between two ceramic blocks which are clamped together using spring clamps. ....	32
<i>Figure 25:</i> The first side to be bonded for the leak test using the sandwich method.....	33
<i>Figure 26:</i> A leak test specimen using the sandwich method after it had failed the leak test. Note the red dye in the bottom right corner of the specimen, on the entire left edge of the specimen and the top center right dot of the specimen, all of these areas were where the specimen leaked. Also note the patch on the left edge using a soldering iron because the copper heat spreader kept tearing holes in that side.....	34
<i>Figure 27:</i> A diagram of the internal components of the LCP battery .....	35
<i>Figure 28:</i> LCP used to package the LCP with graphite drawn around the edges.....	36
<i>Figure 29:</i> LCP battery successfully lighting up an LED light. ....	36
<i>Figure 30:</i> Temperature plot of Cu heat spreader with 2 nanofoils and 2 LCPs .....	38
<i>Figure 31:</i> Von Mises Stress plot of Cu heat spreader with 2 Nanofoils and 2 LCPs .....	39
<i>Figure 32:</i> Temperature plot of Al heat spreader with 2 Nanofoils and 2 LCPs .....	39
<i>Figure 33:</i> Stress plot of Al heat spreader with 2 Nanofoils and 2 LCPs.....	40
<i>Figure 34:</i> Temperature plot of Al heat spreader with 2 Nanofoils and 1 LCPs. ....	40
<i>Figure 35:</i> Temperature distribution at interface between the heat spreader and the substrate. ....	42
<i>Figure 36:</i> Distribution through the thickness of the model (Actual Penetration Depth of numerical model) .....	43
<i>Figure 37:</i> Pi 6 verses Pi 1, Peak Temperature verses Thermal Penetration depth in the substrate. ....	44
<i>Figure 38:</i> Pi 6 verses Pi 2, peak temperature verses melting potential .....	45
<i>Figure 39:</i> Pi 6 verses Pi3, peak temperature verses energy density .....	45
<i>Figure 40:</i> Pi6 verses Pi4, peak temperature verses thermal strain .....	46
<i>Figure 41:</i> Pi 6 verses Pi 5, peak temperature verses thermal penetration in chip .....	47
<i>Figure 42:</i> Pi7 verses Pi1, interfacial stress verses thermal penetration depth in substrate.....	48
<i>Figure 43:</i> Pi7 verses Pi2, interfacial stress verses melting potential.....	48
<i>Figure 44:</i> Pi7 verses Pi 3, Interfacial stress verses energy density. ....	49
<i>Figure 45:</i> Pi7 verses Pi4 interfacial stress verses thermal strain.....	50
<i>Figure 46:</i> Pi7 verses Pi5, interfacial stress verses thermal penetration in chip .....	50
<i>Figure 47:</i> Pi8 verses Pi1, heat affected zone verses thermal penetration depth in substrate .....	51
<i>Figure 48:</i> Pi8 verses Pi2, Heat affected zone verses melting potential.....	52
<i>Figure 49:</i> Pi8 verses Pi3, heat affected zone verses energy density .....	52
<i>Figure 50:</i> Pi8 verses Pi4, heat affected zone verses thermal strain. ....	53

Figure 51: Pi8 verses Pi5, heat affected zone verses thermal penetration in chip .....	54
Figure 52: Pi9 verses Pi1, adhesion strength verses penetration depth in substrate .....	54
Figure 53: Pi9 verses Pi2, adhesion strength verses melting potential.....	55
Figure 54: Pi9 verses Pi3, adhesion strength verses energy density.....	56
Figure 55: Pi9 verses Pi4, adhesion strength verses thermal strain.....	57
Figure 56: Pi9 verses Pi5, adhesion strength verses thermal penetration in chip .....	57
Figure 57: Pi6 verses Pi1, peak temperature verses thermal penetration depth in substrate. ....	58
Figure 58: Pi6 verses Pi2, peak temperature verses melting potential.....	59
Figure 59: Pi6 verses Pi3, peak temperature verses energy density .....	60
Figure 60: Pi6 verses Pi4, peak temperature verses thermal strain .....	61
Figure 61: Pi6 verses Pi5, peak temperature verses thermal penetration of the chip .....	62
Figure 62: Pi7 verses Pi1, interfacial stress verses thermal penetration in substrate .....	63
Figure 63: Pi7 verses Pi2, interfacial stress verses melting potential.....	63
Figure 64: Pi7 verses Pi3, interfacial stress verses energy density.....	64
Figure 65: Pi7 verses Pi5, interfacial stress verses thermal strain .....	65
Figure 66: Pi7 verses Pi5, interfacial stress verses thermal penetration in chip. ....	65
Figure 67: Wiring diagram of LCP battery connected in series with a hearing aid battery and an LED light. ....	68
Figure 68: Picture of the LCP Aluminum Carbon air battery lighting up an LED.....	69
Figure 69: Pi6 verses Pi1, peak temperature verses thermal penetration depth in the substrate .....	70
Figure 70: Pi6/Pi2 verses Pi3, distance to melt point verses heat put in/energy density.....	71
Figure 71: Pi6 verses Pi3, peak temperature verses energy density .....	72
Figure 72: Pi6 verses Pi4, peak temperature verses thermal strain.....	73
Figure 73: Pi6 verses Pi5, peak temperature verses thermal penetration in chip.....	74
Figure 74: Pi8 verses Pi3, measured heat affected zone verses energy density.....	75
Figure 75: Pi9 verses Pi3 adhesion strength verses energy density .....	76
Figure 76: Comparison of Macro-Model and Micro-Model with Pi 6 .....	77

## List of Tables

<b>Table 1: The change in stress and temperature as the number of elements are increased .....</b>	<b>15</b>
Table 2: This table shows all the possible combinations of the DOE.....	22
Table 3: Results from the 8 runs on COMSOL.....	<b>Error! Bookmark not defined.</b>
Table 4: The average strength of the sandwich method pull tests. ....	66
Table 5: Physically Measured Heat Affected zone and heat affected zone of numerical .....	67



# 1 Introduction

## 1.1 Significance

As applications in microelectronics, sensors, medical devices and diagnostics, and energy and information storage strive towards smaller, more integrated, and multi-material/multi-functionality designs, the challenge of joining dissimilar materials in small and non-flat regions represents a significant barrier. Typical joining methods, such as bulk heating or direct contact, cannot meet the challenges and demands of microscale joining. Novel nanoheater structures have the potential to meet the challenges that microscale joining inherently poses. Nanoheaters have been proven to generate a defined localized exotherm when ignited and are small and discrete which make them ideal for microjoining.

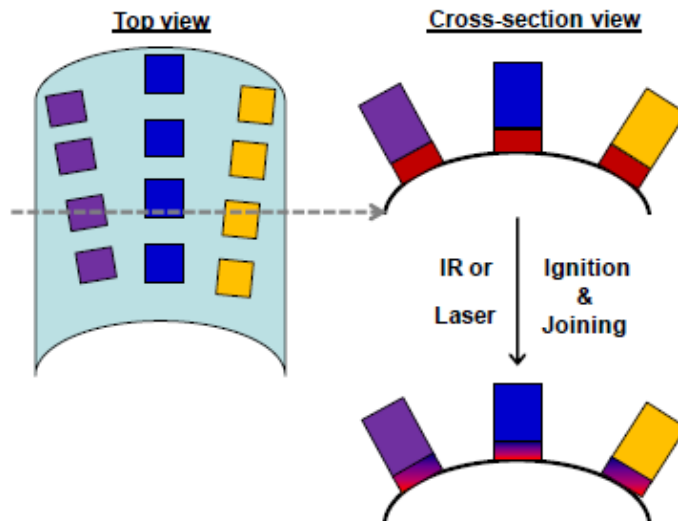


**Figure 1: Concept of microscale joining on flexible (or curved) substrates using nanoheater structures. Colored squares indicate different types of functional components (such as electronics or sensors elements). On the right side (cross-section view) it shows the joining of components using thin nanoheater layers (different shades of red indicate nanoheaters designed for different heat output) with non-contact (i.e., IR or lase) ignition**

## 1.2 State of Knowledge in Joining

There are various forms of existing welding/joining methods that are potentially applicable to the joining of small objects, e.g., microelectronics components (C.T.Ko, K.-N. Chen.), (J. Cecil, Powell, D. Vasquez 580-588), (C. L. Bauer, G. G. Lessmann 361-387). They may be classified into two groups, fusion joining and solid-state joining. Diffusion bonding, deformation welding, friction joining and ultrasonic joining exemplify the solid-state joining processes (G. Cam, M. Kocak 1-44). Due to their ability to produce metallurgical bonding at a relatively low joining temperature, these solid-state processes are advantageous in applications where excessive heating of the materials being joined is not tolerated. However, except for thermocompression wedge bonding and ultrasonic joining, conventional solidstate joining processes are not applicable to the joining of very small parts and hence are hardly applicable to microelectronics packaging. Fusion joining processes that potentially apply to small components are represented by electron-beam joining and laser joining (G. Smolka, A. Gillner, L. Bosse, R. Lüzeler 187-192), (Z. Sun, R. Karppi 257-267), (A. P. Mackwood, R. C. Crafer 99-115) in which focused application of high energy results in pinpoint melting and re-solidification of the materials being joined. These fusion processes, however, have their own limitations, particularly in applications where melting and/or excessive heating of the parts being joined is not allowed. Joining processes that involve melting of a filler metal may also be categorized as fusion joining processes. The latter processes are represented by brazing (R. M. do Nascimento, A. E. Martinelli, A. J. A. Buschinelli) and soldering (H. H. Manko), (J. S. Hwang) . While the above methods all have different degrees of applicability to small-part joining, the microelectronics industry currently adopts only soldering and ultrasonic joining. Ultrasonic joining, when applied to microelectronics, takes the form of wire bonding in which interconnects are produced by

ultrasonic joining of an integrated circuit to a printed circuit board with Al, Cu or Au wire (W. H. Kearns), (G. Harman), (R.R. Tummala) (S. Nakada). bonding, another ultrasonic joining method used in microelectronics, does the same, except it involves partial melting of the bonding wire and thus is not strictly a solid-state process.

Soldering techniques have been very successful in the microelectronics assembly and MEMS integration (H. H. Manko), (J. S. Hwang). Solders are low-melting point metal alloys, and the most widely used solder is eutectic tinlead (Sn/Pb, 63/37). However, due to the toxicity of lead, lead-free solders are being developed for electronic components assembly onto PCB (printed circuit board). In recent years, energy cost and demand have been increasingly high due to the energy shortage. In this sense, pursuit of less energy consuming or more energy efficient processes is much referred. However, the current lead-free alternatives being used, e.g., tin/silver/copper (Sn/Ag/Cu, SAC), have melting points around 217°C or higher (> 30°C higher than that of the Pb/Sn solder, 183°C) and have to be processed (reflowed) at much higher temperatures than that of the Sn/Pb solders, which can negatively affect product reliability due to higher residual stresses in PCB assemblies. **Thus, lower temperature processing using nanosolders** (Q. Cui, F. Gao, S. Mukherjee, Z. Gu 1246-1257), (Z. Gu, H. Ye, D. H. Gracias 60-64), (Z. Gu, H. Ye, D. Smirnova, D. Small, D. H. Gracias 225-229), (F. Gao, Z. Gu) **or self-heating methods are strongly desired for microscale joining.** Similarly, in other lower temperature applications where a polymer adhesive (e.g., hot melt thermoplastic or cured thermoset) is desirable, the powder or liquid can be applied in small volumes (e.g., in powder or droplet form) for microscale joining (S. Bohm, K. Dilger, J. Hesselbach, J. Wrege, S. Rathmann, W. Ma, E. Stamman, G. Hemken 676-679), (S. Bou, D. Fratila, A. Boglea, D. Andrijasevic, A. Almansa, W. Palfinger, W. Mann, A. Olowinsky, W.

Brenner, R. Most, Z. Rozynek). Most current methods, however, require bonding by external bulk heating, with some processes incorporating additives for UV curing or utilizing laser heating.

Joining using a filler material provides another approach to joining of small parts such as microelectronics components. However, due to the restriction that IC interconnects must be created at sufficiently low temperature, conventional brazing techniques that require furnace heating are not advantageous. Thus, use of a self-heating brazing material is essential. Reactive *in-situ* heating through exothermic solid material transformations has been well developed in macroscale, for example, in thermite welding of rail sections (N. Ilic, M. T. Jovanovic, M. Todorovic, M. Trtanj and P. Saponji 243-250) by ignition of iron oxide and Al powder mixtures (C. Meric, E. Atik, S. Sahin 172-176), the Ni-Al system for thermal joining applications (J. Wang, E. Besnoin, O. M. Knio, T. P. Weihs). The Ni-Al system is a pre-eminent system for joining since its intermetallic compounds ( $\text{NiAl}_3$ ,  $\text{Ni}_2\text{Al}_3$ ,  $\text{NiAl}$ ,  $\text{Ni}_3\text{Al}$ ) are accompanied by large exothermic formation enthalpies (-37.85 to -71.65 kJ/mol, room temperature) (J. C. Trenkle, J. Wang, T. P. Weihs, T. C. Hufnagel), (J. C. Trenkle, L. J. Koerner, M. W. Tate, S. M. Gruner, T. P. Weihs, T. C. Hufnagel). The Ni-Al system has been studied in solid-state combustion synthesis using pressed foil laminates (e.g, RNT foils), and ultrasonically welded or electroplated layers on metal substrates. **However, the Ni-Al system has not been used in microscale joining, and more importantly, due to the brittle nature of foil laminates, it cannot be applied on flexible or curved substrates. This is a significant need to develop new types of nanoheater structures (Al-Ni and others such as thermites) that satisfy such demand.** It is well-known that nano-sized materials exhibit novel electrical, optical, magnetic and mechanical properties. (A. P. Alivisatos 933-937), (C. J. Murphy, T. K. Sau, A. M. Gole, C.

J. Orendorff, J. Gao, L. Gou, S. E. Hunyadi, T. Li 13857-13870), (C. Lieber 486-491), (S. Iijima 56-58), (P. M. Ajayan 1787-1799). In the past two decades, techniques for nanomaterial synthesis and fabrication have progressed rapidly. However, joining and interconnect formation techniques have lagged behind and are becoming the bottleneck of circuit formation and electronics assembly. Two examples have shown promise in interconnect formation and joining at micro- and nanoscale: (1) annealing or sintering (F. Mafune, J.-Y. Kohno, Y. Takeda, T. Kondow 1686-1687), (R. Klajn, K. J. M. Bishop, M. Fialkowski, M. Paszewski, C. J. Campbell, T. P. Gray, B. A. Grzybowski 261-264) and (2) focused E-beam (FEB) or focused Ion-beam (FIB). (M. Wang, J. Wang, Q. Chen, L. M. Peng 1825-1831), (D. N. Madsen, K. Mølhave, R. Mateiu, A. M. Rasmussen, M. Brorson, C. J. H. Jacobsen, P. Bøggild 47-49), (F. Banhart 329-332) Annealing is one way to lower contact resistance between components, which is similar as diffusion bonding or welding; however, the annealing temperature is normally high and this may damage certain electronic components. FEB/FIB-based joining has been used in the bonding of carbon nanotubes to substrates, nanotubes to nanotubes, and nanowires to nanowires; however, this technique suffers from slow processes and contamination. Even though facing various challenges, microscale joining has been shown promise. More promisingly, joining property may be increased by the enabling of nanotechnology. (Y. Lu, J. Y. Huang, C. Wang, S. Sun & J. Lou) **Thus, it is attractive to develop nanoheater structures as a new technique for the enabling of microscale joining.**

## 2 Research Goals

The primary goal of this thesis research is to study the feasibility of joining flexible polymer materials using nanoheaters in flexible electronics and more specifically flexible batteries. A numerical model is needed to show the general properties and characteristics of

nanoheaters when configured to join many different material combinations. For the creation of an experimental flexible battery, a material that is impermeable to water and does not degrade in electrolytic solutions is needed. A numerical model must match a physical model with experiments that can be tested. Experimental tests to measure the strength of the flexible material bonds needs to be conducted. Methods must be developed to seal the flexible materials using nanoheaters. Finally tests to measure the quality of the hermetic seal and a prototype battery cell are desired.

### 3 Nanofoil

While nanoheaters are made in our research group Nanofoil was the primary nanoheater that was used for the experiments. Nanofoil is a commercial type of nanoheater that uses thousands of alternating layers of nickel and aluminum which are fabricated by vapor depositing to create a thin and very rigid Nanoheater (NanoFoil®). Nanofoil was picked do to a few favorable parameters. First Nanofoil is cheaper to buy than to make a nanoheater powder in the quantities needed, with the lower lead times. The approximate reaction speed is well documented and consistent along with the energy released per gram. This allowed for the calculation of energy released at a specified time. Lastly Nanofoil has the lowest ignition temperature of which is 200C.

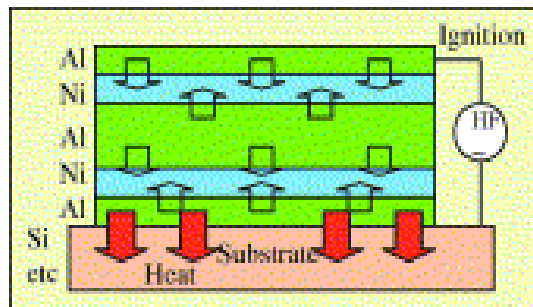


**Figure 2: Nanofoil composition (NanoFoil®.)**

## 4 Numerical Model

The interest of this project is to understand how well nanoheaters can join two flexible materials together in a macro and micro scale. A simple micro and macro model was created to simulate this, as shown in figure 3 & 4, a very thin sheet was placed at the top of the model to simulate the Nanofoil. Underneath that a thicker block was placed underneath the Nanofoil to represent the heat spreader and another larger block was placed at the bottom representing the LCP.

### 4.1 Finite Element Analysis in COMSOL

Finite Element Analysis (FEA) software was used to solve the numerical calculations. COMSOL Multiphysics 4.3 was the primary software used to solve the numerical simulations. COMSOL is able to calculate 3D heat transfer models with high precision when set up correctly. In this case the time dependent thermal stress module of COMSOL was used to understand how nanofoil reacts in a joining environment.

### 4.2 Geometry & Boundary Conditions

The external ambient temperature as well as the initial temperature of all the materials was set to 293.15K to simulate room temperature. A convective cooling of  $10,000\text{W}/(\text{m}^2\text{-K})$  was applied to the bottom of the substrate to simulate the conduction of the heat through the ceramic blocks when pressure was applied as shown in figure 8. For the rest of the outside faces  $5\text{W}/(\text{m}^2\text{-K})$  was used to simulate the convective cooling of the model to the ambient air of the room. A domain heat source was also applied to the top of the chip to simulate the energy

released from the Nanofoil as shown in figure 6. Figure 5 shows all the areas where symmetry was applied. The faces on the side of the model cut the model in a quarter to reduce the number of elements and the top symmetry cuts the height of the model in half further reducing the elements. Two separate models were made a macro model as shown in figure 3 and a micro model as shown in figure 4.

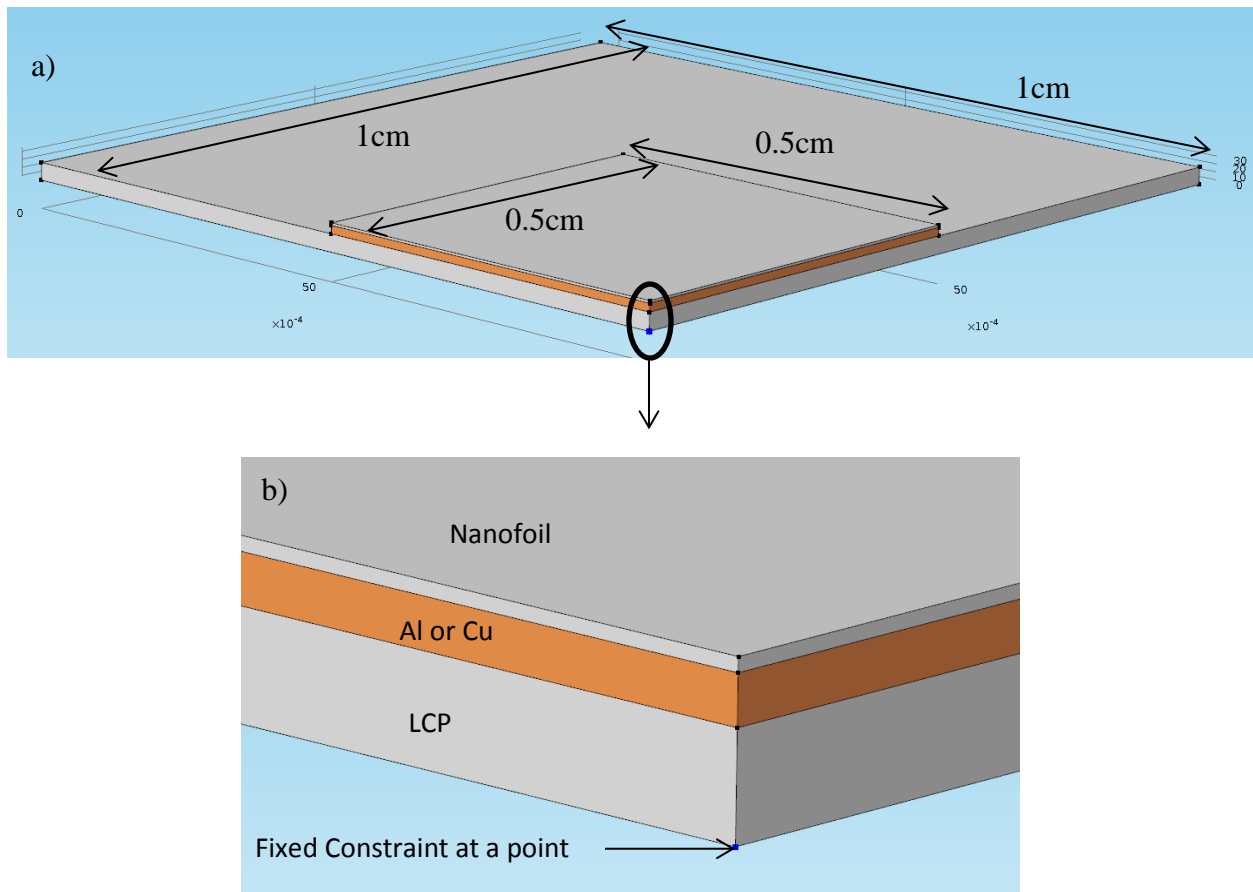


**Figure 3: The full COMSOL model (a) and a close up of the layers in the model (b) featuring Nanofoil as the top layer, Al and Cu as the middle layer and LCP as the bottom layer. The thickness of the nanofoil was 60 microns but since symmetry was imposed the nanofoil was represented as 30microns when one nanofoil was used and 60microns when two nanofoils were used. The thickness of the heat spreaders when either Al or Cu were used was 0.1016mm and the LCP was .11mm when one LCP was needed and .22 when two were needed**

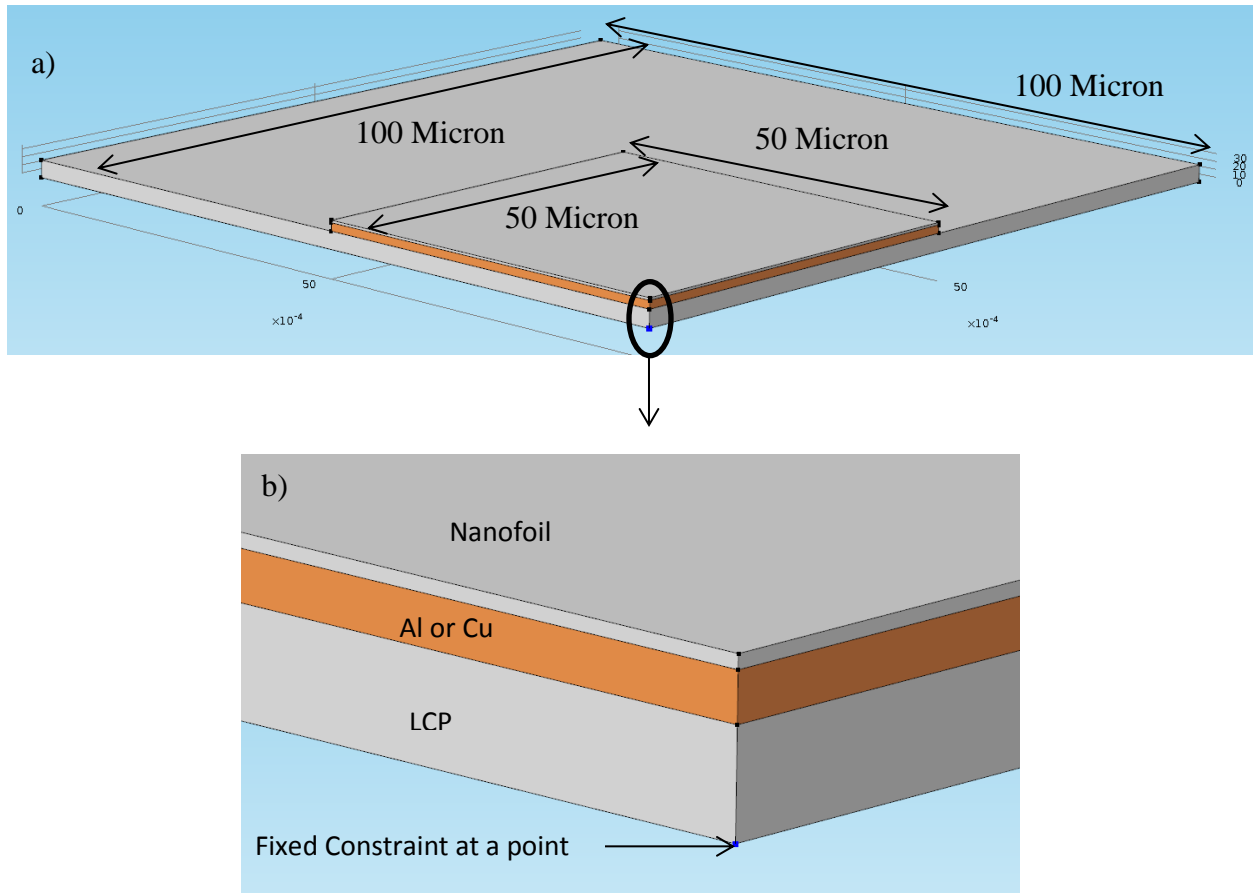


**Figure 4: The microscale COMSOL model (a) and a close up of the layers in the model (b) featuring Nanofoil as the top layer, Al and Cu as the middle layer and LCP as the bottom layer. The thickness of the nanofoil was 0.6 microns but since symmetry was imposed the nanofoil was represented as 0.3 microns when one nanofoil was used and 0.3 microns when two nanofoils were used. The thickness of the heat spreaders when either Al or Cu are used was 1.016 microns and the LCP was 1.1 microns when one LCP was needed and 2.2 microns when two were needed.**

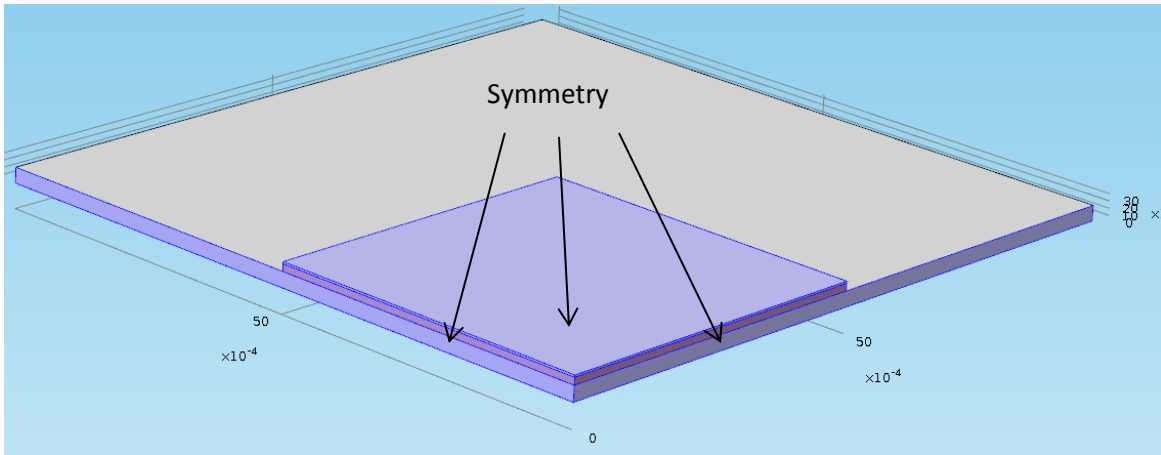


**Figure 5:** The blue colored faces are all of the areas where a symmetry boundary condition was applied.

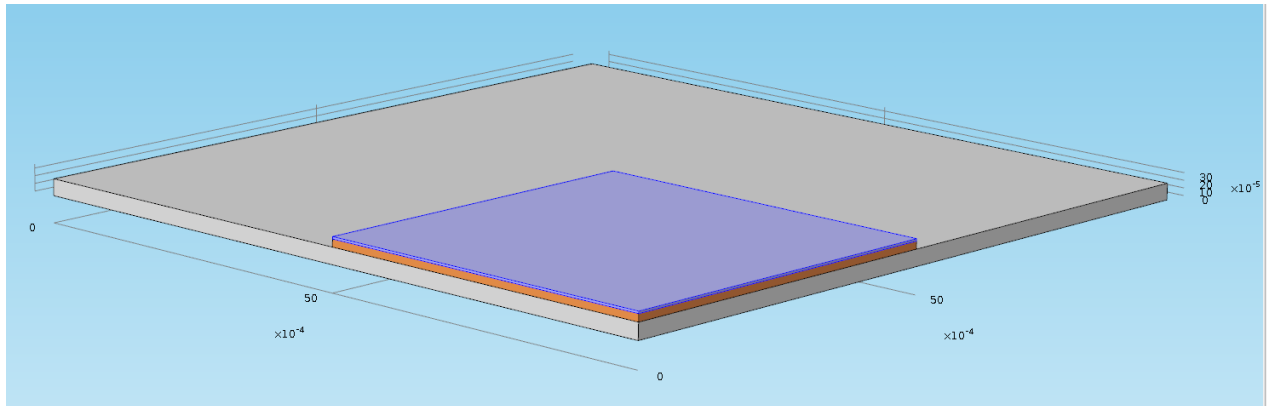


**Figure 6:** The blue colored domain is the domain which represents the nanofoil and which the heat source is specified.

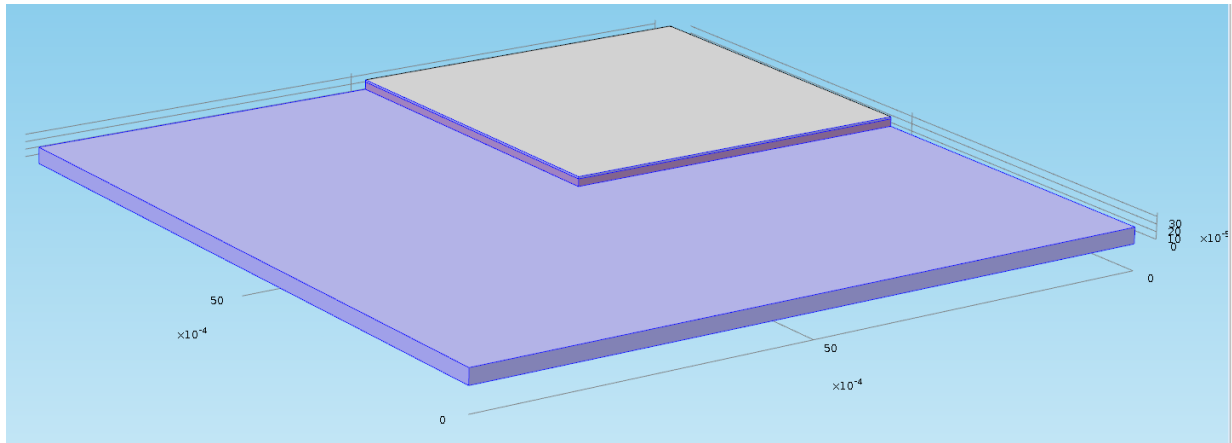


**Figure 7: The blue colored faces indicate an area where a convective cooling parameter of  $5\text{W/m}^2$  are placed.**

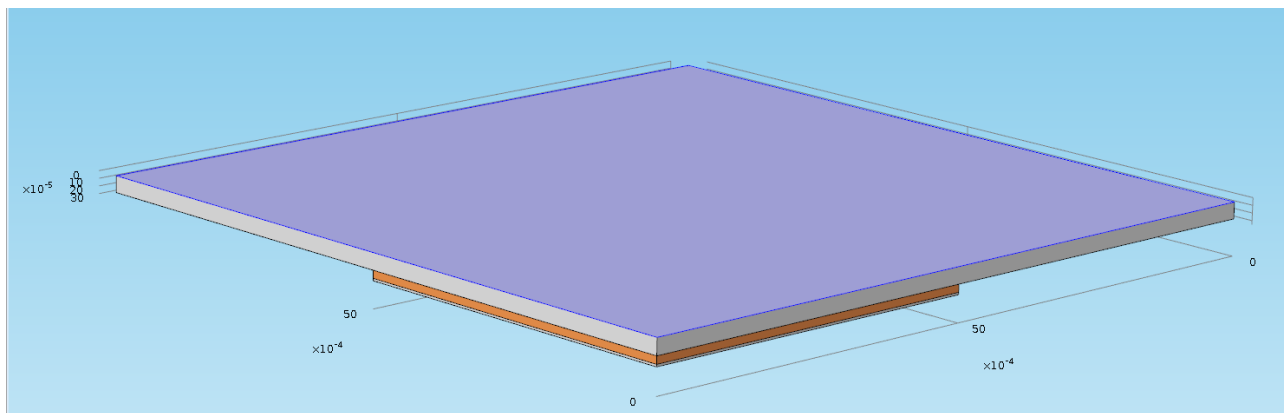


**Figure 8: The blue colored face indicates an area where a convective cooling parameter of  $10,000\text{W/m}^2$  is placed.**

#### 4.2.1 Mesh

In finite element analysis software selecting a proper mesh is very important in obtaining accurate results. Generally speaking a more refined mesh or a model with a lot of elements will produce better results than a course mesh or a mesh with fewer elements. (J. Fish, and T.

Belytschko 77) The elements used in this analysis were basic tetrahedral elements. Special attention was given to the corners and the small thickness. Extra elements were added through the thickness since the temperature and stress gradient was shown to be so great through the thickness rather than through the sides. At the corner where the heat spreader material meets the LCP more elements were added as well to increase accuracy (C. Felippa). The maximum element size was specified as  $2e-4$  and the minimum element size was  $2e-6$  and the maximum element growth rate was set to 1.3. The elements in the nanoheater and the heat spreader were scaled. The x & y direction scale was set to 0.3 and the z direction scale was set to 6 to increase the elements in the z direction. The LCP material's elements were scaled as well. The x & y direction scale was set to 0.2 and the z direction scale was set to 3 to increase the elements in the z direction. A distribution selection was also selected on the edges where the heat spreader meets the LCP. The number of elements on each edge was set to 40.

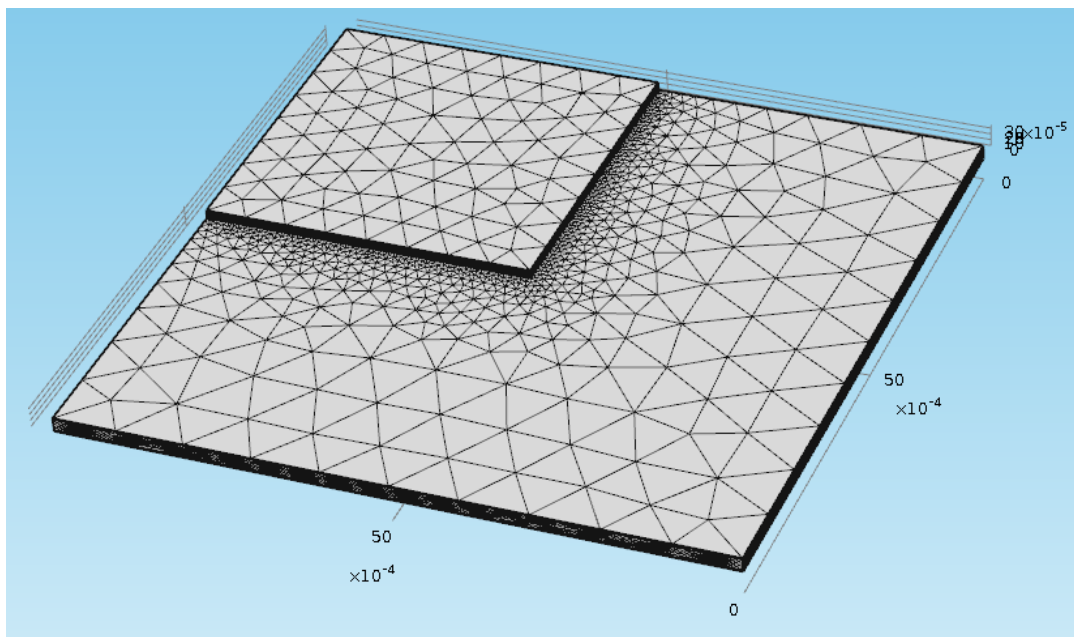


**Figure 9: Final Mesh Configuration**

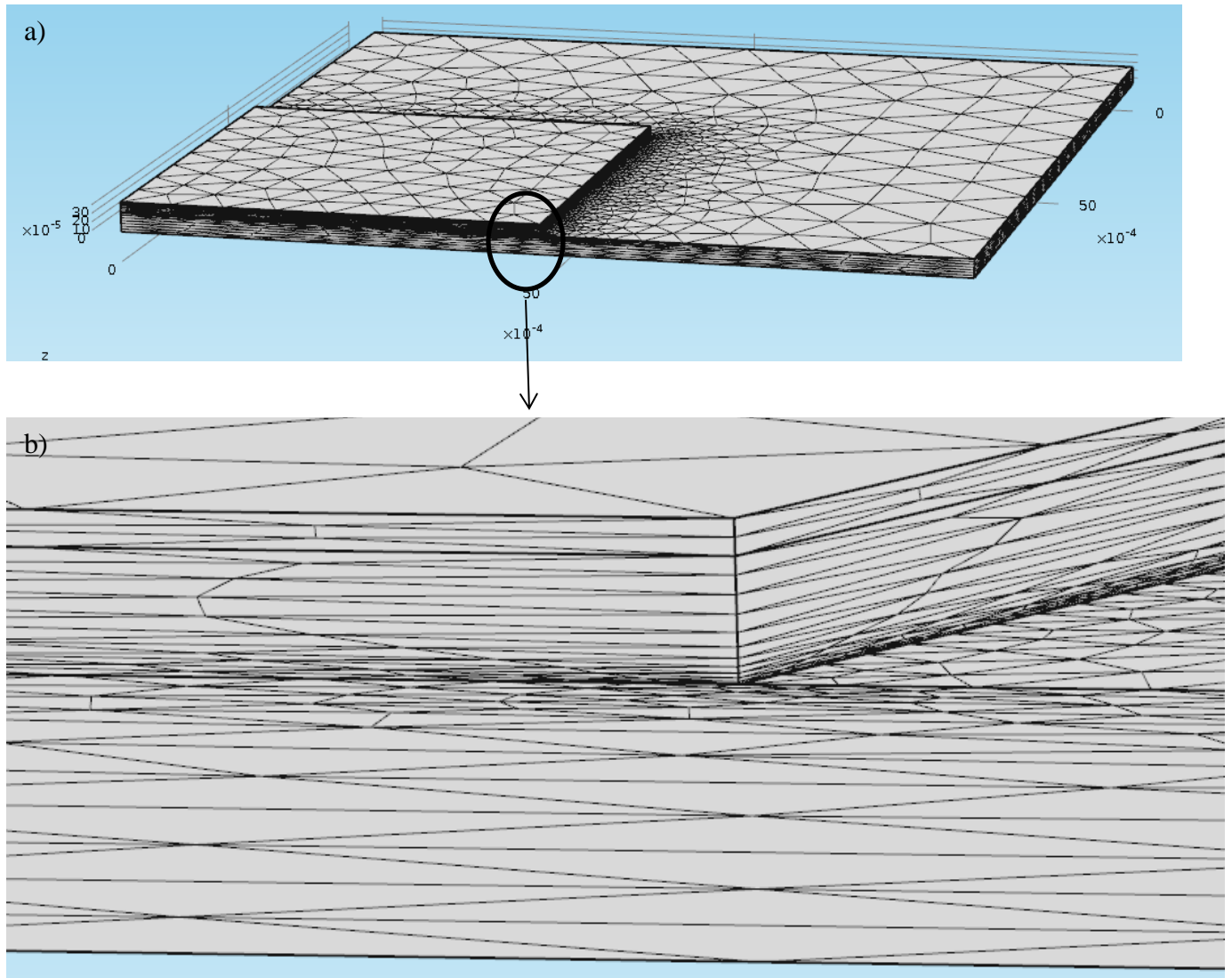


**Figure 10:** The final mesh (a) with an enlargement of the area where there are many elements through the through the thickness of the model (b)

Table 1 and figure 11 are checks to make sure the mesh is fine enough. Since the percent difference in both the temperature and the stress of the model is under 1.5% when the second highest mesh goes to the highest it is safe to say that adding more elements won't change the values very much. The model with 27,846 to about 2 hours to run depending on which study it was.

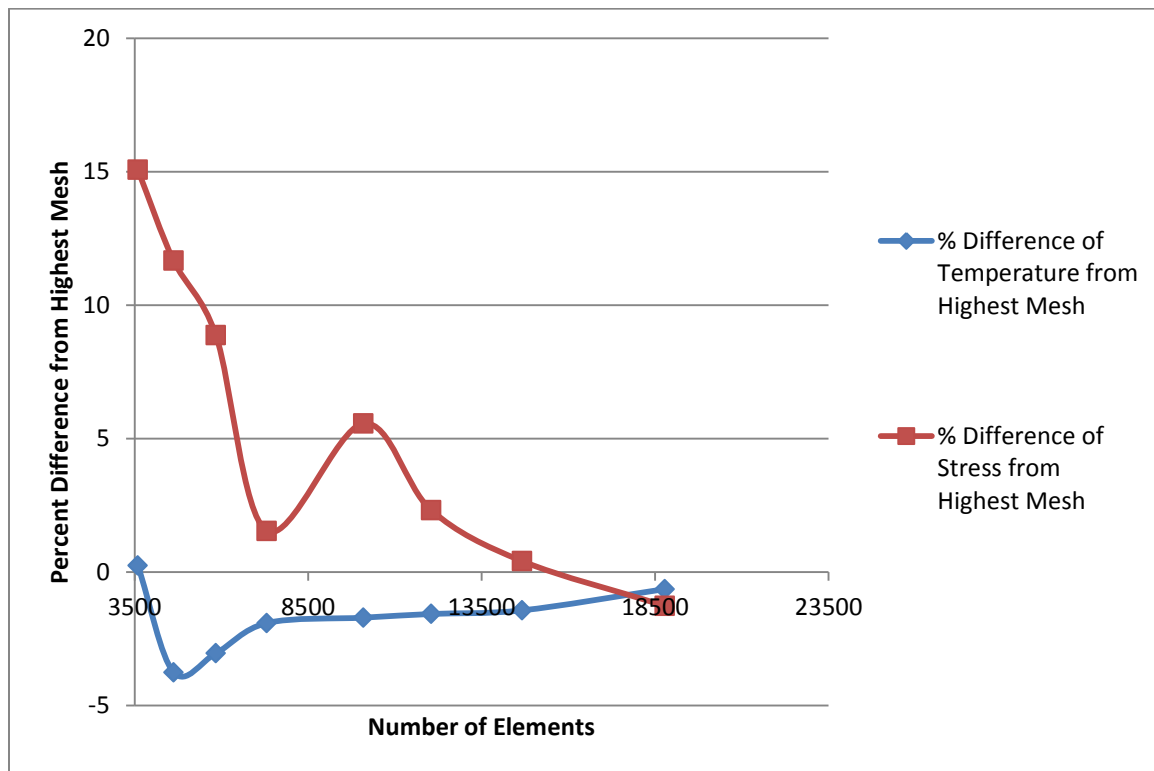
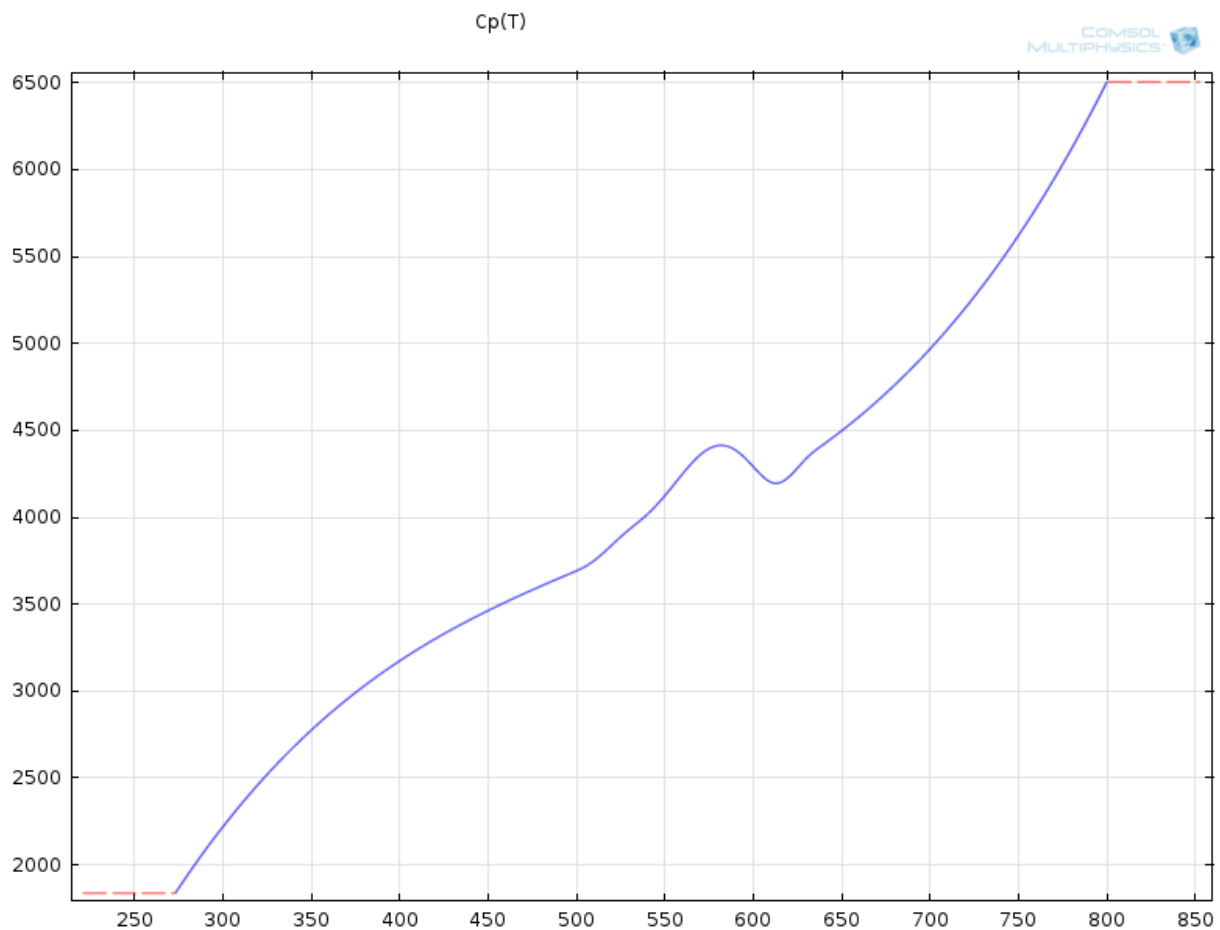


**Figure 11: The percent difference in stress and temperature compared to the mesh with the most elements which has 27846 elements.**

**Table 1: The change in stress and temperature as the number of elements are increased**

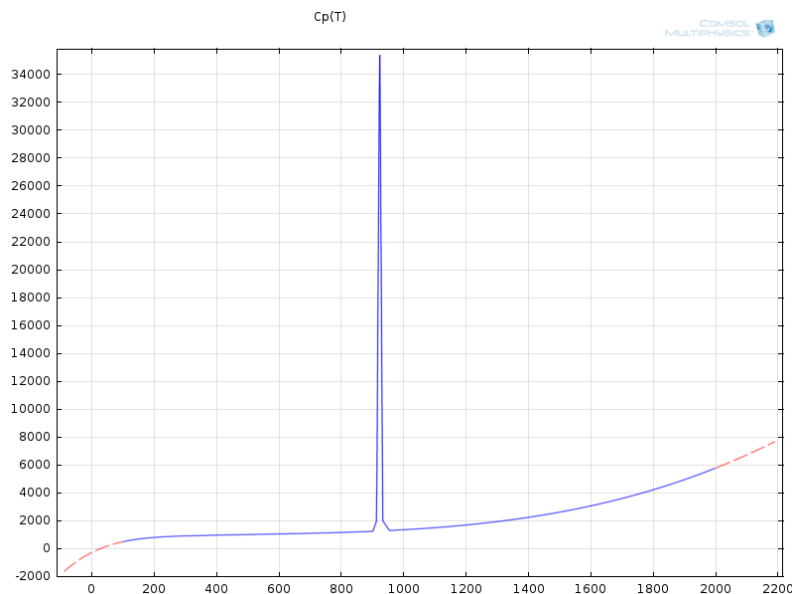
<b># of Mesh Elements</b>	<b>Temp (K) at End of Heating</b>	<b>Stress (N/m<sup>2</sup>) at End of Heating</b>	<b>% Difference of Temperature from Highest Mesh</b>	<b>% Difference of Stress from Highest Mesh</b>
3592	625.97	68756300	0.25	15.07
4623	624.42	66722100	-3.75	11.66
5842	629.03	65054000	-3.04	8.87
7311	636.38	60673900	-1.90	1.54
10096	637.68	63079400	-1.71	5.57
12046	638.58	61140200	-1.57	2.32
14671	639.46	59998200	-1.43	0.41
18779	644.62	58999700	-0.64	-1.26
27846	648.75	59752500	1	1

Figure 12 below is a graph of the heat capacity of LCP measured by a differential scanning calorimeter. A conservative estimate is that 2,990 J/kg of heat is needed to melt the LCP over a temperature of 577K-598K. A more generous estimate is that 12,600 J./kg of heat is needed over a temperature range of 513K-598K. This graph shows that the phase change from solid to liquid is much less abrupt than from metal and that there is a considerable range in temperature where the LCP is very soft. Perhaps joining can take place before the melting point is reached. The melting point of this LCP is 598K.



**Figure 12: Measured heat capacity curve in relation to temperature of LCP from differential scanning calorimeter with the increase in heat capacity to account for latent heat of fusion for melting. The X axis is temperature and the Y axis is k/kg-K**

Figure 13 below is a graph of the specific heat capacity curve of Al 1145. Aluminum has a relatively high latent heat of fusion at 498,000 J/Kg. The original specific heat capacity curve was taken from the COMSOL Material Library. A spike in the specific heat capacity was made as seen in the middle of Figure 13. The area under the triangular spike is equal to the latent heat of fusion of aluminum. Metals go from a solid to a liquid in less than a degree but a temperature range was needed for the calculations to work in COMSOL. It was found that if the LCP specific heat capacity spike started 20 degrees before melting than the model would indicate that it was at melting temperature and melted when precisely enough heat was added. The only problem with this is that the 20 degrees before the melting of aluminum will give results that are not entirely accurate but within 20 degrees of accuracy. A very important aspect of these simulations was to know if the aluminum got hot enough to melt and the specific heat capacity graph in Figure 13 below made sure that was the case.



**Figure 13: Specific heat capacity curve in relation to Temperature obtained by COMSOL Model Library for Al 1145 which incorporates a spike in LCP needed to represent the latent heat of fusion. The X axis is temperature and the Y axis is J/kg-K**

### **4.3 Thermomechanical Settings**

The physics used in COMSOL was thermal stress. Thermal stress was chosen because the main outputs that are needed in the model are temperature and stress when a heat source is applied. Thermal stress physics in COMSOL allows for this to be done.

### **4.4 Nanoheater Simulation Approximation**

The representation of a nanoheater in FEA can be very difficult given to the nearly instantaneous energy generated for such a small amount of time. A nanoheater creates its heat through a chemical reaction which travels from the point at which the nanoheater is ignited and radiates out like a wave. The reaction can travel between 6.5-8 m/s and releases 1050-1250J/g (Indium Corporation). The average time it takes for the reaction to take place was calculated to be 0.0007s. Since this is such a short amount of time the numerical model has been simplified to produce 1150j/g during 0.0007s across the whole area of the nanoheater. The physical dimensions of the nanoheater itself were represented as close as possible to the actual nanoheater while the material properties used for the Nanofoil were that of Al1145 since the material properties of the nanoheater are not known. An aluminum alloy was used since the nanoheater is made up of half aluminum. The material properties are not of great importance and more of just a place holder.

### **4.5 Study Parameters**

A time dependent study was used because the Nanofoil releases energy for such a small amount of time and the time after heating is of importance because the maximum temperature at

the interface, time it takes for the model to cool and the residual stress is needed to understand if a good joint is made.

## **4.6 Solver**

A Multifrontal Massively parallel sparse (MUMPS) direct solver was used which is a linear solver. In general direct sparse solvers use more memory but are very accurate when displacement is linear, this is due to the way the matrices are calculated direct sparse solvers calculate the equations directly and do not require iterations. The large matrices require more memory but the absence of iterative calculations allows for a low error (J. D. Hoffman). MUMPS also have the added benefit of using computer memory and multicore processors in parallel. (Comsol Multiphysics Reference Guide Version 4.3 607) The reordering algorithm was set to automatic so the computer would choose when to use minimum or maximum weight matching strategy while solving. Pivoting was used and a pivot threshold of 0.1 was used to prevent zeros in the pivot element of the calculated matrices when the elimination step of the LU factorization was being calculated.

## **4.7 Generalized Numerical Analysis and Pi Numbers**

It is important to know how much heat the nanoheaters need to produce to properly join a variety of materials with a variety of geometries. In order to generalize the inputs along with the outputs of the joining using nanoheaters, a dimensionless analysis was created using the Buckingham Pi theorem (P. J. Pritchard and J. C. Leylegian 292-303). It was found that to generalize the joining of a chip on a substrate 12 physical variables occur in the model.

The 12 parameters are as shown below

Heating time,  $\Delta t$  (s)

Thickness of Substrate,  $H$  (m)

Heat Generation,  $\dot{Q}_{gen}$  (W) or  $(kg \frac{m^2}{m^2 K})$

Specific Heat Capacity,  $C_p$  ( $\frac{J}{kg K}$ )

Melting point of substrate,  $T_{melt}$ (K)

Thermal diffusivity in substrate,  $\alpha_{diffusivity}$  ( $\frac{m^2}{s}$ )

Density of the substrate,  $\rho_{sub}$  ( $\frac{kg}{m^3}$ )

Delta in Coefficient of expansion,  $\Delta\alpha_{expansion}$  ( $\frac{1}{K}$ )

Change in temperature,  $T_{max} - T_{init}$  or  $\Delta T$  (K)

Heat Affected Zone, HAZ ( $m^2$ )

Maximum Interfacial Stress,  $\sigma_{interface}$  (Pa) or ( $\frac{kg}{m s^2}$ )

Pull Strength from experimental testing,  $\sigma_{pull}$  (Pa) or ( $\frac{kg}{m s^2}$ )

Three independent physical units are present in the model; these three units are length, time and temperature. The physical units are subtracted from the physical variables to obtain the number of Pi groups. The 12 physical variables were arranged into 9 different expressions where the dimensions canceled out to create a dimensionless expression. The six dimensionless expressions were 9 Pi groups as seen below.

$$\Pi_1 = \frac{\Delta\alpha_{diff}.\Delta t}{H^2} \text{ [Thermal Penetration Depth in Substrate]}$$

$$\Pi_2 = \frac{T_{melt}Cp\Delta T^2}{H^2} \text{ [Melting Potential]}$$

$$\Pi_3 = \frac{\dot{Q}_{gen}\Delta T^2}{\rho_{sub}H^5} \text{ [Energy Density]}$$

$$\Pi_4 = \frac{\Delta\alpha_{exp}.H^2}{Cp\Delta t^2} \text{ [Thermal Strain]}$$

$$\Pi_5 = \frac{\alpha_{diff.chip}\Delta t}{H^2} \text{ [Thermal Penetration in Chip]}$$

$$\Pi_6 = \frac{\Delta T Cp \Delta t^2}{H^2} \text{ [Peak Temperature]}$$

$$\Pi_7 = \frac{\sigma_{int}H^3}{\dot{Q}_{gen}} \text{ [Interfacial Stress]}$$

$$\Pi_8 = \frac{HAZ}{H^2} \text{ [Heat Affected Zone]}$$

$$\Pi_9 = \frac{\sigma_{pull}H^3}{\dot{Q}_{gen}} \text{ [Adhesion Strength]}$$

The Pi groups were arranged in a way so that the first 5 Pi groups consisted of input variables and the last 4 pi groups consisted of output variables, measured from COMSOL or measured from experiments. With the 9 Pi groups a numerical model was created using the multi physics Finite Element Analysis software, COMSOL. The simulations were conducted to find relationships between the variables we are able to change and the results. The numerical simulations have much more flexibility in how we can change the variables and how we can obtain data for the results.

#### 4.7.1 Design of Experiments Using Pi Numbers

A Design of Experiments (DOE) was conducted which incorporated 3 key parameters and each parameter was given a high and a low value. 8 simulations needed to be conducted since each parameter had 2 values and there were 3 parameters giving  $2^3 = 8$  (How to Perform a Design of Experiments). The 3 key parameters were the material of the heat spreader either Aluminum or Copper, the amount of Nanofoil 1 or 2 Nanofoils and the thickness of the LCP either 2 LCPs fused together to make 1 double thick LCP or 1 LCP. This will give us a broad understanding of the properties that joining using nanoheaters possess, Table 2 below shows all the possible combinations.

**Table 2: This table shows all the possible combinations of the DOE**

Run #	Material	Material high or low	Nanofoil	Nanofoil high or Low	LCP thickness	LCP high or low
1	Al	low	1	low	1	low
2	Al	low	2	high	1	low
3	Al	low	1	low	2	high
4	Al	low	2	high	2	high
5	Cu	high	1	low	1	low
6	Cu	high	2	high	1	low
7	Cu	high	1	low	2	high
8	Cu	high	2	high	2	high

## 5 Experimental Models

4 different experiments were conducted using LCP to first tangibly understand the properties of the LCP and optimal temperatures and pressures needed to join LCP to itself. The second experiment was the first experiment using nanoheaters to join LCP which used a method

which resembled a taco and tested the bond strength. The third experiment tested how well the taco joining method could hermetically seal an LCP pouch. The 4th experiment used a joining method using nanoheaters which resembled a sandwich and which tested the bond strength of the sandwich. The 5<sup>th</sup> experiment used the sandwich method but flipped everything inside out and was used to attempt to seal an LCP pouch hermetically. The final experiment was the construction of a LCP battery.

## **5.1 General Welding of LCP**

The LCP supplied by iQLP melts at roughly 598K degrees C. An experiment was conducted using a variable temperature soldering iron. The experimental test was conducted from the lowest setting at which the LCP softens which is 553K to the highest setting 713K. The optimal temperature for welding was found to be in the 573 to 583 range. This temperature is consistent with the temperature that is used to bond LCP to copper circuits for industrial purposes. In industry the LCP is also bonded using slight pressure as well. As the temperature goes further below the melt point, more pressure is required generally until 553K is reached in which case the soldering Iron is not hot enough to melt the LCP. At 553K and 563K the LCP is soft and malleable but very difficult to bond to itself. Above the melting temperature very little pressure is needed to melt the LCP and have it bond together however it gets much more difficult to not melt through the 2 pieces of LCP as the soldering iron temperature is increased. Furthermore the speed of movement of the soldering iron over the LCP needs to be increased as well to prevent melting through the LCP. The degradation temperature of LCP is 673K and at 673K and above the LCP started to smoke but no visible sign of degradation in the LCP sample was observed presumably do to the increased movement of the soldering iron over the specimen.



**Figure 14:** Testing of optimal temperature for joining LCP with a soldering iron. The top left specimen was joined when 280C (553K) was applied and the temperature was increased by 10 degrees C for each subsequent piece until 440C (713K) was reached which is the bottom right specimen.

## 5.2 Taco Joining Method

LCP has a very low conductivity of 0.189 W/m-K and when using the nanoheater by itself to join two pieces of LCP, it creates such a high heat that the LCP becomes singed and burnt resulting in a very unfavorable joint. Heat spreaders were used consisting of aluminum and copper with much better results.

The taco joining method is the first method used to join LCP using nanoheaters. The method resembles a taco in which the meat in the middle is the nanofoil and the shell is household aluminum foil used as a heat spreader. The thickness of this particular aluminum foil is 0.012mm. The taco is then laid width and length wise in between two pieces of LCP. The point where the bottom of the taco ends is where the two pieces of LCP are pushed together as shown in figure 15.

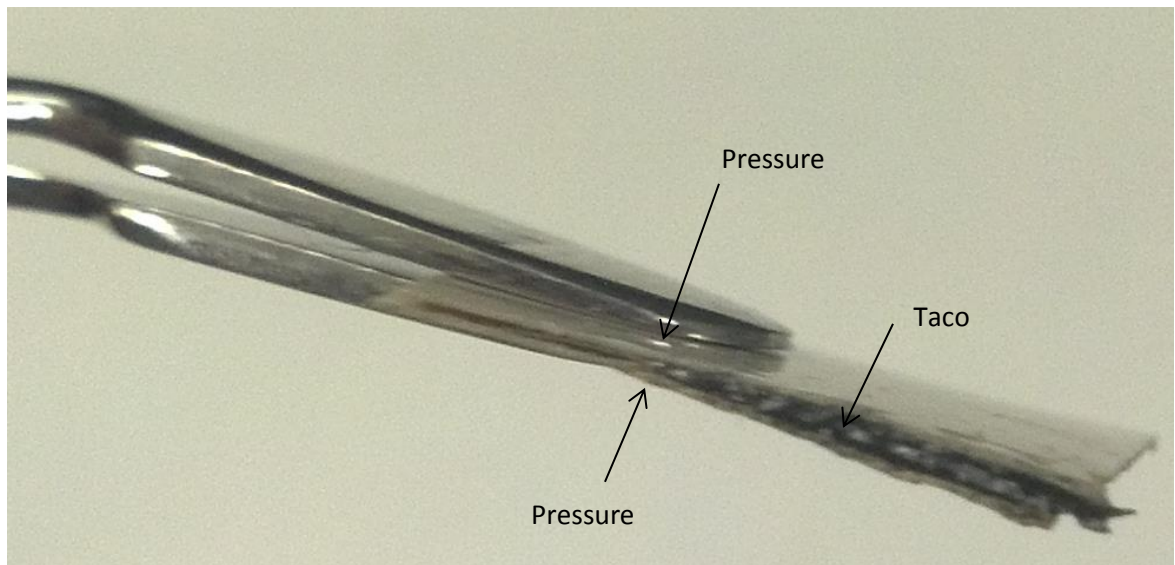


**Figure 15: A cross section of a joining specimen using the taco method. The area where the pressure is applied is where the joining LCP to LCP bond is formed.**

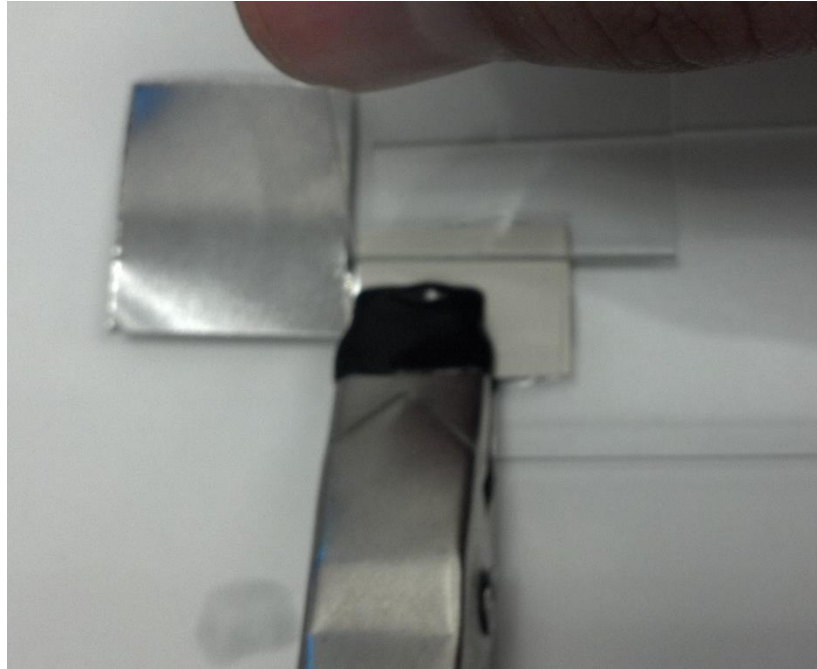


**Figure 16: Joining set up of taco method. The taco and LCP are clamped down with clamps to a glass slide while a second glass slide is used to apply pressure where the Taco ends and the two pieces of LCP meet. The piece of metal on the left of the LCP is an ignition antenna used to ignite the Nanofoil using an induction heater. This method of ignition was later dropped in favor of spark ignition.**

### **5.2.1 Taco Peel Tests**

A small pull-test machine was built using a small drill press with the drill piece removed. A small pull scale was attached to the area where the drill was as shown in figure 17. The test specimens were glued to a glass slide and a golf tee was then glued to the other side of the test specimen and an eye hook was screwed into the top of the golf tee as shown in figure 18. The glass slide was clamped down to the bottom of the pull-test machine using 2 C-clamps as shown in figure 17. The pull-test machine was used to measure the force needed to peel the two bonded pieces of LCP together.

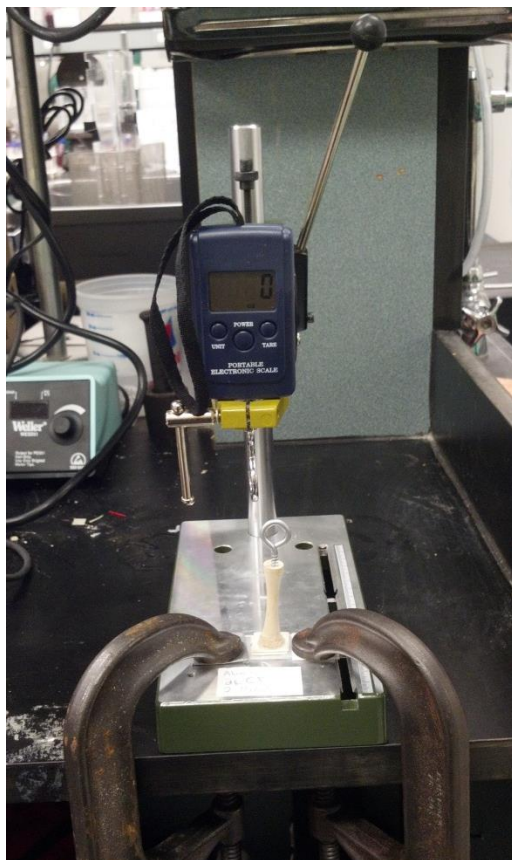


***Figure 17:*** Custom pull-testpull-test machine used for conducting pull tests.



***Figure 18:*** LCP specimens are glued onto a glass slide and a golf tee is glued to the LCP. These test specimens have the aluminum and nanofoil taco not cut out.



**Figure 19:** LCP specimens are glued onto a glass slide and a golf tee is glued to the LCP. A hole is drilled into the top of the golf tee and an eye hook was screwed into the hole. These test specimens have the aluminum and nanofoil taco cut out.

### 5.2.2 Taco Leak Test

A leak test was conducted by joining the LCP using a soldering iron to compare the results to a taco method leak test. Baking soda and red dye were placed inside the leak specimen before it was sealed and the specimens were submerged in vinegar and left for 24 hours. If red bubbles were initially observed or if after the 24 hours the vinegar was pink or red then the specimen had failed the leak test. Figure 20 is a picture of one of the soldering iron leak tests before it was submerged in vinegar. 3 specimens were tested using the taco method to seal the

specimen and 3 more specimens were tested using a soldering iron to seal the specimen. Figure 21 is a picture of the only test specimen that did not leak after the 24 hour period.



***Figure 20:*** Leak test specimen using a soldering iron to seal the LCP

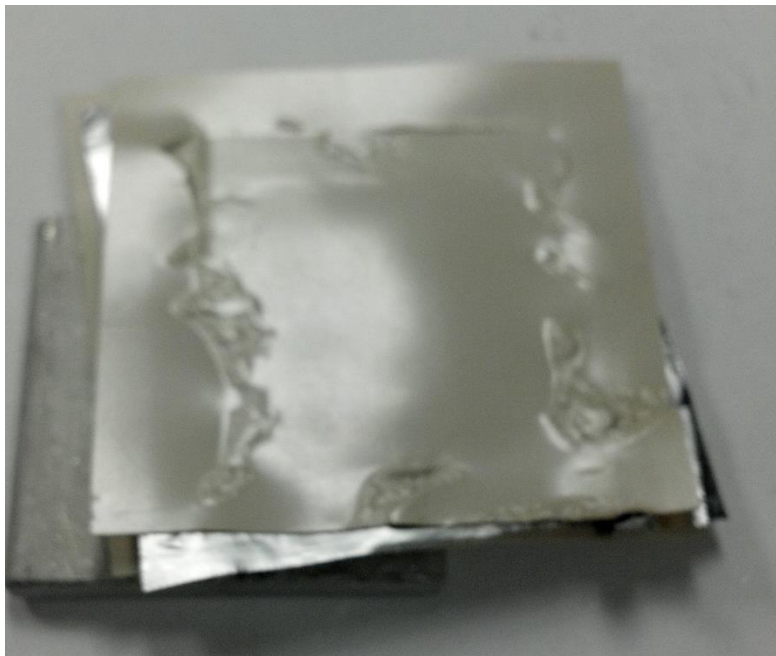


***Figure 21:*** Leak test specimen using nanofoil to seal the LCP

### 5.3 Sandwich Joining Method

Another joining method was found to be more beneficial than the taco method since the taco method has a very small amount of joining area. The sandwich method had the LCP as the bread of a sandwich and the meat in the middle was the Nanofoil and the copper or aluminum heat spreaders, the Nanofoil being in the exact center of the sandwich and the heat spreader material being on both sides of the Nanofoil. Figure 22 is a layout of the materials that make up the specimen. The copper and aluminum heat spreaders are 4mils or 0.1016mm thick and the grade of aluminum used is Al 1145 and the grade of copper used is Cu 10100. A small ignition antenna made up of a slender piece of Nanofoil is placed on the Nanofoil (as seen in Figure 23) that protrudes out of the side of the specimen to allow for easy ignition. Once the sandwich specimen is made 1 ceramic block is placed below the specimen and another ceramic block on top, 2 spring clamps are then used to clamp the specimen down and the Nanofoil is ignited from igniting the Nanofoil antenna. The specimens are glued to golf tees and glass slides just the same way as discussed in the previous section taco joining section.

To verify the numerical model LCP that was twice the thickness of the ordinary LCP was made. This was done by taking two pieces of LCP and placing them on top of each other and sandwiching them between two pieces of silicon. The silicon and LCP were then put on top of an induction stove top and the stove top was set to 613K. The soldering iron was set to its maximum temperature of 729C and the tip was placed in the center of the top piece of silicon and pressure was applied for 20 seconds. This process produced a piece of LCP that was roughly twice the thickness of the ordinary LCP. A piece of ordinary LCP was measured to an average of 0.11mm thick. The range for acceptable double thick LCP was between 0.2mm and 0.22mm. To verify the 8 numerical model simulations 1 piece of nanofoil was used as well as 2 pieces of nanofoil.

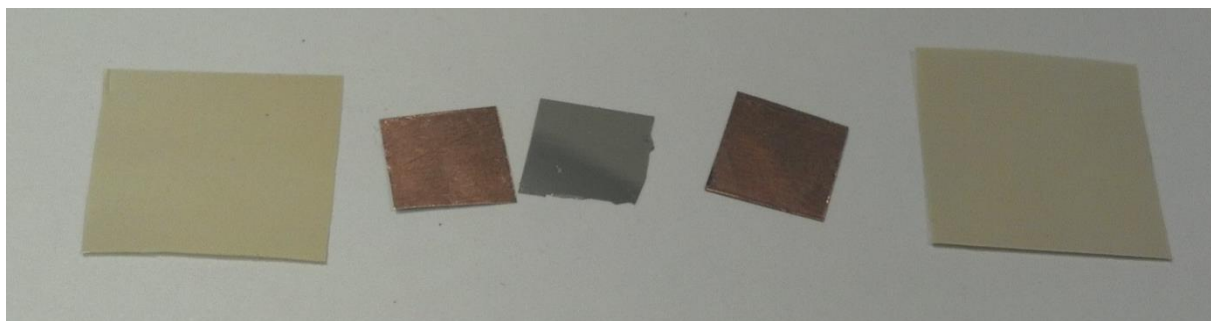


**Figure 22: The pieces used in the sandwich joining tests. The two outside tan colored pieces are LCP, the two copper colored pieces are copper and the shiny metallic piece in the center is nanofoil. The antenna used for igniting the nanofoil is no shown in this picture**

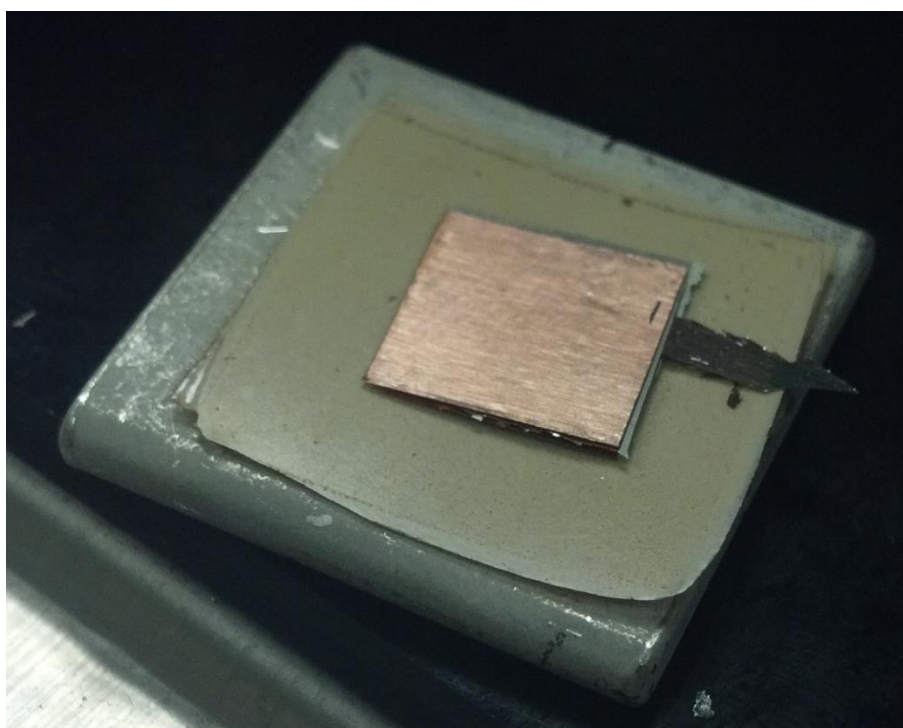


**Figure 23: A partially completed sandwich test before the final piece of LCP is placed on top. The metallic protrusion on the right side of the specimen is the antenna.**



**Figure 24: Test specimen before ignition. The sandwich specimen is in between two ceramic blocks which are clamped together using spring clamps.**

## **5.4 Sandwich Joining & Leak Test**

To create a strong flexible joint the sandwich method was flipped inside out. The two pieces of LCP were in the very middle of the sandwich and then copper heat spreaders were placed on the top and bottom of the LCP and on the very outside the Nanofoil was placed. This new method would allow for rather large LCP to LCP bond areas. The size of the LCP used was 4cm by 4cm squares. The copper heat spreaders were 1cm wide and 4.5cm long. The nanofoils were cut into strips 0.5cm wide and 5 cm long.

The numerical simulations conducted earlier showed that the LCP gets to melting temperature through the entire thickness of the LCP but since the latent heat of fusion was not known at that time for the phase change for LCP it was not known if the LCP actually changed phase. The numerical model did show that the face where the two LCPs met only reach 30 degrees above melting while the opposite side where the copper was on reached nearly 1000K. To find out how much Nanofoil was needed, an experiment was conducted 2 Nanofoils per side were used to join the LCP and then 3 Nanofoils per side were used to join the LCP. It was

determined that 3 Nanofoils achieved a much more consistent bond which appeared to show no holes.

Copper was used instead of aluminum as the heat spreader because it is a better conductor and has a higher melting temperature so copper would be less likely to stick to the LCP. Copper also oxidizes faster than aluminum making it more difficult to stick to the LCP. From the pull tests it was found that the copper does not stick as well to the LCP than aluminum does. Silicon was used as the material to clamp down the specimen before ignition because from previous experiments which are not covered in this document it was found that silicon wafers do not stick to any material currently found in the laboratory.

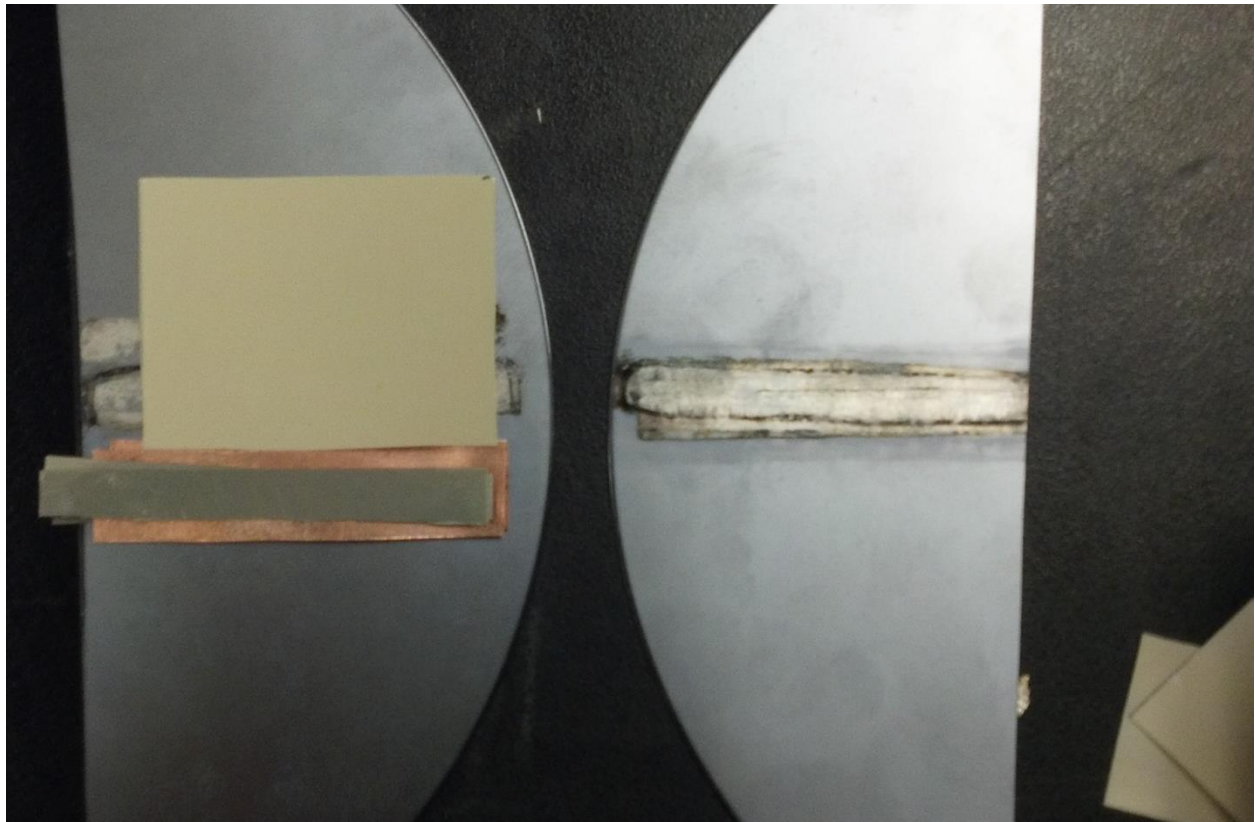


***Figure 25: The first side to be bonded for the leak test using the sandwich method.***

Below in figure 26 is a picture of the leak test specimen after it leaked. With this particular specimen one side had difficulty bonding using Nanoheaters do to the LCP sticking to the copper heat spreader and tearing holes in the specimen. A patch was performed using the soldering iron in which case the area where the patch was made leaked as well as other areas of the specimen.



**Figure 26:** A leak test specimen using the sandwich method after it had failed the leak test. Note the red dye in the bottom right corner of the specimen, on the entire left edge of the specimen and the top center right dot of the specimen, all of these areas were where the specimen leaked. Also note the patch on the left edge using a soldering iron because the copper heat spreader kept tearing holes in that side.

### 5.3 LCP Battery Prototype

The Prototype LCP battery was manufactured the same exact way that the leak test pouches were made, using the same dimensions, amount of Nanofoils and technique. The big difference with the LCP battery were the contents inside the. A sheet of AL1145 aluminum was used as the anode which was 0.1016mm, a small cut out piece of a coffee filter was used as the paper separator and 6 layers of carbon paper were used as the carbon cathode. 0.1016mm thick Cu10100 copper was used as the material for the leads. Salt water was used as the electrolyte and table salt was used as the salt and tap water as the water source. A picture of the main internal components is shown in figure 27 below

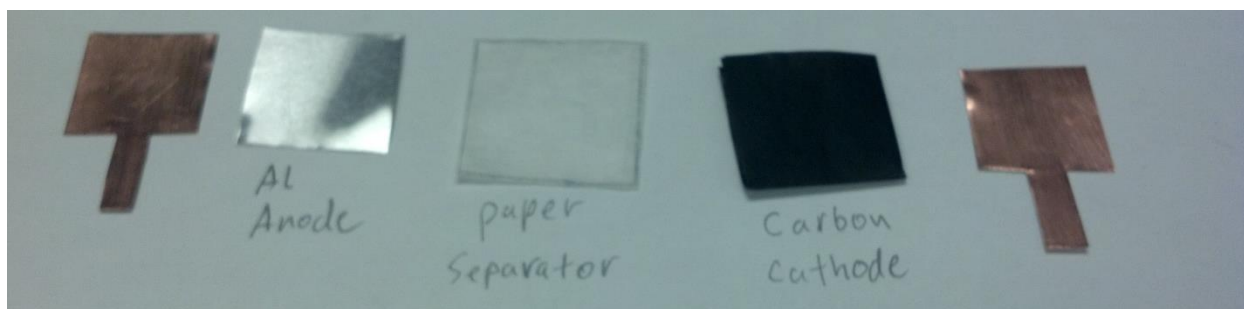


**Figure 27: A diagram of the internal components of the LCP battery**

Graphite from a mechanical pencil was put on the corners of the LCP that were to be joined together. The graphite was used to try and create a thin layer of material that was fairly thermally conductive that was in between the copper and LCP so that the copper wouldn't stick to the LCP as much. The graphite appeared to help but it was only tried to join the LCP during the making of the battery.

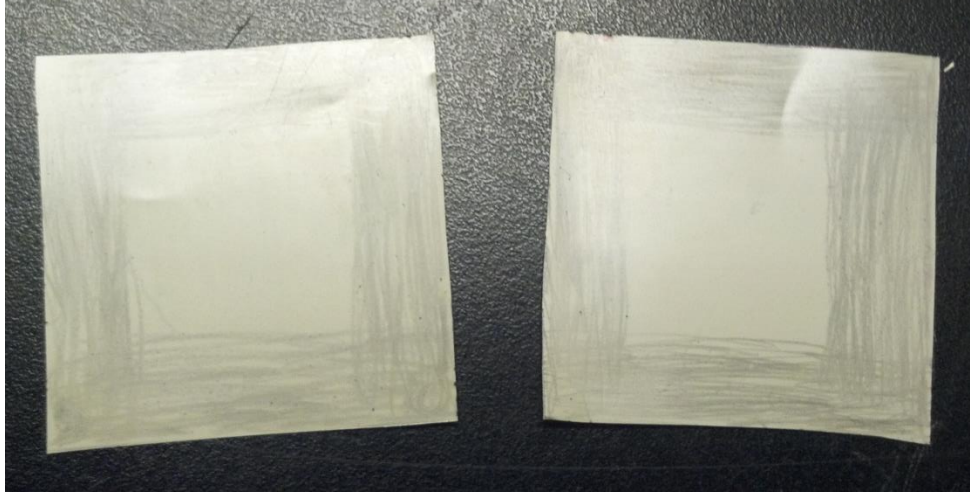


**Figure 28: LCP used to package the LCP with graphite drawn around the edges.**

The copper leads that stuck out of the battery were difficult to seal with Nanofoil since the copper was so thick and because the solution inside the battery was liquid. Liquid electrical tape was used to seal around the leads and one side of the LCP since there was not enough nanofoil to join the last side. Figure 29 below shows the completed LCP battery lighting up a small red LED light with the help of a hearing aid battery.



**Figure 29: LCP battery successfully lighting up an LED light.**

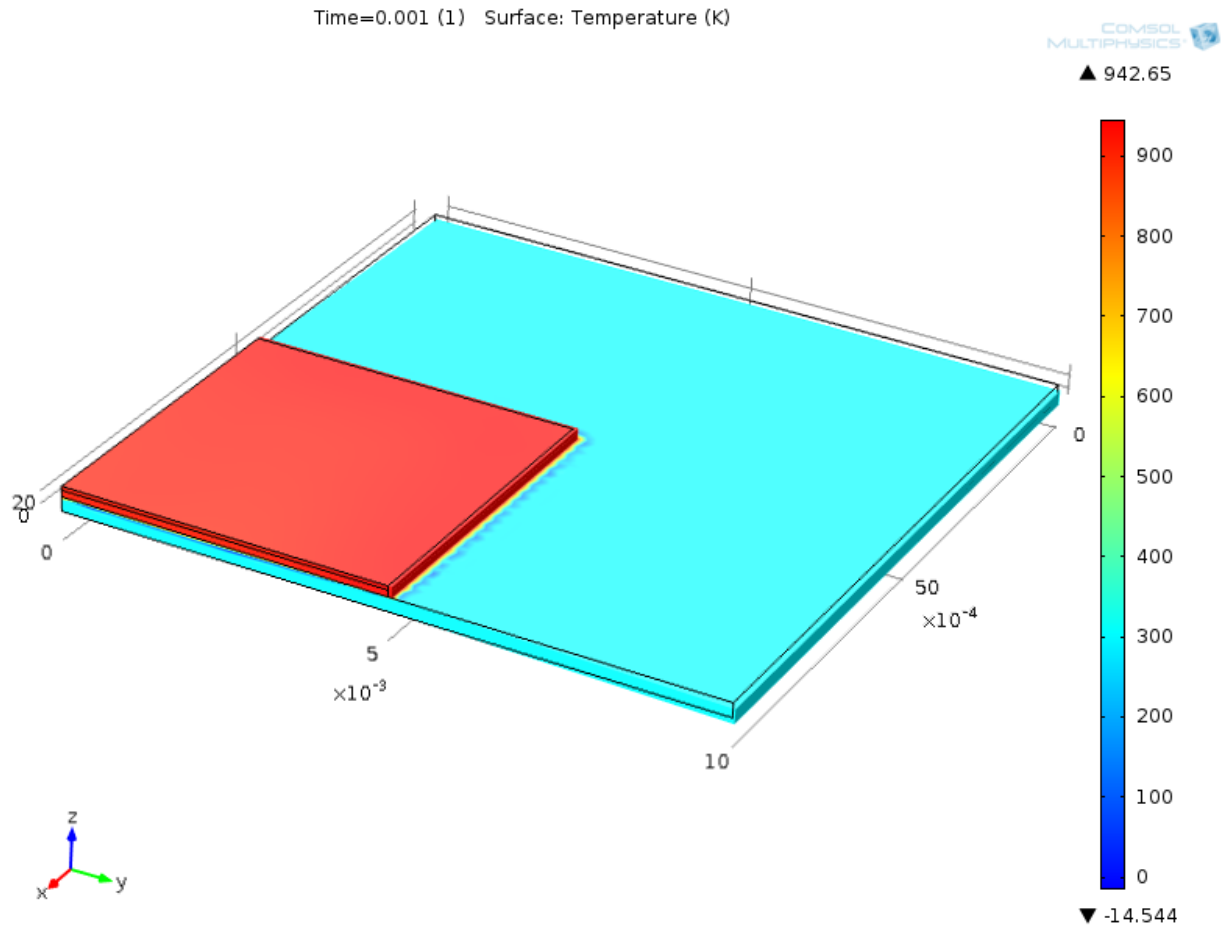
## 6 Results

### 6.1 Taco Results

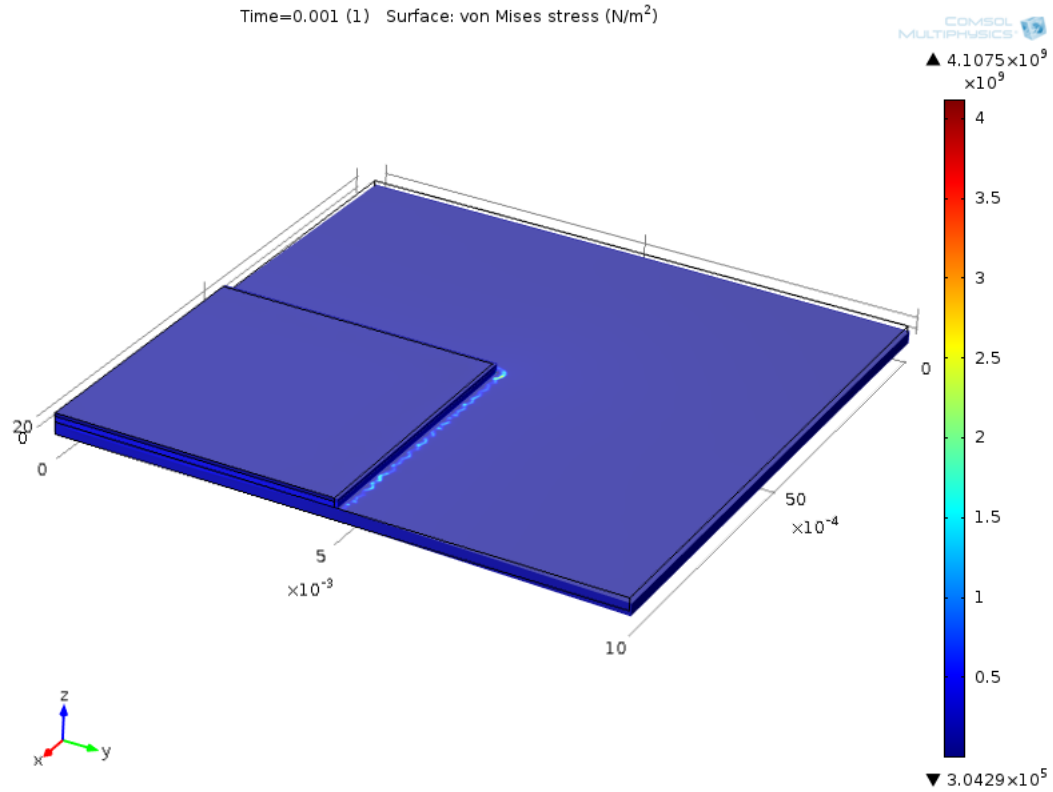
The results from the Taco method of joining shows that only a very small area of LCP to LCP joining is achieved due to the need to pinch the 2 pieces of LCP together at the area where the taco ends and the two pieces of LCP meet. From the pull tests it was found that a large portion of aluminum foil bonded to the LCP and helped in providing strength to the bond since the strength of the bond was lower when the majority of the taco was cut out. The average weight that the bond with the aluminum and Nanofoil not cut out was 29 ozf or 8.06 N which is nearly 2 pounds and when the aluminum and Nanofoil were mostly cut out, the average weight the bond could hold was 18 ozf or 5 N which is a little more than a pound. When the taco method was used to create the leak test another noticeable fault in this method was found. The nanofoil joined to the aluminum and continued to remain stiff and brittle after ignition. One of the three specimens that used the taco method to seal the specimen did not leak for 24 hours but when the specimen was flexed the seal was instantly broken. All of the 3 soldering iron sealed specimens leaked within the 24hr period. At the joining area very small sleeks were found.

## 6.2 Numerical Model results

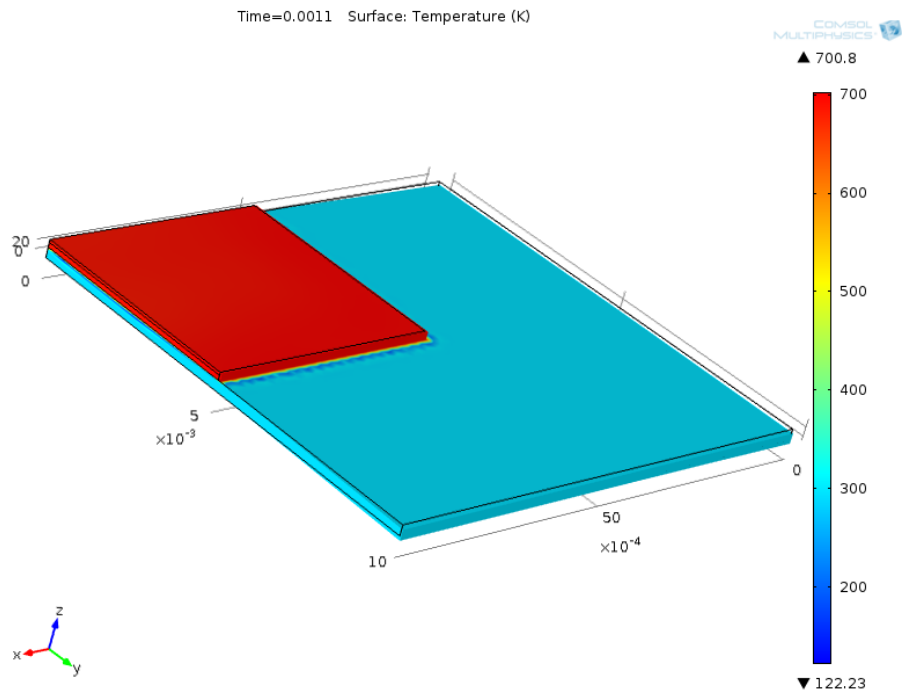
### 6.2.1 Sample of Temperature and Stress Distributions



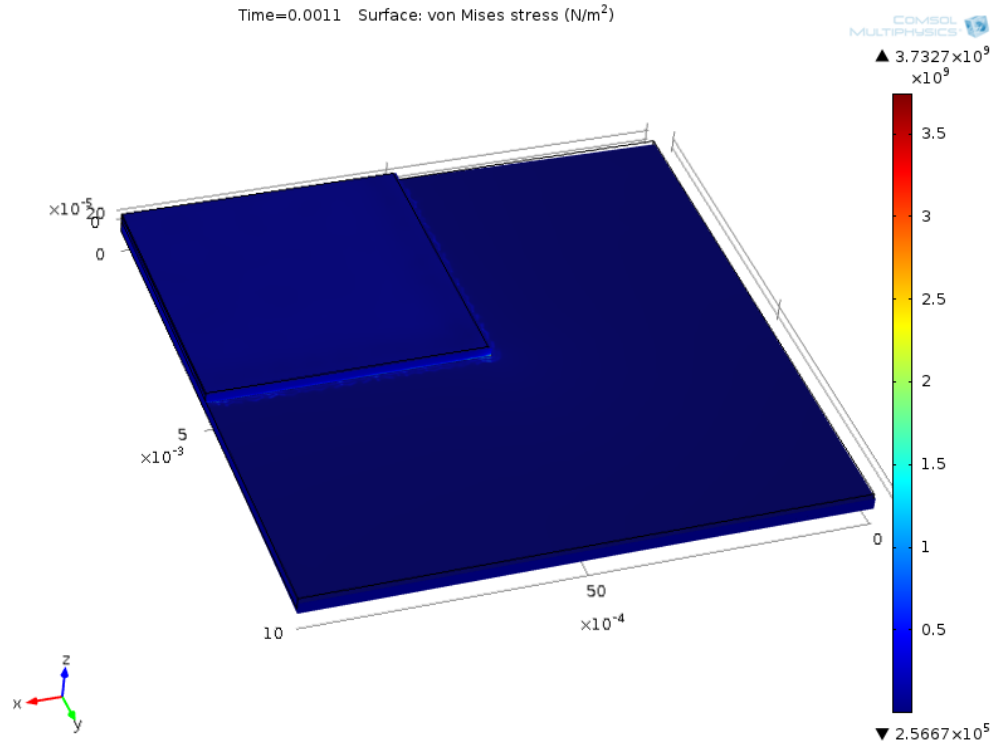
**Figure 30: Temperature plot of Cu heat spreader with 2 nanofolds and 2 LCPs**



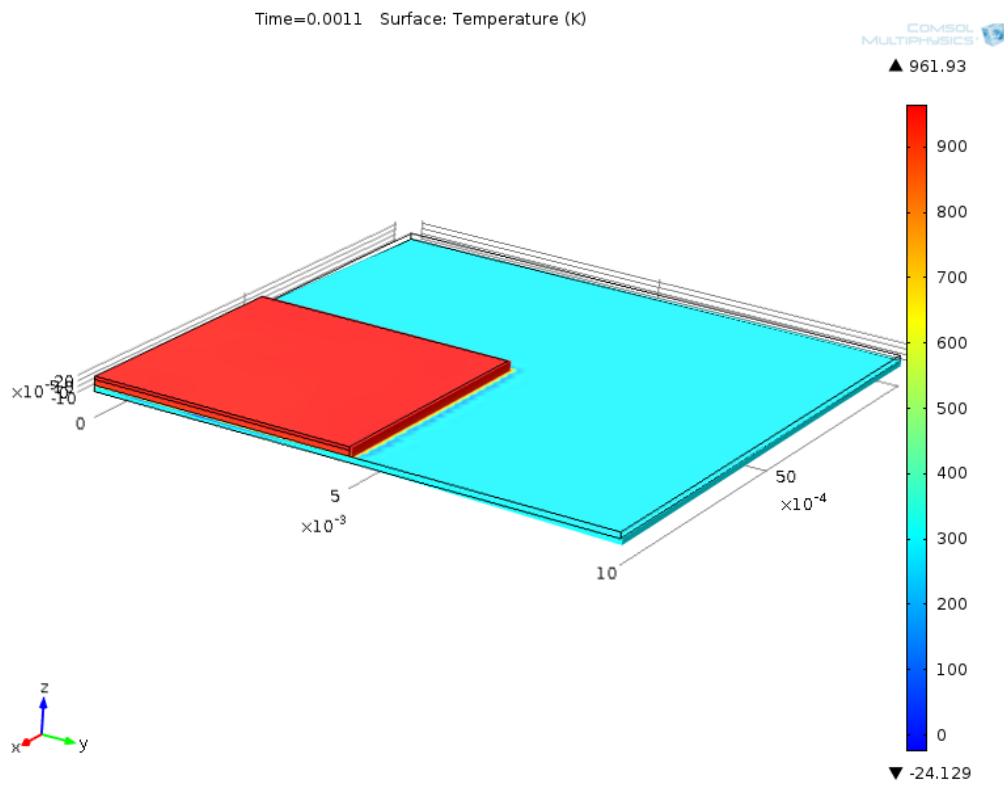
**Figure 31: Von Mises Stress plot of Cu heat spreader with 2 Nanofuels and 2 LCPs**



**Figure 32: Temperature plot of Al heat spreader with 2 Nanofuels and 2 LCPs**



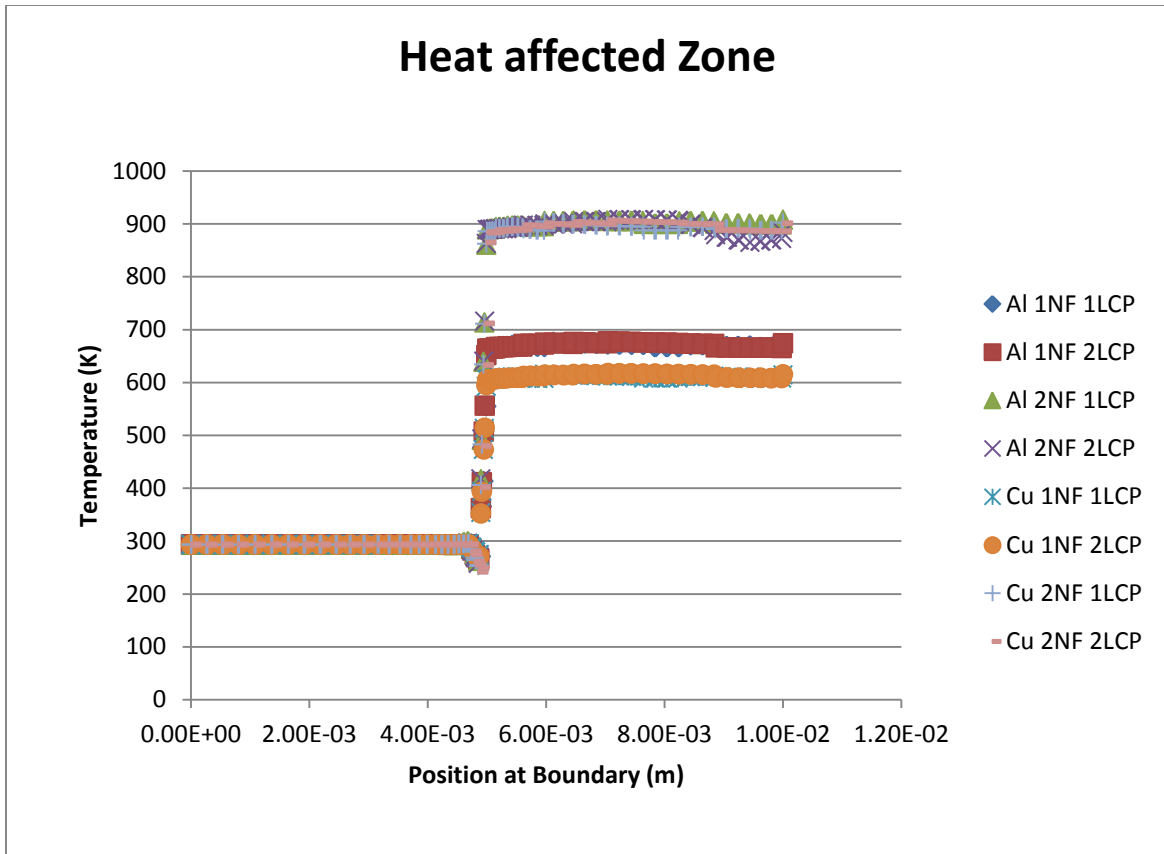
**Figure 33: Stress plot of Al heat spreader with 2 Nanofoils and 2 LCPs.**



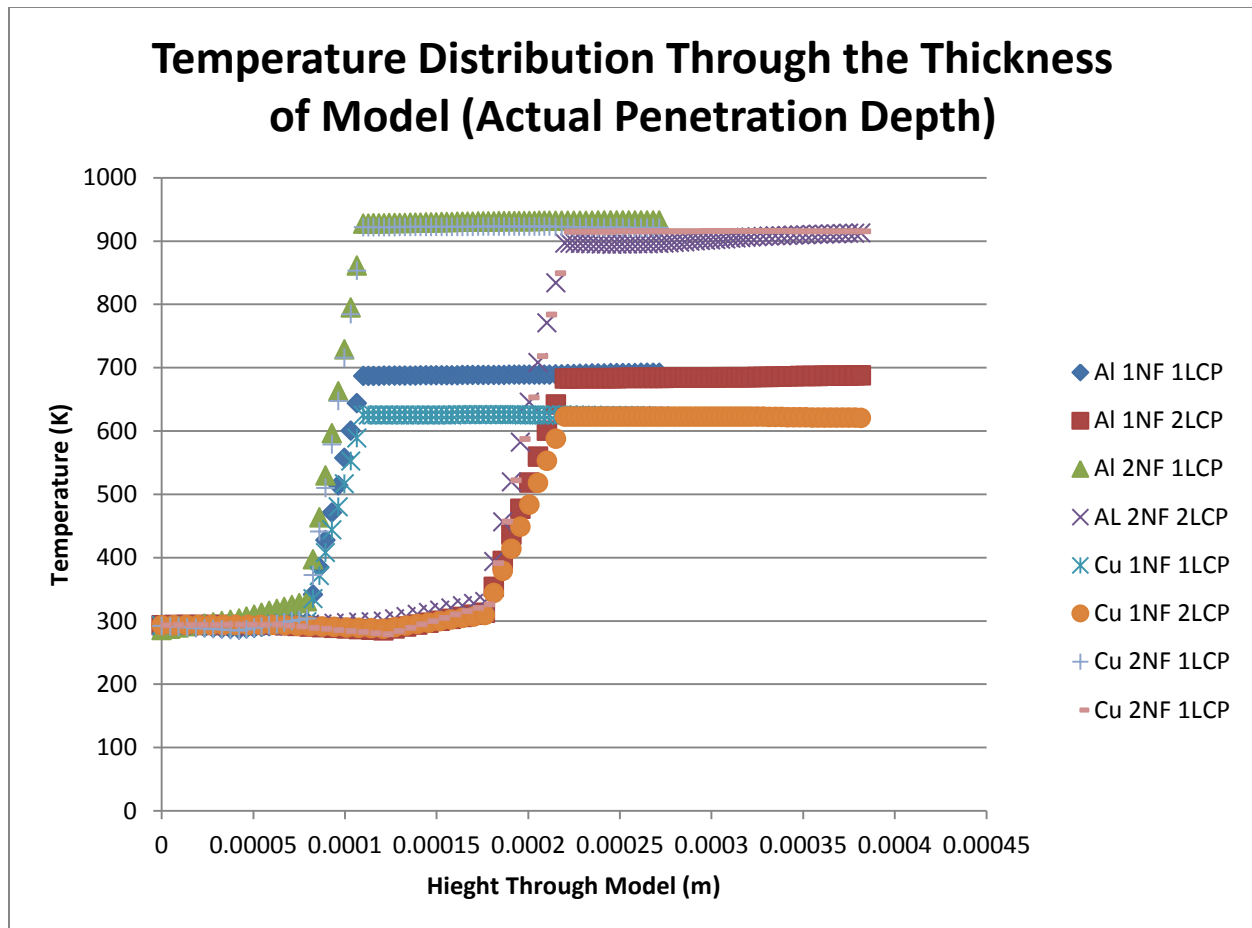
**Figure 34: Temperature plot of Al heat spreader with 2 Nanofoils and 1 LCPs.**

**Table 3: Dimensional results of numerical simulations in tabular form**

Material Heat & Thickness	oint (Pa)	Max Temp (K)	Heat Affected Zone	
			Melting away from heat spreader (m)	Total Melting Area (m <sup>2</sup> )
AL 1NF 1LCP	5.49E+07	690.47	7.85E-05	4.8566E+05
AL 2NF 1LCP	4.82E+07	928.6789	7.86E-05	9.6886E+05
AL 1NF 2 LCP	9.61E+07	692.5624	1.50E-05	6.7053E+05
AL 2NF 2LCP	6.70E+07	923.4113	1.51E-05	2.8627E+05
Cu 1NF 1LCP	2.86E+07	627.2221	6.06E-05	8.6722E+05
Cu 2NF 1LCP	8.62E+07	927.0289	6.18E-05	2.5291E+05
Cu 1NF 2 LCP	2.51E+07	628.0455	3.01E-05	1.5736E+06
Cu 2NF 2LCP	1.57E+08	927.3939	3.01E-05	1.0060E-04

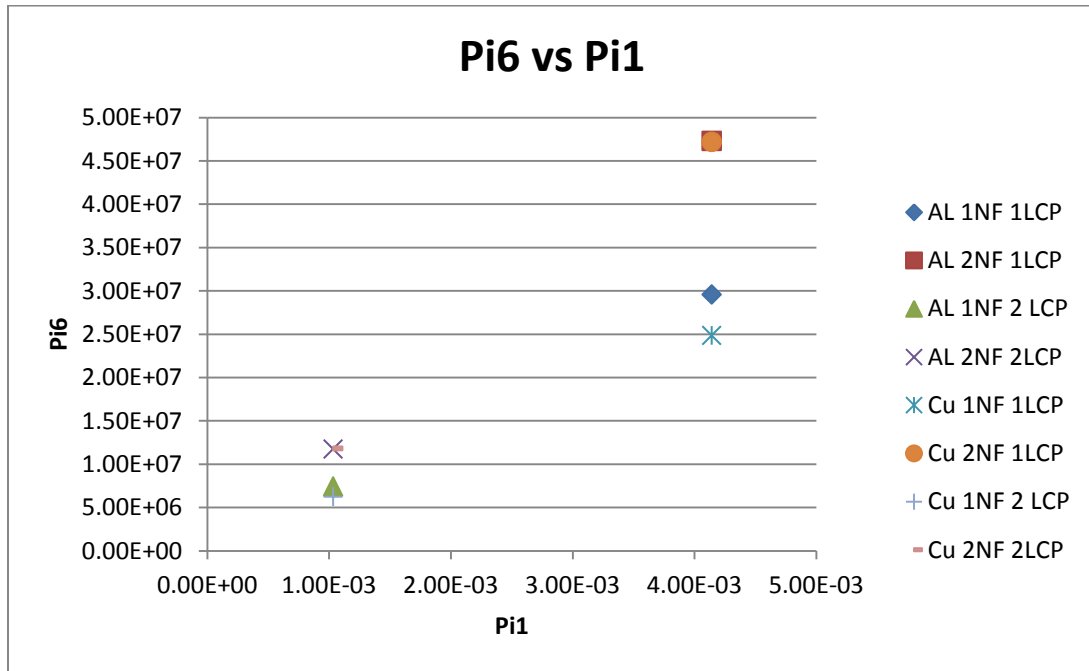


**Figure 35: Temperature distribution at interface between the heat spreader and the substrate.**



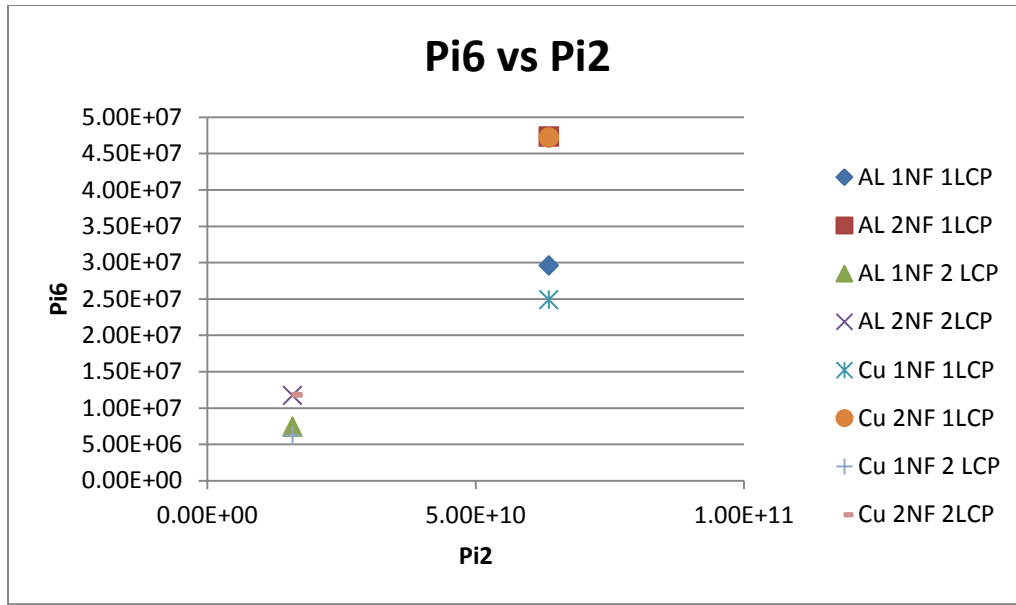
**Figure 36: Distribution through the thickness of the model (Actual Penetration Depth of numerical model)**

## 6.2.2 Pi Group Results



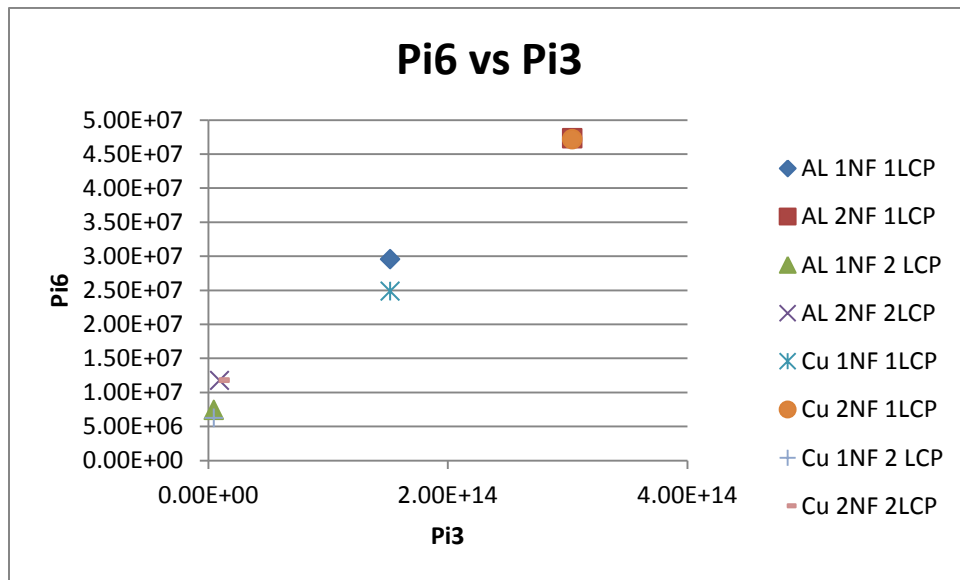
**Figure 37: Pi 6 verses Pi 1, Peak Temperature verses Thermal Penetration depth in the substrate.**

In Figure 37 above it can be seen that with increasing heat using Nanofoil, the Pi6 increases. All of the models with 1 LCP fall similarly on the bottom left of the graph while all of the specimens on the top right have 2 LCP. When only looking at the change in heat spreader material, most of the values stay the same. The two models with 1LCP and 1 Nanofoil do not follow each other as well and the aluminum model has a higher Pi6 than the copper.



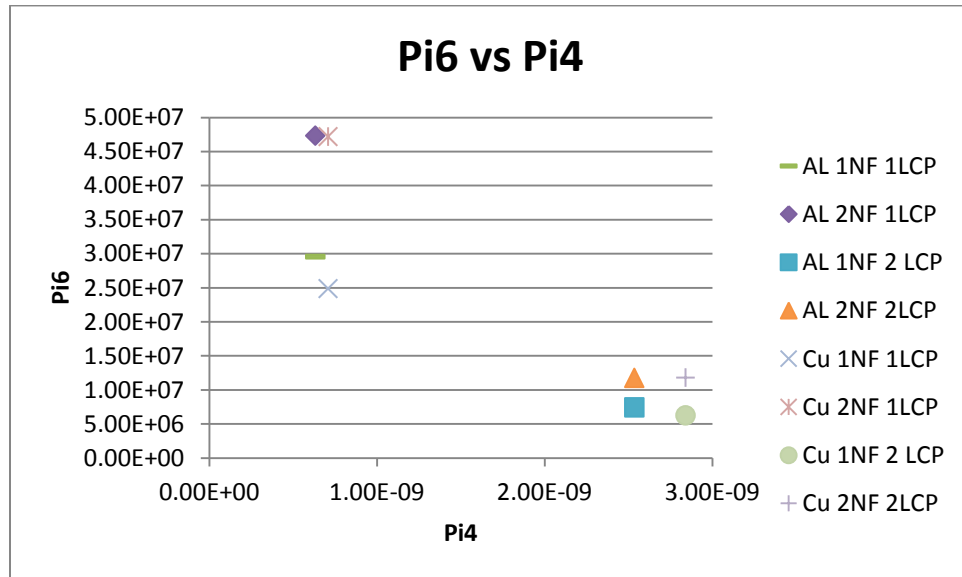
**Figure 38: Pi 6 verses Pi 2, peak temperature verses melting potential**

Figure 38: above is very similar to figure 37 in the relations of the different models. Pi6 increases again when more Nanofoil is added. Pi2 decreases when the LCP increases in thickness and the change in material doesn't change by very much.



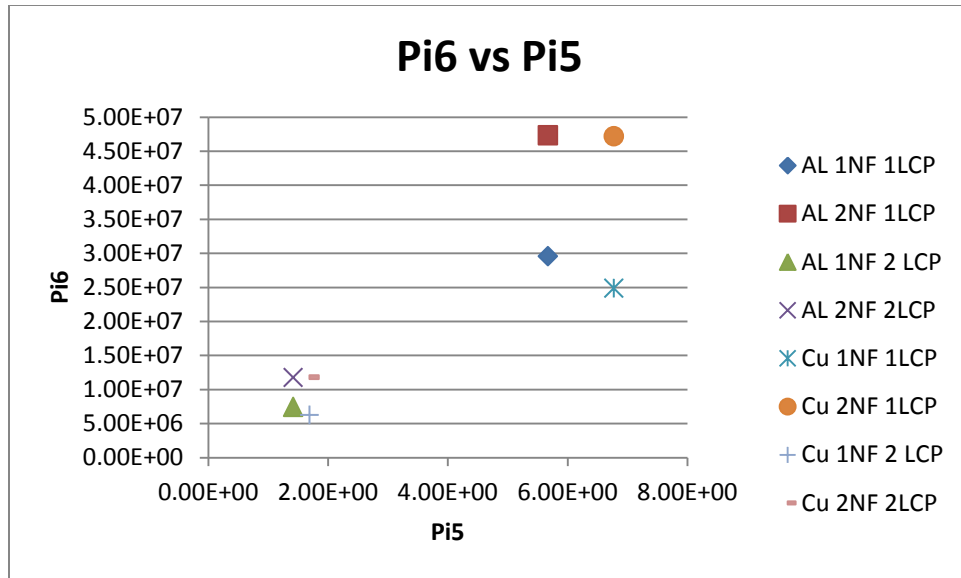
**Figure 39: Pi 6 verses Pi3, peak temperature verses energy density**

Figure 39, above shows that all of the models with a 2LCP thickness have a relatively low Pi3 and Pi6. Single nanofoil and LCP models have Pi6 and Pi3 numbers that are higher than double thick LCP models but not as high as 2 Nanofoil and single LCP models.



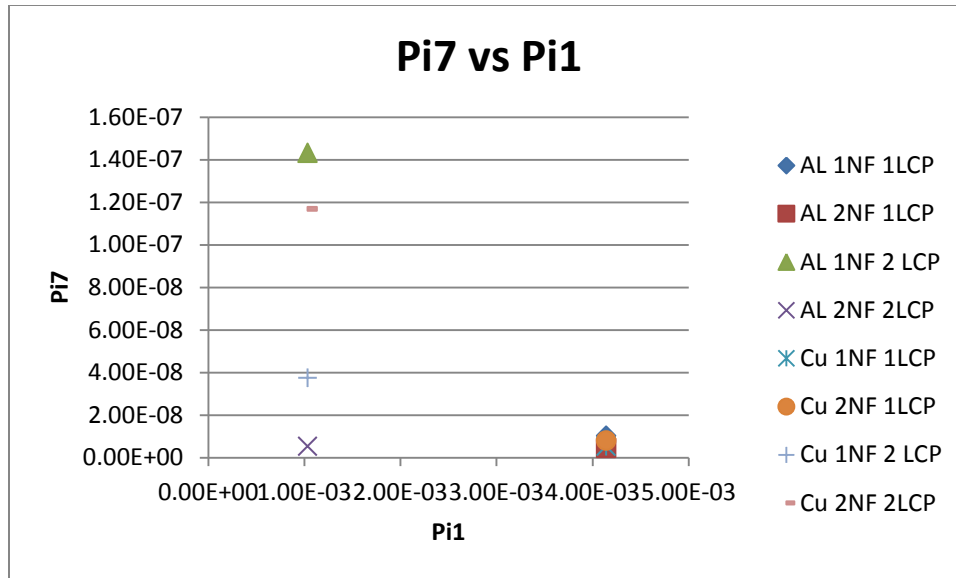
**Figure 40: Pi6 verses Pi4, peak temperature verses thermal strain**

Figure 40 shows that the models with a 2 LCP thickness have high Pi4 values but low Pi6 values. The copper and aluminum models with 1 Nanofoil and 1 LCP have lower Pi4 values and higher Pi6 values when compared to the models with 2 LCP thicknesses. The Models with the 2 Nanofoil and 1 LCP have the highest Pi 6 values and have similar Pi3 values when compared to the single Nanofoil and LCP thickness models.



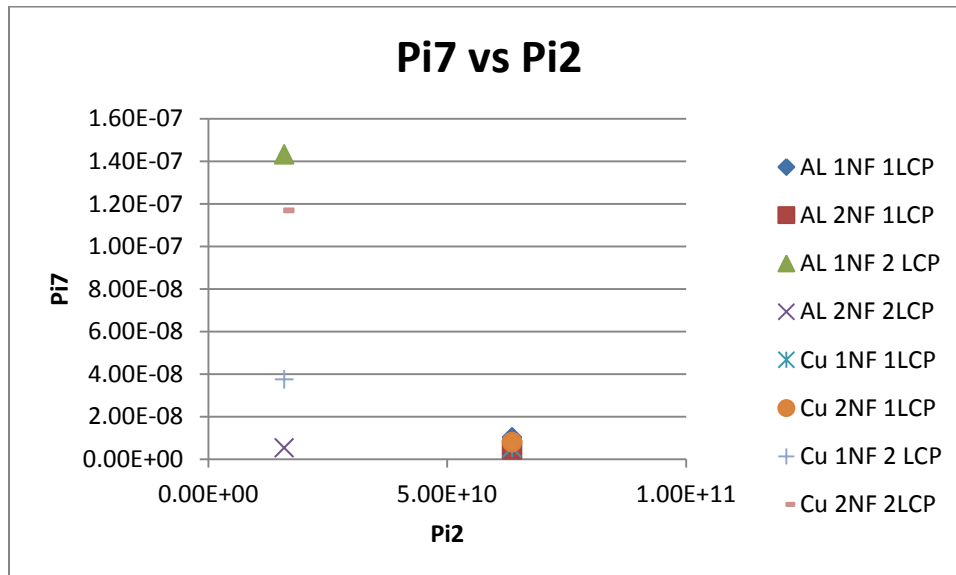
**Figure 41: Pi 6 verses Pi 5, peak temperature verses thermal penetration in chip**

Figure 41 shows a similarity between the thicknesses of LCP. The models that have a LCP thickness of 2 have lower Pi6 and Pi5 values while the single thick models have higher Pi6 and Pi5 values. This chart also shows that when switching from aluminum to copper the Pi5 value will increase. The Pi5 value will increase more for the 1 LCP thick. Pi6 also decreases slightly when the material is changed from aluminum to copper, this change is most pronounced in the models that use only 1 Nanofoil.



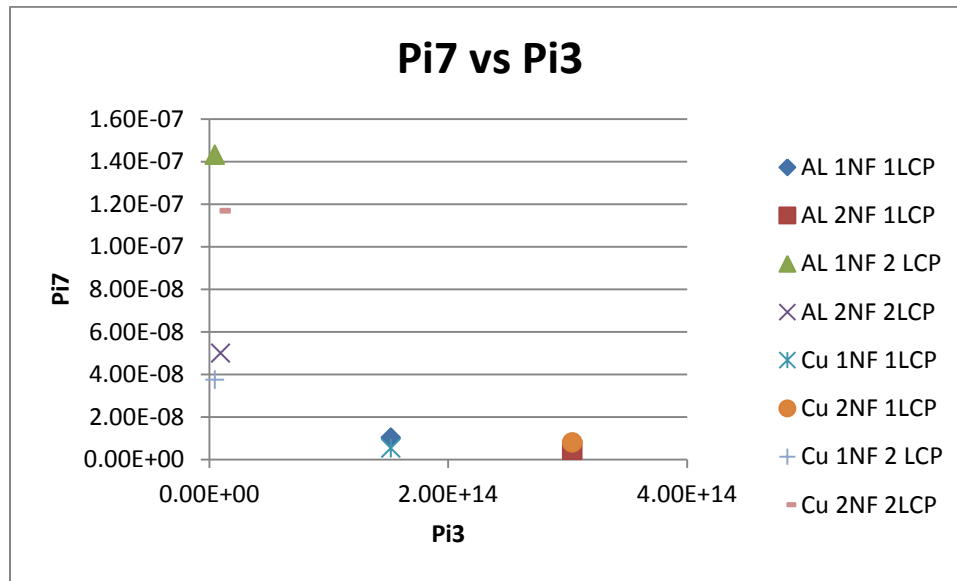
**Figure 42: Pi7 verses Pi1, interfacial stress verses thermal penetration depth in substrate.**

Figure 42 shows that Pi1 is relatively the same for all models that have an LCP thickness of 2. Figure 42 also shows that adding heat in the form of more nanofoils will decrease Pi7. While the single thickness LCP model's values are much closer together they follow the same trend as the double thick LCP.



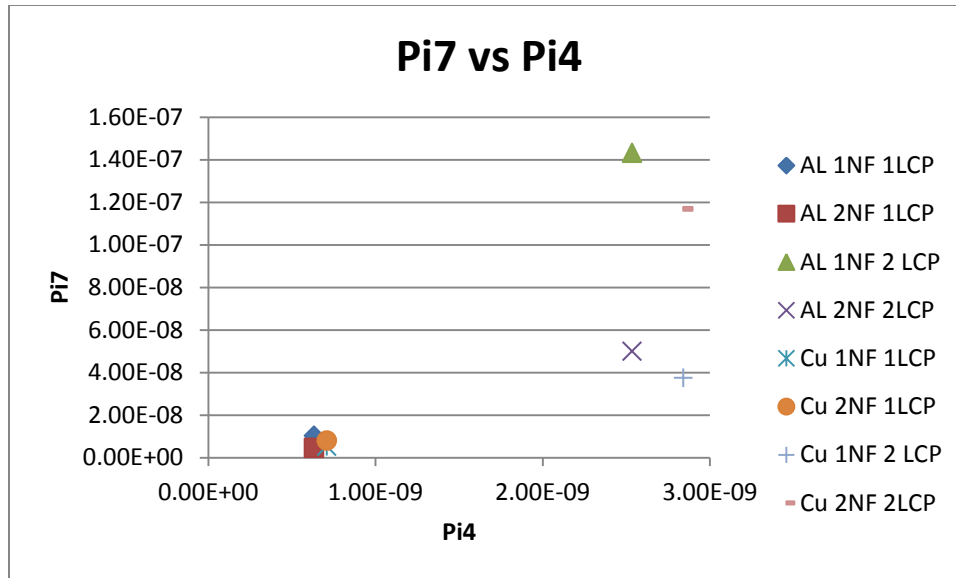
**Figure 43: Pi7 verses Pi2, interfacial stress verses melting potential.**

Figure 43 is very similar to figure 42. All of the double thick LCP models have very similar Pi2 values which are lower than the single thickness LCP models. The Pi7 value also decreases in value when heat is added for the double LCP models. The single LCP models stay relatively the same value and have low Pi7 values.



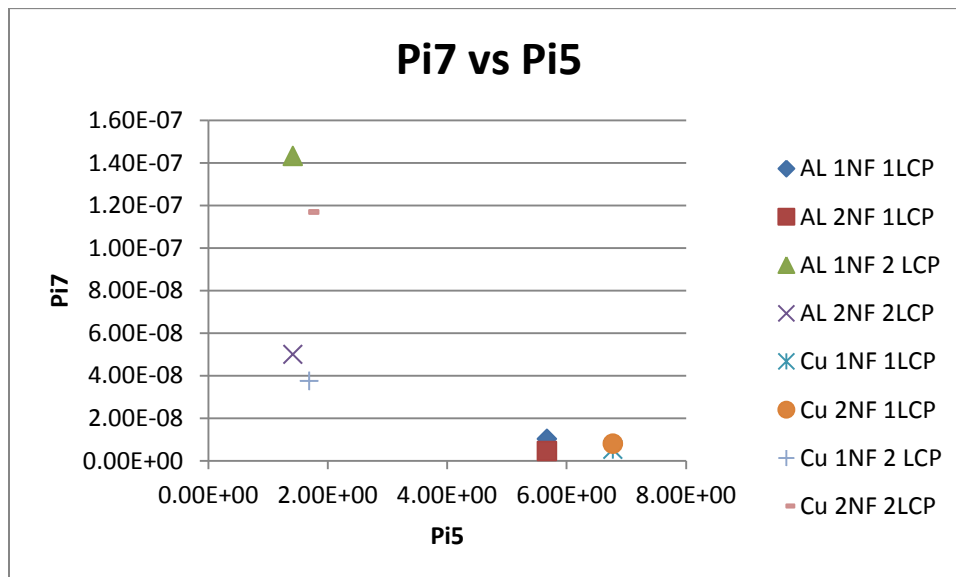
**Figure 44: Pi7 verses Pi 3, Interfacial stress verses energy density.**

In Figure 44 above the Pi3 value is relatively the same for all models with an LCP thickness of 2. The Pi7 values also increase the most when copper, 1 Nanofoil and 2 LCP is changed to aluminum, 1 Nanofoil 2 LCP. The Pi value of copper, 2 Nanofoil 2 LCP is much higher than aluminum, 2 Nanofoil 2 LCP. In the single thickness LCP models when copper is changed to aluminum Pi 7 changes slightly.



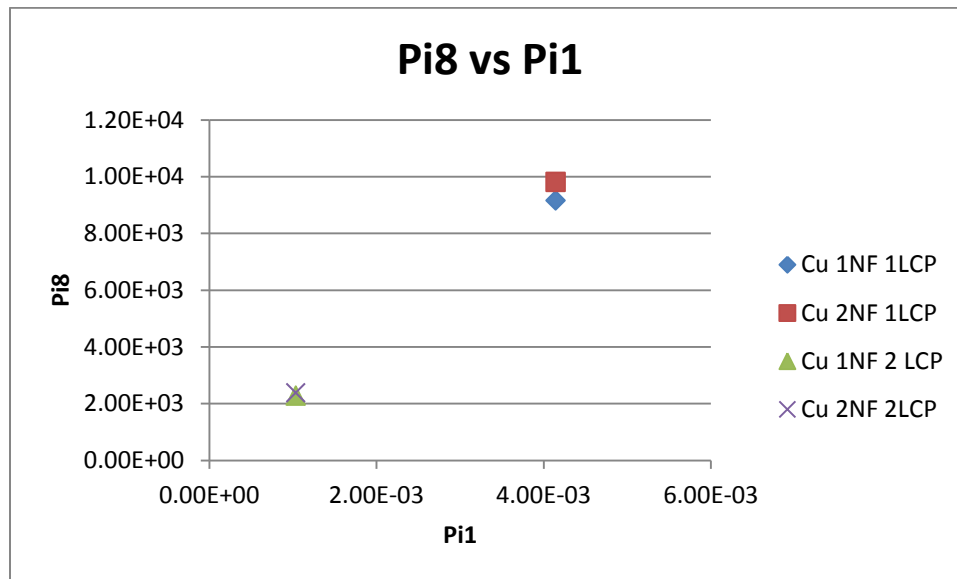
**Figure 45: Pi7 verses Pi4 interfacial stress verses thermal strain.**

In Figure 45 above, a small tight cluster of the 4 single thickness LCP models can be seen which are shown to have low Pi7 and Pi4 values. Pi7 is very high for the Aluminum, 1 Nanofoil 2 LCP model but when the heat is increased the Pi7 value goes down while the Pi4 value does not change. Copper, 1 Nanofoil 2LCP starts out low but when heat is added the Pi 7 value increases dramatically.



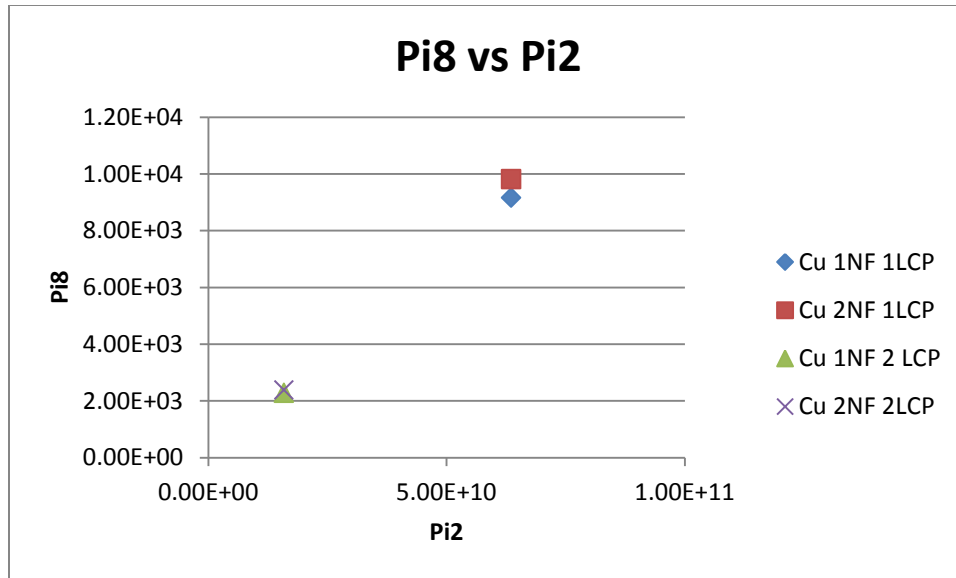
**Figure 46: Pi7 verses Pi5, interfacial stress verses thermal penetration in chip**

Figure 46 above shows that all of the models with an LCP thickness of 2 have low Pi5 values. For copper, 1 Nanofoil 2 LCP the Pi7 value is rather low when compared to copper, 2 Nanofoils 2LCPs. The opposite is the case for aluminum. Aluminum 1 Nanofoil 2 LCPs has a much higher Pi7 value than Aluminum, 2 Nanofoils 2 LCPs. This same relationship can be found but at a much smaller level with the single thickness LCP models. When comparing materials, going from aluminum to copper shifts the models higher in value in the Pi5 direction. This shift is more pronounced in the single LCP models than the double LCP models.



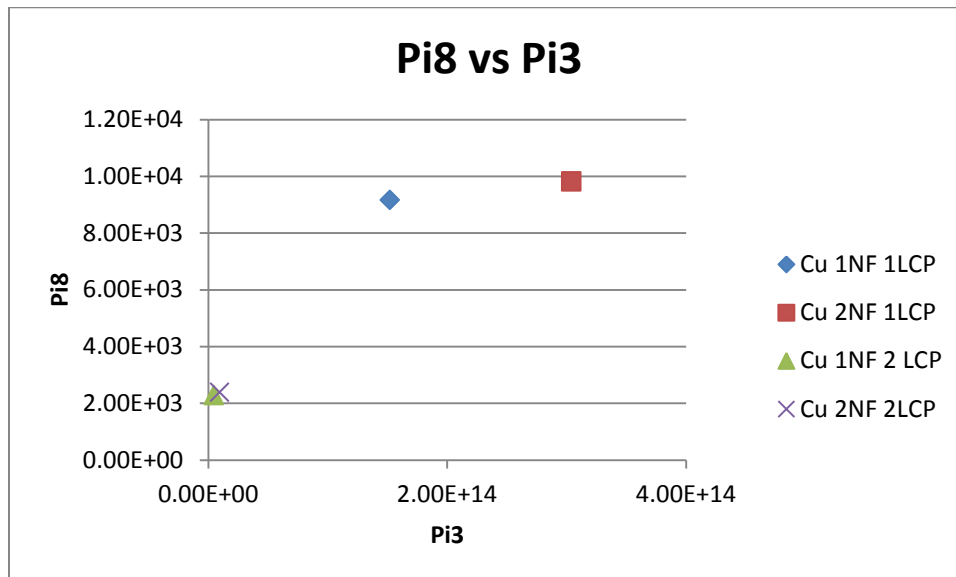
**Figure 47: Pi8 verses Pi1, heat affected zone verses thermal penetration depth in substrate**

Figure 47 above shows that with a decrease in the thickness of the LCP the Pi8 and Pi1 values increase. Figure 47 also shows that increasing the heat generation can raise the Pi8 value slightly when compared to the lower heat generation value.



**Figure 48: Pi8 verses Pi2, Heat affected zone verses melting potential.**

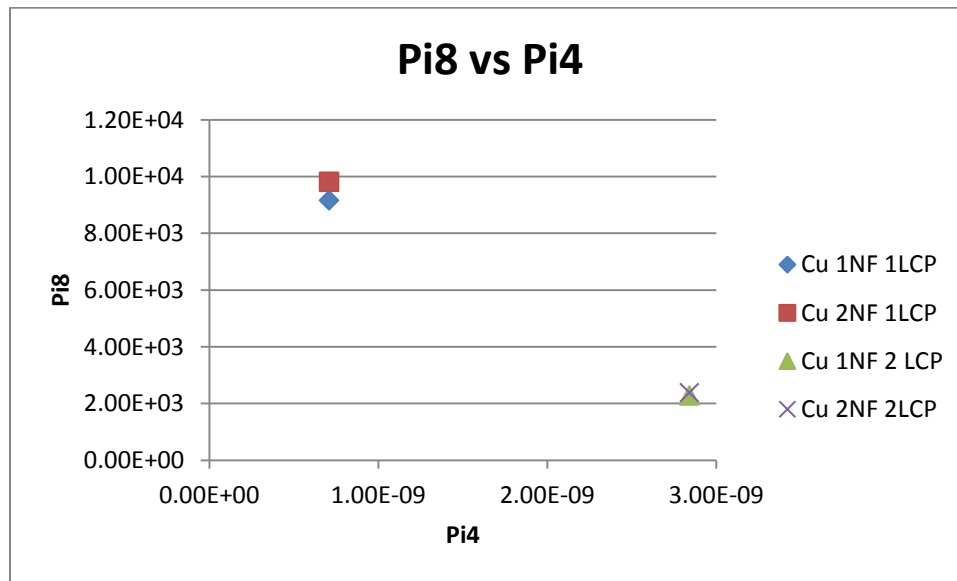
Figure 48 above shows nearly identical relationships as Figure 42 as discussed above.



**Figure 49: Pi8 verses Pi3, heat affected zone verses energy density**

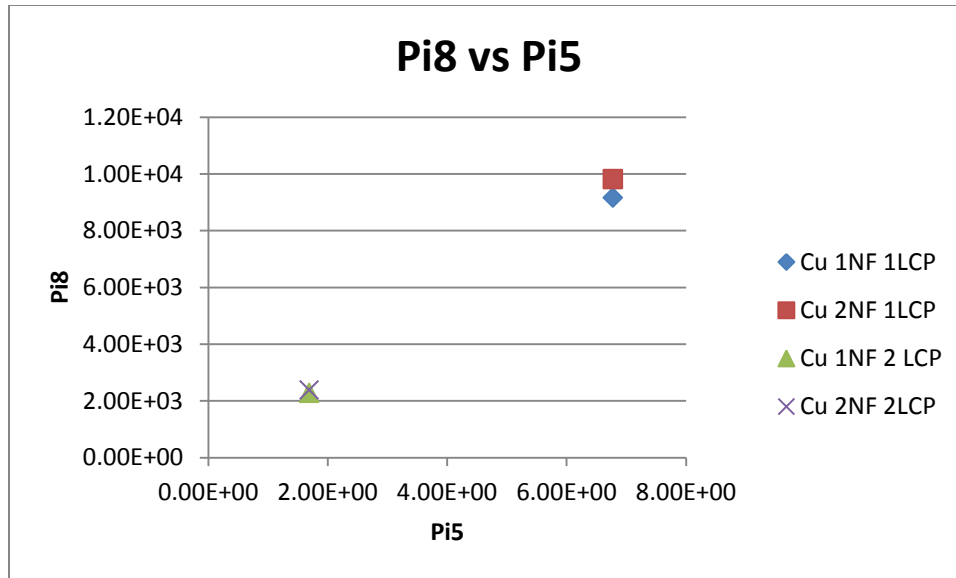
Figure 49 above shows that copper, 1 Nanofoil 2LCP and copper, 2 Nanofoil 2 LCP don't change very much and that the increase in temperature only increases the Pi8 and Pi3 values slightly when comparing the changes to the other larger changes with the 2 single LCP

thickness models. When heat is added to copper with 1 LCP, the Pi3 value increases in value much more than the Pi8 value increases in value.



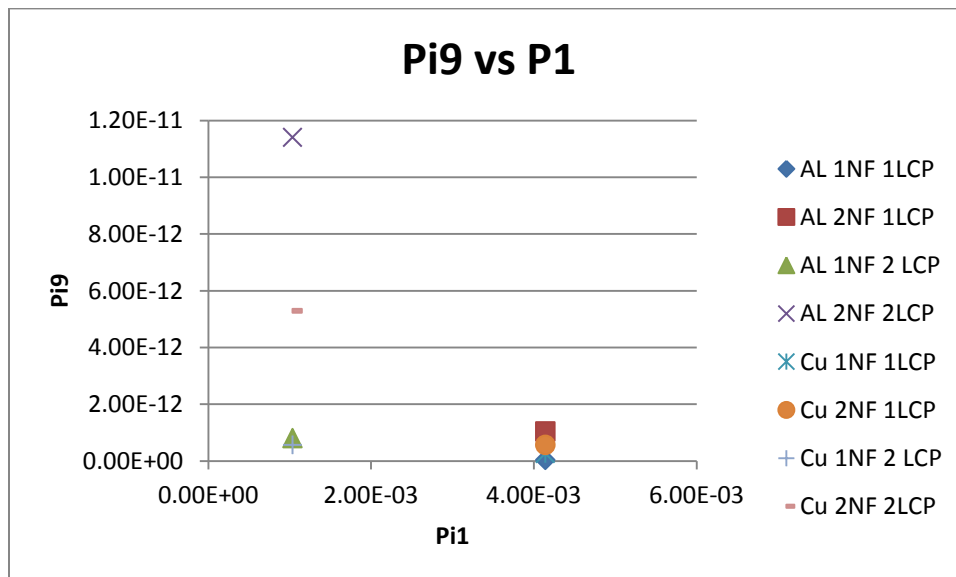
**Figure 50: Pi8 verses Pi4, heat affected zone verses thermal strain.**

Figure 50 above is very similar to Figure 47. Figure 50 shows that with a decrease in the thickness of the LCP the Pi8 values increase and Pi 4 values decrease. Figure 50 also shows that increasing the heat generation can raise the Pi8 value slightly when compared to the lower heat generation value.



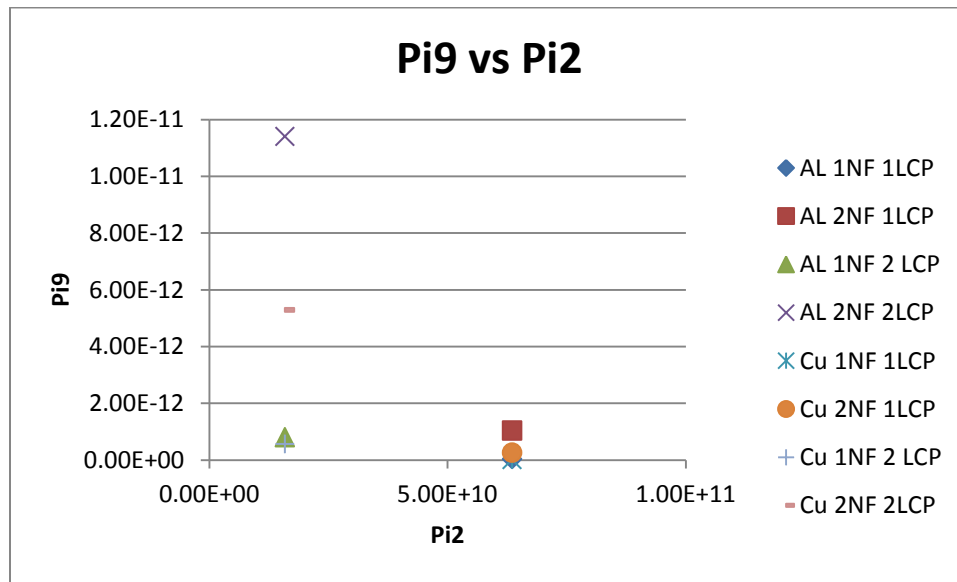
**Figure 51: Pi8 verses Pi5, heat affected zone verses thermal penetration in chip**

Figure 51 above is very similar to Figure 50. Figure 51 shows that with a decrease in the thickness of the LCP the Pi8 and Pi5 values increase. Figure 51 also shows that increasing the heat generation can raise the Pi8 value slightly when compared to the lower heat generation value.



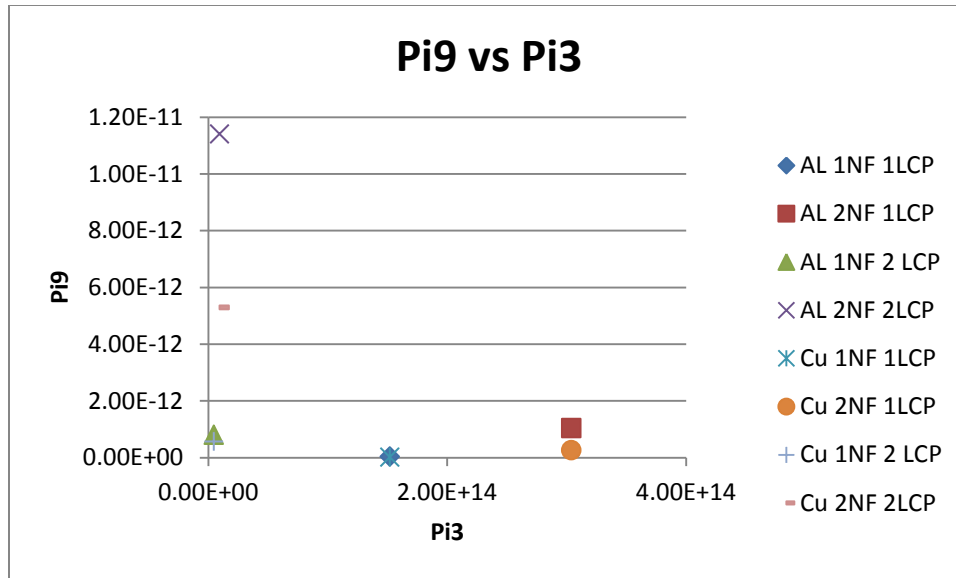
**Figure 52: Pi9 verses Pi1, adhesion strength verses penetration depth in substrate**

Figure 52 above shows two distinct lines that the data falls into and the line with spread out data on the left of figure 52 with low  $Pi_1$  values are all the models with 2LCP thicknesses. The line of data on the lower left side consists of all the models with 1LCP thickness. The two highest values of  $Pi_9$  both have 2 Nanofoils and 2 LCP. In general increases in nanofoil increase the  $Pi_9$  values of the models.



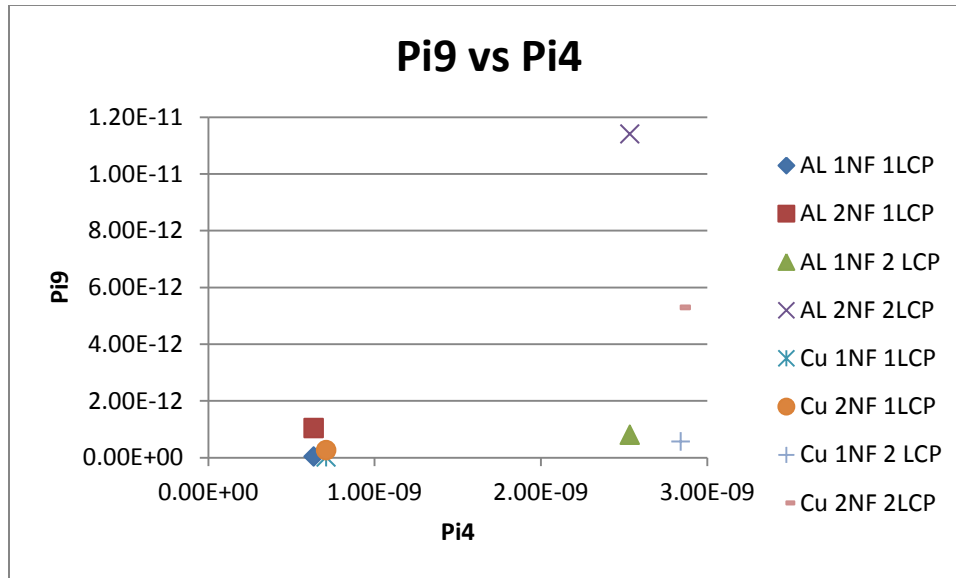
**Figure 53:  $Pi_9$  verses  $Pi_2$ , adhesion strength verses melting potential.**

Figure 53 above shows two distinct lines that the data falls into and the line with spread out data on the left of figure 53 with low  $Pi_2$  values are all the models with 2LCP thicknesses. The line of data on the lower left side consists of all the models with 1LCP thickness. The two highest values of  $Pi_9$  both have 2 Nanofoils and 2 LCP. With all of the models when nanofoil was added  $Pi_9$  increased.



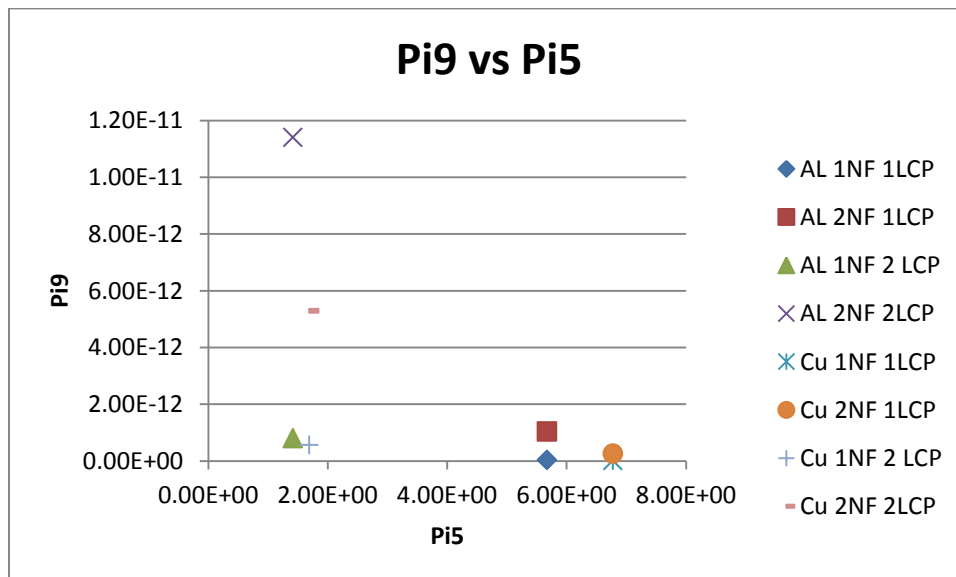
**Figure 54: Pi9 verses Pi3, adhesion strength verses energy density.**

In figure 54, 4 of the models have relatively similar Pi3 values. These are all of the models with 2LCP thicknesses. The aluminum and copper models with 1 Nanofoil and 2 LCPs have very similar Pi9 values. Copper and aluminum with 1 Nanofoil and 1 LCP have very similar Pi9 and Pi3 values. Both 2 Nanofoil and 1 LCP models have similar Pi3 values but the copper model has a slightly larger Pi9 value and in general when nanofoil is added to a model Pi9 increases.



**Figure 55: Pi9 verses Pi4, adhesion strength verses thermal strain.**

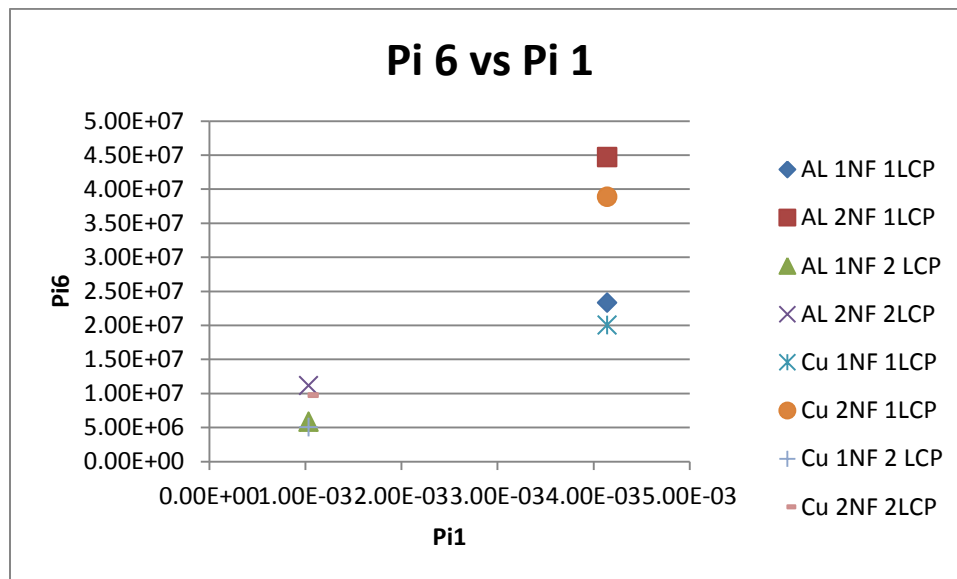
Figure 55 shows a cluster of 4 models in the lower left corner of the graph. All of these models are the models with 1 LCP. When the thickness of the LCP is increase to 2 LCPs the Pi4 values increase. Changes in Pi9 can be attributed to increases in nanofoil and when aluminum is used the increases are more dramatic.



**Figure 56: Pi9 verses Pi5, adhesion strength verses thermal penetration in chip**

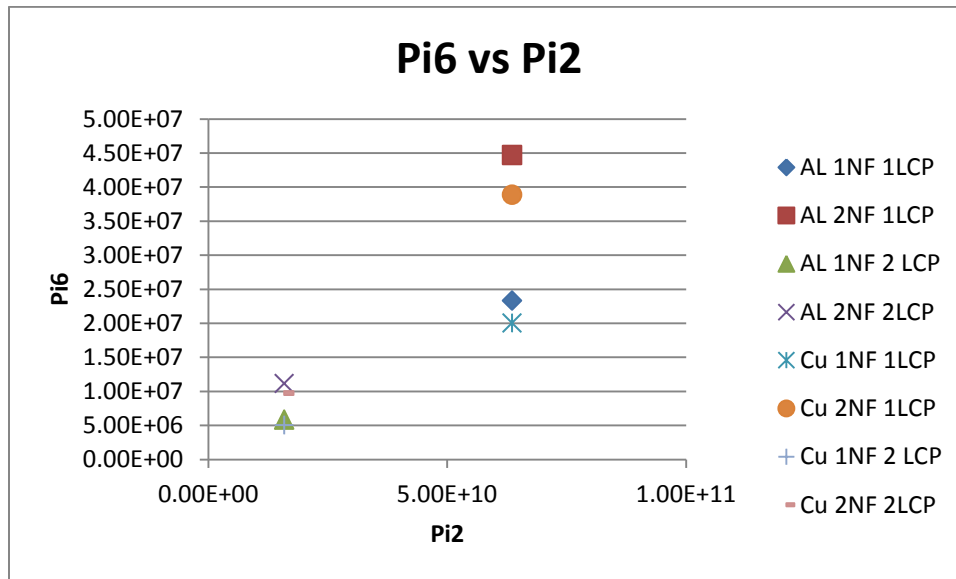
Figure 56 above shows that all of the models with an LCP thickness of 2 have low Pi5 values. For copper and aluminum, 1 Nanofoil 2 LCP the Pi9 value is rather low when compared to, 2 Nanofoils 2LCPs. This same relationship can be found but at a much smaller level with the single thickness LCP models. When comparing materials, going from aluminum to copper shifts the models higher in value in the Pi5 direction. This shift is more pronounced in the single LCP models than the double LCP models.

### 6.2.3 Micro-Model Results



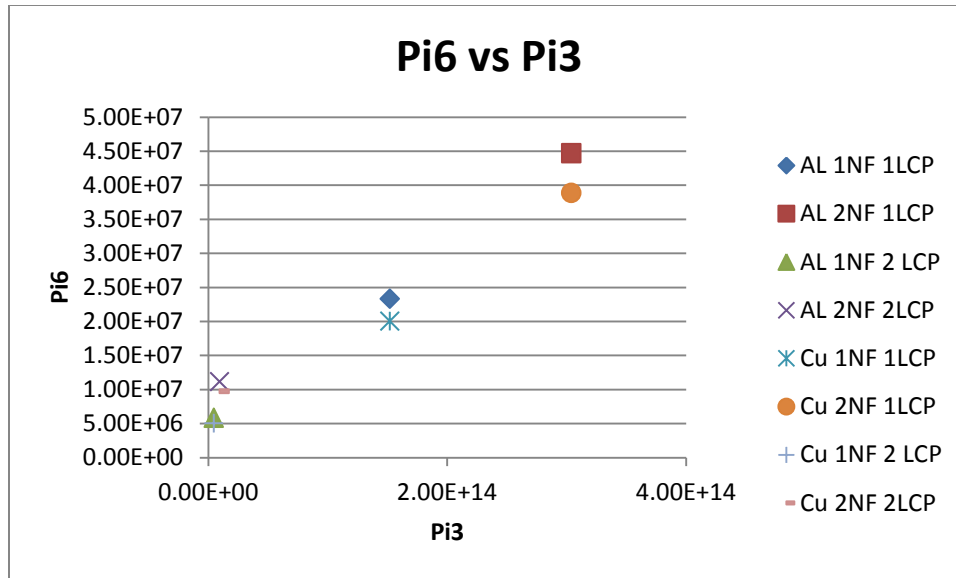
**Figure 57: Pi6 verses Pi1, peak temperature verses thermal penetration depth in substrate.**

In Figure 57 above it can be seen that with increasing heat using Nanofoil, the Pi6 value increases. All of the models with 1 LCP fall similarly on the bottom left of the graph while all of the models on the top right have 2 LCP. When only looking at the change in heat spreader material, most of the values increase slightly in Pi6 when going from copper to aluminum this relationship is most pronounced with the two, 2 Nanofoil 1 LCP models.



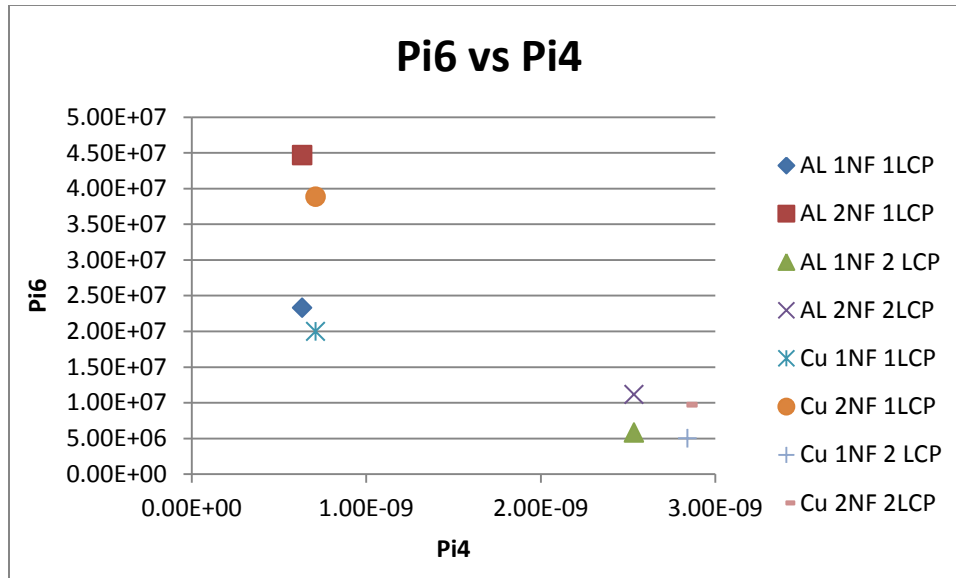
**Figure 58: Pi6 verses Pi2, peak temperature verses melting potential**

Figure 58 above is very similar to figure 57 in the relations of the different models. Pi6 increases again when more Nanofoil is added. Pi2 decreases when the LCP increases in thickness and when changing a model from copper to aluminum the only change that occurs is an increase in the Pi6 direction which in general is small.



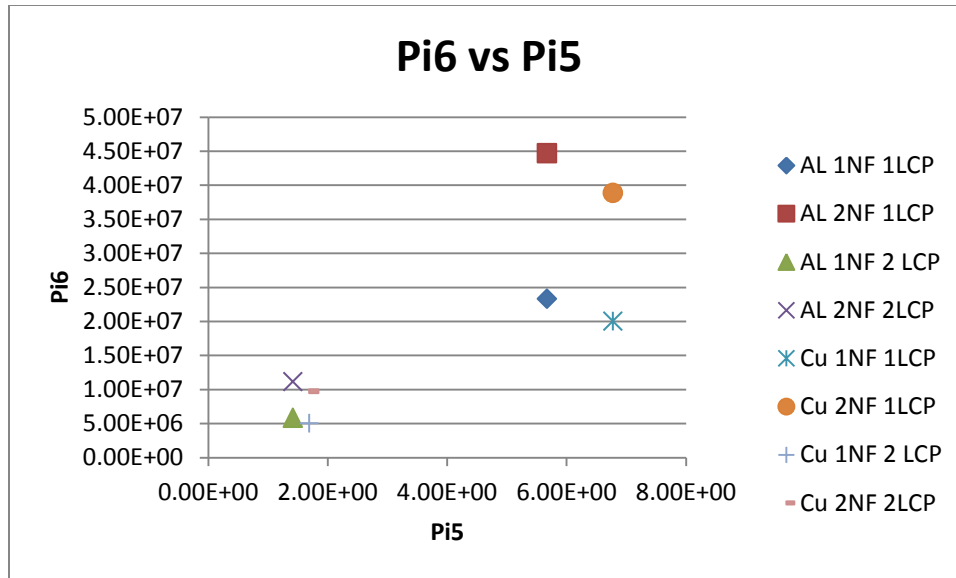
**Figure 59: Pi6 verses Pi3, peak temperature verses energy density**

Figure 59, above shows that all of the models with a 2LCP thickness have a relatively low Pi3 and Pi6. Single nanofoil and LCP models have Pi6 and Pi3 numbers that are higher than double thick LCP models but not as high as 2 Nanofoil and single LCP models which have the highest Pi6 and Pi3 values. When heat is added Pi6 and Pi3 increase. Pi6 increases more than Pi3 in the 2 LCP models and Pi6 and Pi3 increase relatively the same when heat is added for the single LCP models. When material changes from copper to aluminum Pi6 increases slightly.



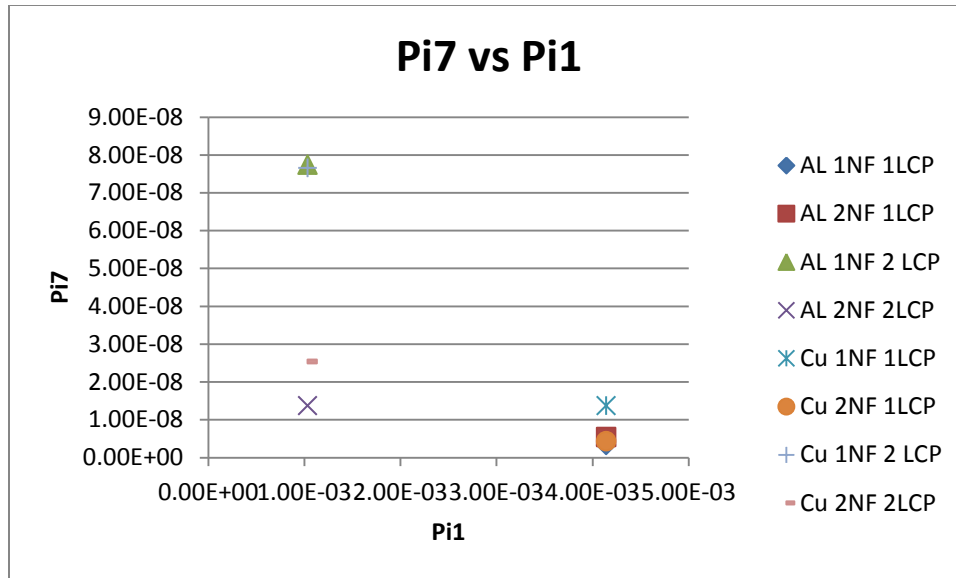
**Figure 60: Pi6 verses Pi4, peak temperature verses thermal strain**

Figure 60 shows that the models with a 2 LCP thickness have high Pi4 values but low Pi6 values. The copper and aluminum models with 1 Nanofoil and 1 LCP have lower Pi4 values and higher Pi6 values than the models with 2 LCP thicknesses. The Models with 2 Nanofoils and 1 LCP have the highest Pi 6 values and have similar Pi3 values when compared to the single Nanofoil and LCP thickness models. When material is changed from copper to aluminum Pi4 decreases slightly.



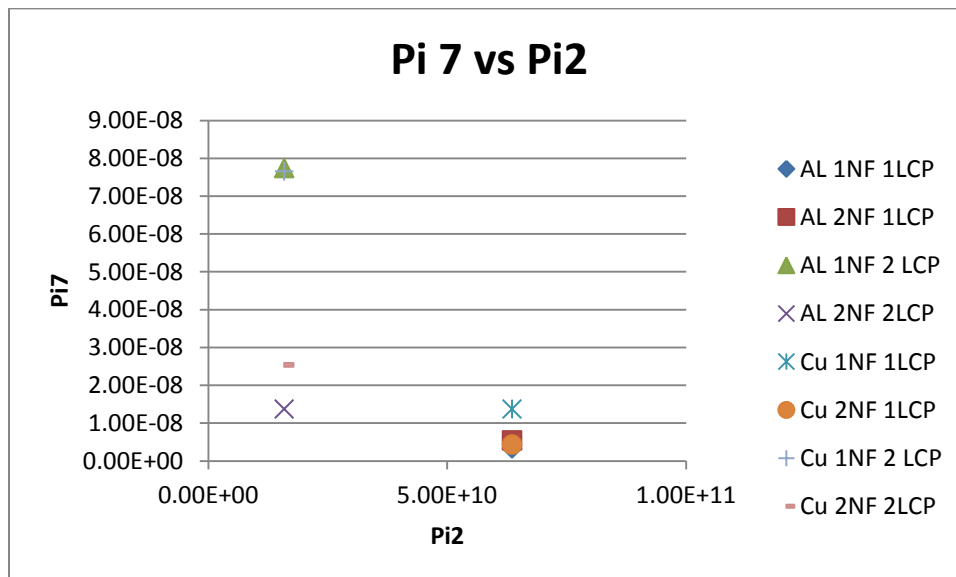
**Figure 61: Pi6 verses Pi5, peak temperature verses thermal penetration of the chip**

Figure 61 shows a similarity between the thicknesses of LCP. The models that have a LCP thickness of 2 have lower Pi6 and Pi5 values while the single thick models have higher Pi6 and Pi5 values. This chart also shows that when switching from aluminum to copper the Pi5 value will increase. The Pi5 value will increase more for the 1 LCP thick. Pi6 also decreases slightly when the material is changed from aluminum to copper, this change is most pronounced in the models that use only 1 Nanofoil.



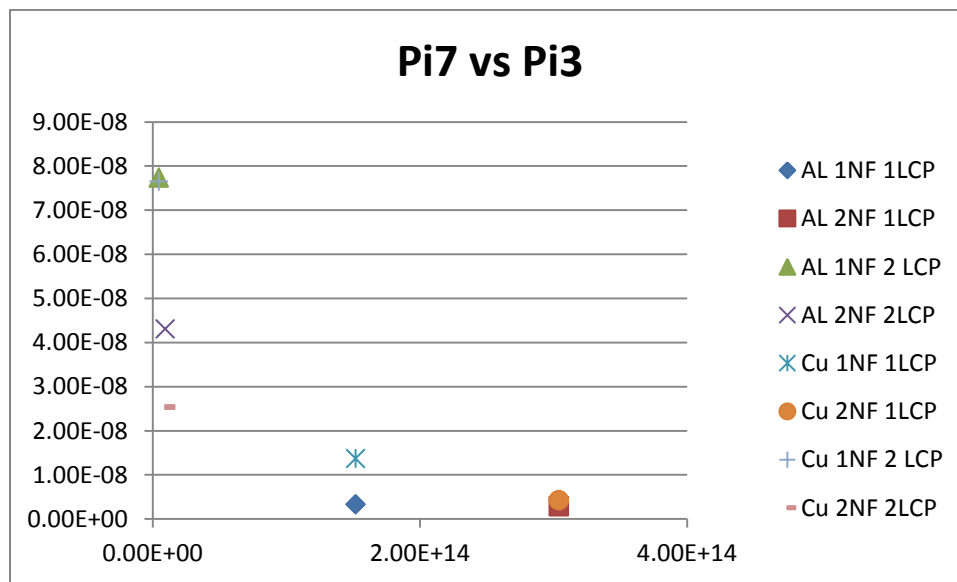
**Figure 62: Pi7 verses Pi1, interfacial stress verses thermal penetration in substrate**

Figure 62 shows that Pi1 is relatively the same for all models that have an LCP thickness of 2. Figure 62 also shows that adding heat in the form of more nanofoils will decrease Pi7. While the single thickness LCP model's values are much closer together they follow the same trend as the double thick LCP.



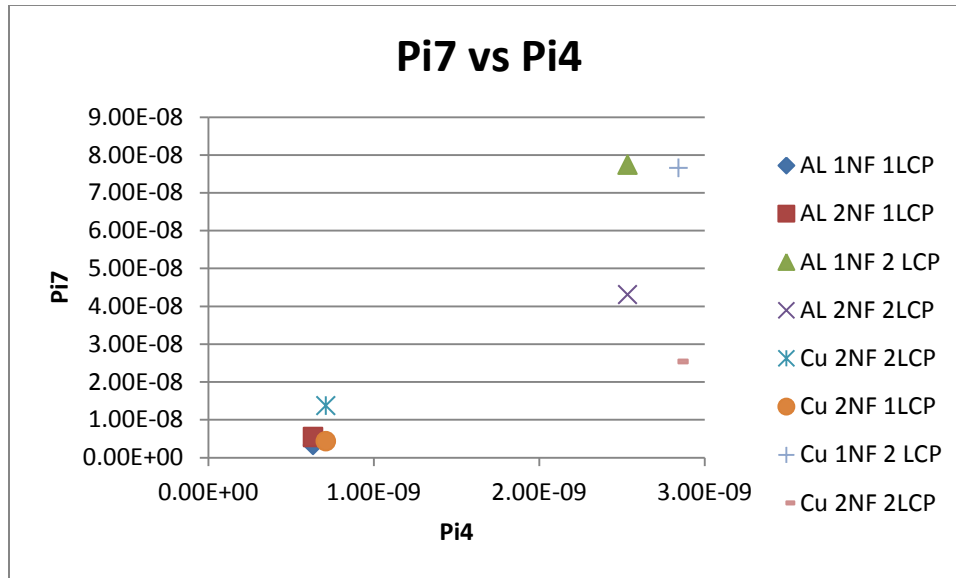
**Figure 63: Pi7 verses Pi2, interfacial stress verses melting potential.**

Figure 63 is very similar to figure 62, all of the double thick LCP models have very similar Pi2 values which are lower than the single thickness LCP models. The Pi7 value also decreases in value when heat is added for the double LCP models. The single LCP models stay relatively the same value and have low Pi7 values. For the 2 LCP models when the material is changed from aluminum to copper the Pi7 value increases.



**Figure 64: Pi7 verses Pi3, interfacial stress verses energy density**

In Figure 64 above the Pi3 value is relatively the same for all models with an LCP thickness of 2. The Pi7 values decreases when copper, 1 Nanofoil and 2 LCP is changed to aluminum, 1 Nanofoil 2 LCP. The Pi7 value of copper, 2 Nanofoil 2 LCP is lower than aluminum, 2 Nanofoil 2 LCP. In the single thickness LCP models when copper is changed to aluminum Pi 7 increases.



**Figure 65: Pi7 verses Pi5, interfacial stress verses thermal strain**

In Figure 65 above, a small tight cluster of the 4 single thickness LCP models can be seen which are shown to have low Pi7 and Pi4 values. Pi7 is very high for the aluminum and copper, 1 Nanofoil 2 LCP model but when the heat is increased the Pi7 value goes down while the Pi4 value does not change. Changing from aluminum to copper increases Pi4.

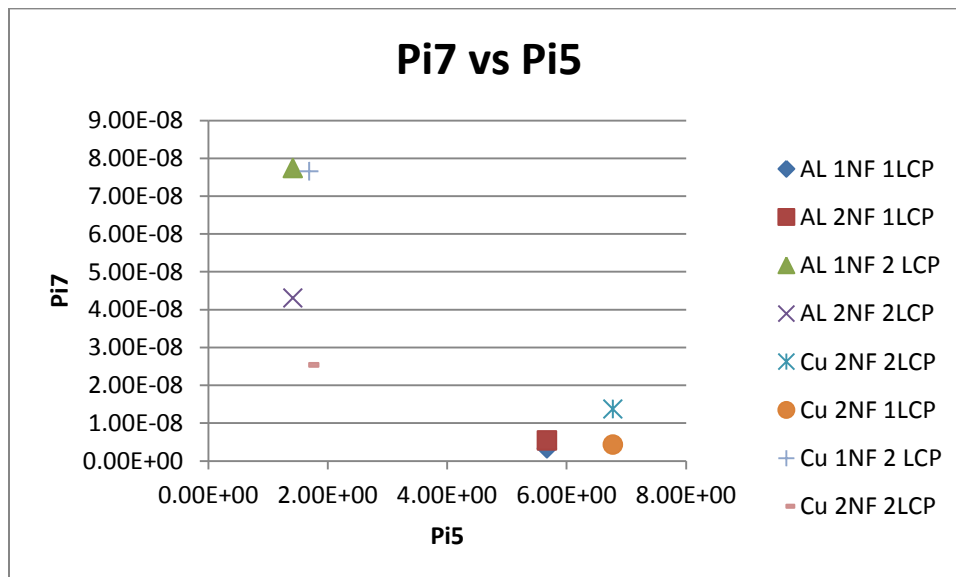


**Figure 66: Pi7 verses Pi5, interfacial stress verses thermal penetration in chip.**

Figure 66 above shows that all of the models with an LCP thickness of 2 have low Pi5 values. Aluminum and copper, 1 Nanofoil 2 LCPs has a much higher Pi7 value than Aluminum and copper, 2 Nanofoils 2 LCPs. This same relationship can be found but at a much smaller level with the single thickness LCP models. When comparing materials, going from aluminum to copper shifts the models higher in value in the Pi5 direction. This shift is more pronounced in the single LCP models than the double LCP models.

### 6.3 Sandwich Joining Results

Table 3 below verifies many of the results from the figures above in the previous section. The strongest bond is between the 2 LCP thicknesses and 2 nanofoils and aluminum. This was predicted because it was seen that aluminum would reach melting point when 2 nanofoils were used creating a good bond between the LCP and the Aluminum as well as the Nanofoil and nanoheater. The heat was able to dissipate into more LCP with 2 LCP thicknesses and because of that some of the LCP bonded to itself.

**Table 4: The average strength of the sandwich method pull tests.**

Material	LCP	Nanofoil	Strength in Ounces				N	Pa
			Pull 1	Pull 2	Pull 3	Average		
AL	1	2	346	452	406	401.33	111.5762	11157.62
AL	2	2	570	529	553	550.67	153.093	15309.3
AL	1	1	4	9	5	6.00	1.668083	166.8083
AL	2	1	16	23	19	19.33	5.374935	537.4935
Cu	1	2	135	68	94	99.00	27.52338	2752.338
Cu	2	2	127	360	280	255.67	71.07889	7107.889
Cu	1	1	2	5	1	2.67	0.74137	74.13704
Cu	2	1	18	7	16	13.67	3.799523	379.9523

**Table 5: Physically Measured Heat Affected zone and heat affected zone of numerical model**

Heat Affected Zone						
Material	Nanofoils	LCPs	Physically Measured		Numerical Model	
			Melting away from heat spreader (m)	Total Melting Area (m <sup>2</sup> )	Melting away from heat spreader (m)	Total Melting Area (m <sup>2</sup> )
Cu	2	2	7.40E-05	1.0149E-04	7.85E-05	1.0153E-04
Cu	2	1	9.00E-05	1.0181E-04	7.86E-05	1.0169E-04
Cu	1	2	1.90E-05	1.0038E-04	1.50E-05	1.0034E-04
Cu	1	1	2.30E-05	1.0046E-04	1.51E-05	1.0038E-04
Al	2	2			6.05791E-05	1.0061E-04
Al	2	1			6.17923E-05	1.0062E-04
Al	1	2			3.00895E-05	1.0030E-04
Al	1	1			3.00896E-05	1.0030E-04

## 6.4 Sandwich Method Leak Test Results

While some sides of the test specimen were bonded well and did not appear to leak, every completed leak test specimen leaked in similar ways to figure 26. The leak test needs a lot of Nanofoil to join 4 or even 3 sides of LCP to make a pouch. The Nanofoil is expensive and supplies were getting low so no successful leak test was performed.

## 6.5 LCP Battery

The LCP battery was successfully made and was able to light up a small LED light that required 2 Volts of power. The LCP battery was measured to produce 0.53 Volts. A small 1.5 Volt hearing aid battery was used to increase the total voltage to 2 volts. Figure 65 below shows a simple wiring diagram of the set up while Figure 66 below is a picture of the setup, which is faintly lighting up a red LED light.

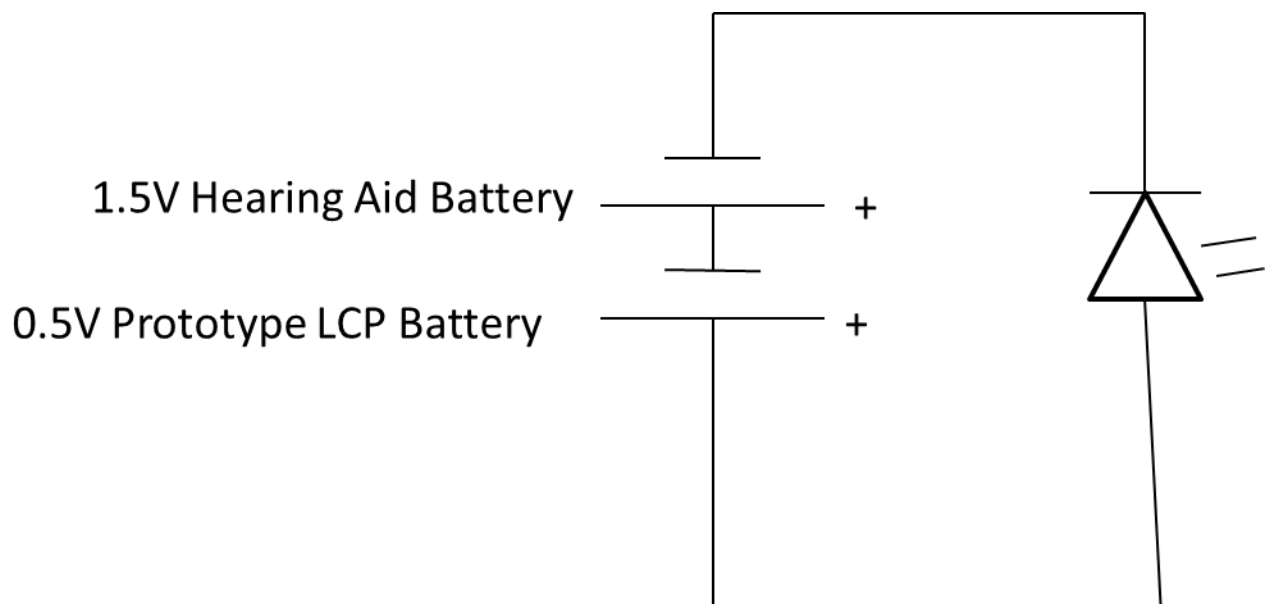


**Figure 67: Wiring diagram of LCP battery connected in series with a hearing aid battery and an LED light.**



**Figure 68: Picture of the LCP Aluminum Carbon air battery lighting up an LED.**

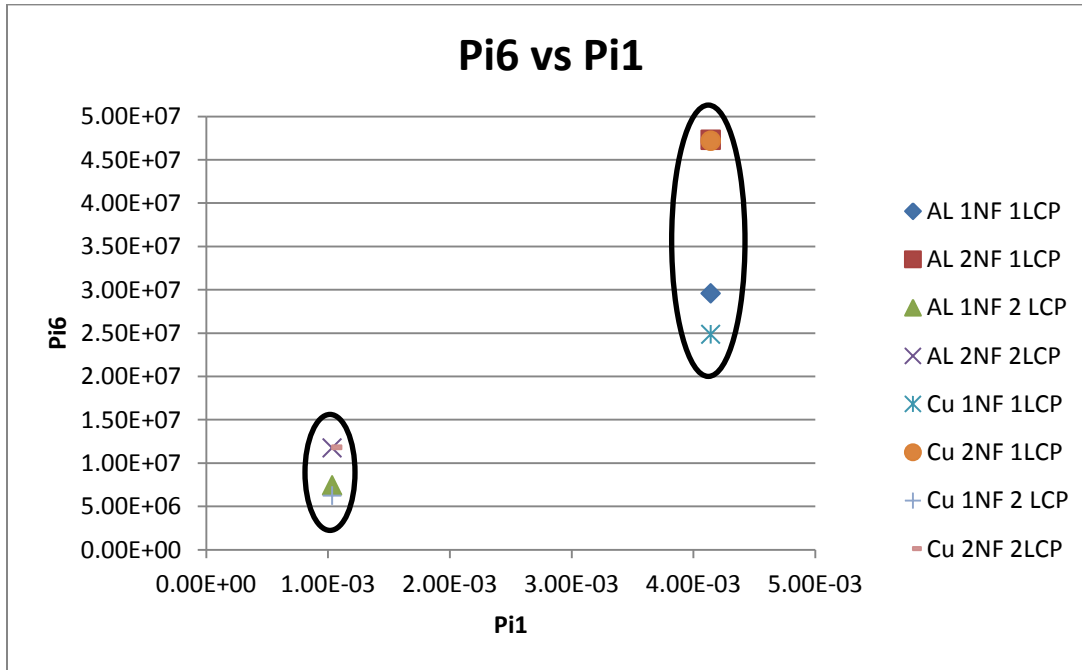
## **7 Discussion**

### **7.1 Discussion of General Welding**

The basic characteristics with general welding of LCP are much different than with welding metals, LCP because of the lower heat transfer coefficient, the lower heat of fusion and the low degradation temperature compared to melting make welding LCP much different and more difficult. When using a soldering Iron to join LCP together. In general a soldering Iron is not recommended to hermetically seal LCP.

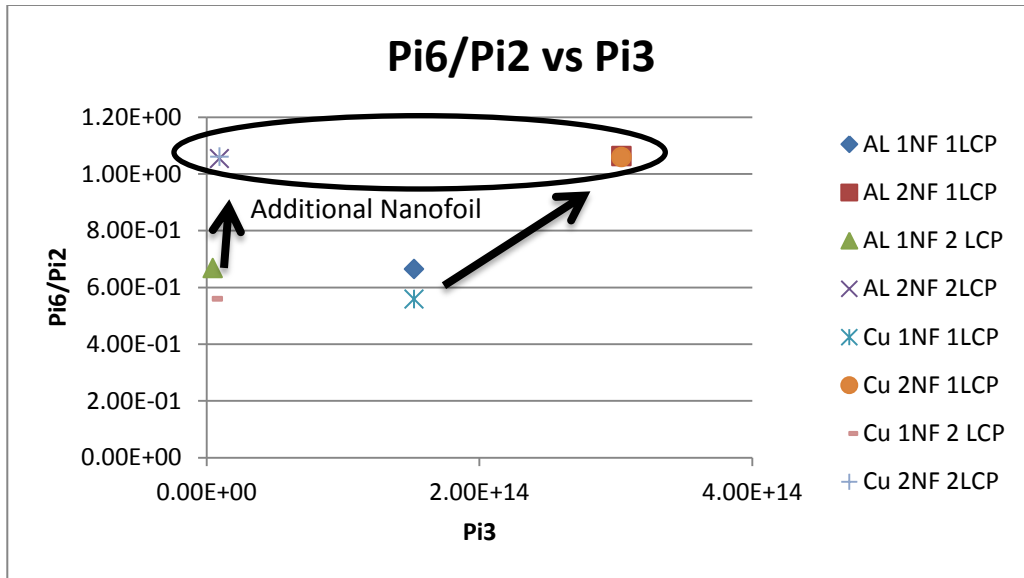
## 7.2 Discussion of Numerical Analysis

### 7.2.1 Physical Size Model



**Figure 69: Pi6 verses Pi1, peak temperature verses thermal penetration depth in the substrate**

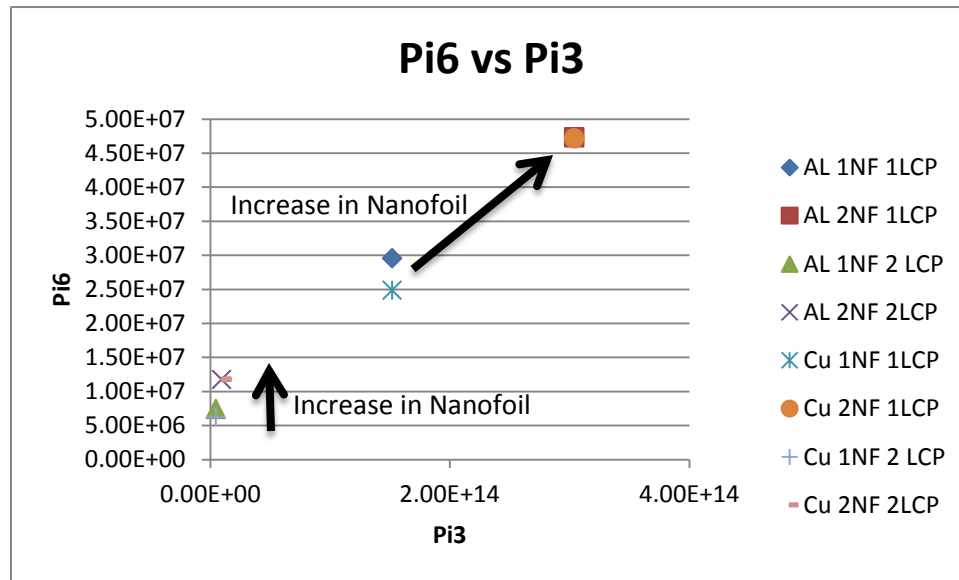
In Figure 69 above, the smaller oval on the right contains all of the models that had 2 LCP thicknesses and the larger oval is all of the models that had single LCP thicknesses. This means that the main factor in the thermal penetration depth in the substrate is how thick the LCP is, the thicker the LCP the lower the penetration depth. This is due to the fact that Pi1 is also dominated by the thickness of the substrate in the denominator of the equation. The peak temperature also rises with increasing heat generation which is to be expected. Since the thickness of the substrate is in the denominator of Pi6 and squared. The Pi6 values are lower for 2 Nanofoils and 2 LCPs than 1 Nanofoil and 1 LCP.



**Figure 70: Pi6/Pi2 versus Pi3, distance to melt point verses heat put in/energy density.**

Figure 70 is an important and interesting graph because it shows how close the LCP gets to melting in relation to the energy density/ heat put in. Any model that gets above 1 on the Y axis reaches a temperature higher than the melt point of the substrate. The two 1 Nanofoil 2 LCP models have low energy density and when the energy is added the substrate gets closer to the melt point but does not increase much in energy density because the  $H^5$  term is in the denominator and dominates the variation in the denominator term. The two, 1 Nanofoil 1 LCP models have a higher energy density than the 1 Nanofoil 2 LCP models because there is the same amount of Nanofoil but less substrate material. When the heat is added to the 1 Nanofoil 1 LCP models the Pi6/Pi2 increases as expected. Pi3 also increases because the lower H number allows the change in heat generated to come into play and affect the heat put in/energy density. As shown in the oval in Figure 70 the copper and aluminum 2 Nanofoil 1 LCP are nearly directly on top of each other. This is because the temperatures are all in the 920K range. In the copper models case the temperature happened to get that hot. With the aluminum models the 920K region was where a heat capacity spike was applied to simulate the melting of Aluminum, if

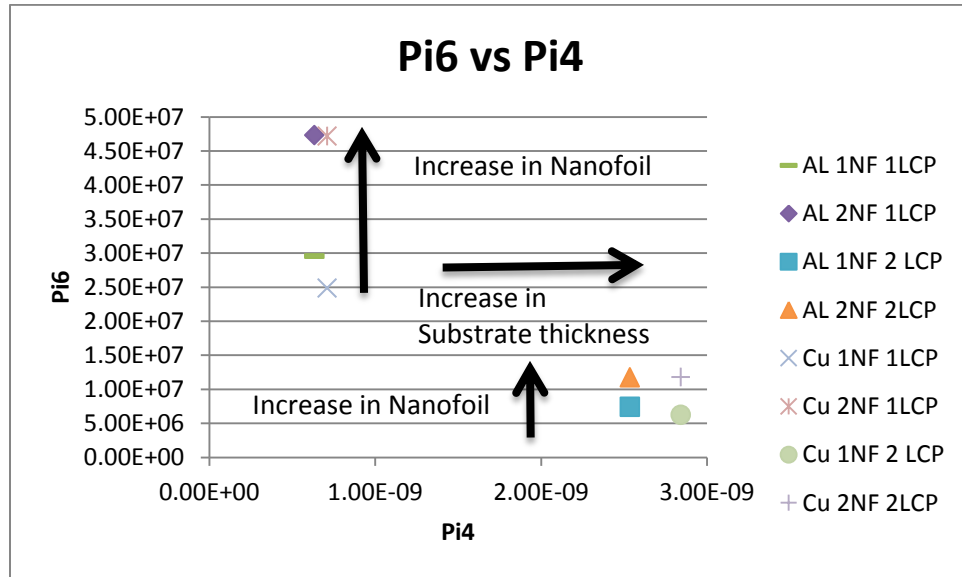
aluminum melted at a higher temperature than the values would be higher. In general copper should be slightly cooler than the aluminum usually because copper has a larger thermal conductivity and can have the heat flow more efficiently through the material than Aluminum. This is why with the 1 Nanofoil models the aluminum has a higher  $Pi6/Pi2$  value.



**Figure 71:  $Pi6$  verses  $Pi3$ , peak temperature verses energy density**

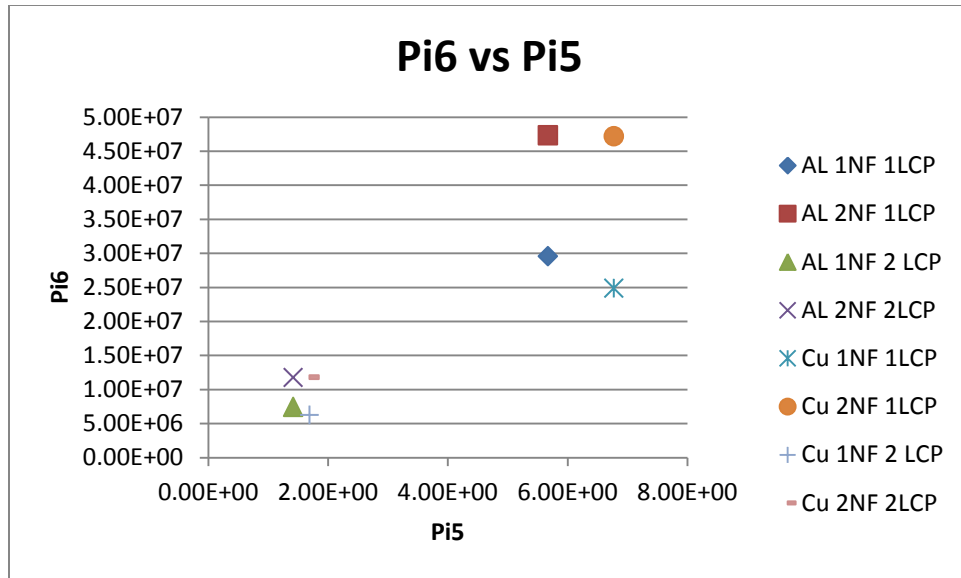
Figure 71 shows the interaction with the peak temperature and the energy density. In this case when heat is added to a model by adding Nanofoil the  $Pi6$  (the peak temperature) goes up. In the case of the models with 2 LCPs the increase is not as much when compared to 1 LCP models and this is because the thickness of the LCP has been put in the denominator and squared so the thinner the LCP the larger the change in  $Pi6$  from larger changes in temperature. This is also the reason why the two models with 1 Nanofoil and 1 LCP have larger  $Pi6$  values when compared with the two, 2 Nanofoil 2 LCP models. The  $Pi6$  value increases from 2 Nanofoils 2 LCPs to 1 Nanofoil 1LCP because the thickness of LCP is a key factor in the  $Pi6$  value as the thickness of the LCP is in the denominator of the equation and put to the 5th power. The single

LCP models increase in  $Pi6$  much more because the smaller thickness of the substrate allows the increase in temperature to be more pronounced.



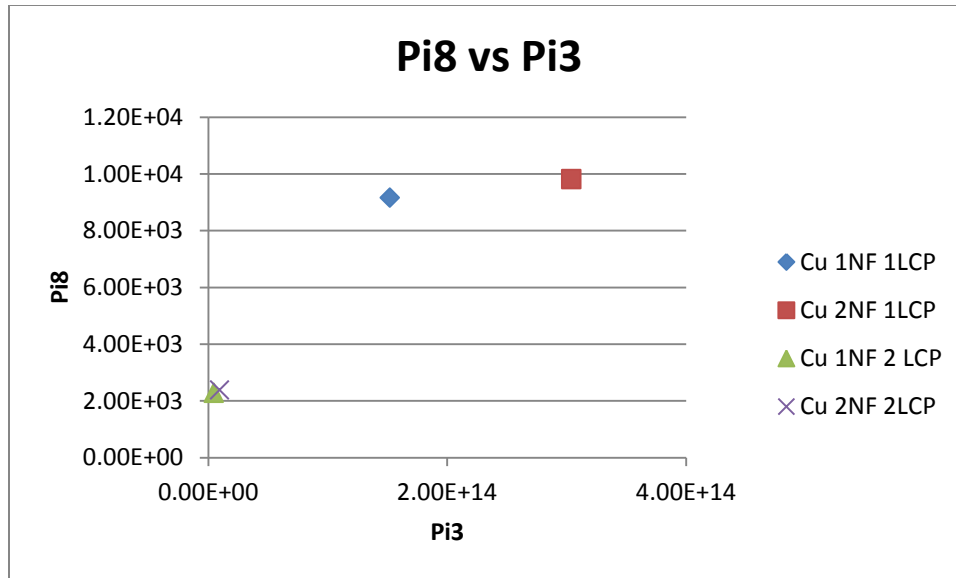
**Figure 72:  $Pi6$  versus  $Pi4$ , peak temperature versus thermal strain.**

Figure 72 above shows that  $Pi6$  (peak temperature) increases with added heat as would be expected. The jumps are less pronounced in the 2 LCP thick models once again because the larger thickness reduces the jump and the thickness is in the denominator of the  $Pi6$  equation and it is squared. The increase in  $Pi4$  is mainly attributed to the increase in thickness since thickness is in the numerator and squared.



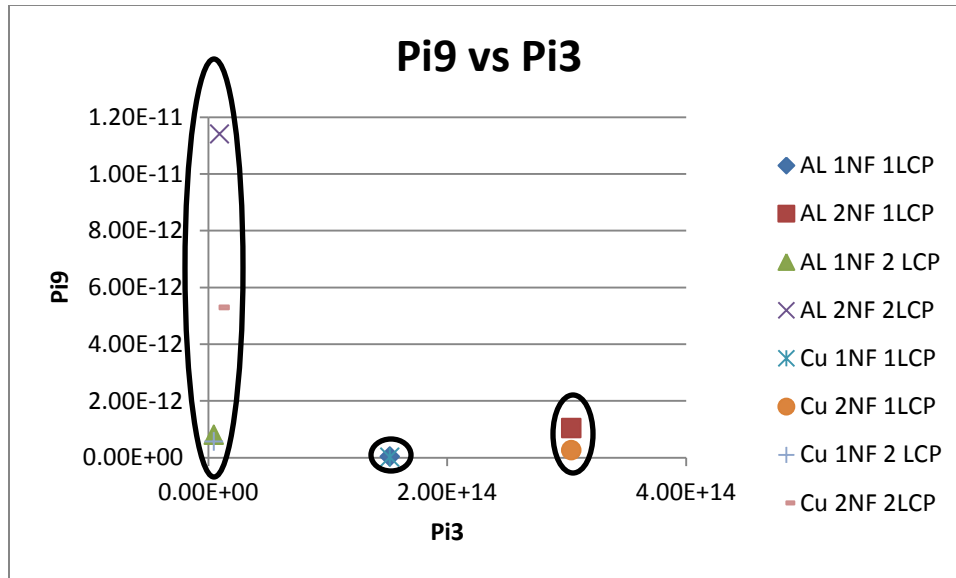
**Figure 73: Pi6 verses Pi5, peak temperature verses thermal penetration in chip.**

Figure 73 above shows the dimensionless relationship between the peak temperature Pi group and the thermal penetration in the chip Pi group. The double thick LCP models have both lower Pi6 values and Pi5 values. Both have the thickness of the LCP in the denominator of the equation for their Pi group and the thickness is also squared. The interesting thing to see in the group of 2 LCP models and the group of 1 LCP models is that switching material from aluminum to copper creates a slight decrease in Pi6 in every instance the decrease is more subtle in the 2 Nanofoil models because both copper and aluminum models are at nearly the same temperature.



**Figure 74: Pi8 verses Pi3, measured heat affected zone verses energy density.**

Figure 74 above is a figure that just takes into account the results of copper since the results of the aluminum results were not reliable and had too much variation do to glass slides breaking and LCP tearing. Figure 74 shows that the heat affected zone increases with Nanofoil albeit in this graph it is rather small in comparison to the other factors. It also shows that the increase in heat generated increases the energy density. The energy density is significantly increased a single thickness LCP substrate is used. Since the thickness is again in the denominator of the Pi8 and squared the relationship may skew the understanding of the real-world variation in heat affected zone. Table 5 can more accurately represent the real world dimensional heat affected zone.



**Figure 75: Pi9 verses Pi3 adhesion strength verses energy density**

Figure 75 above is a good representation of the three different energy densities. The first oval on the left are all the models with a double thick LCP. The circle in the middle shows the two models with 1 Nanofoil and 1 LCP. The second oval has the two models with 2 Nanofoils and 2 LCP. For more about adhesion strength please see Table 3.

### 7.2.1 Comparison with micro model

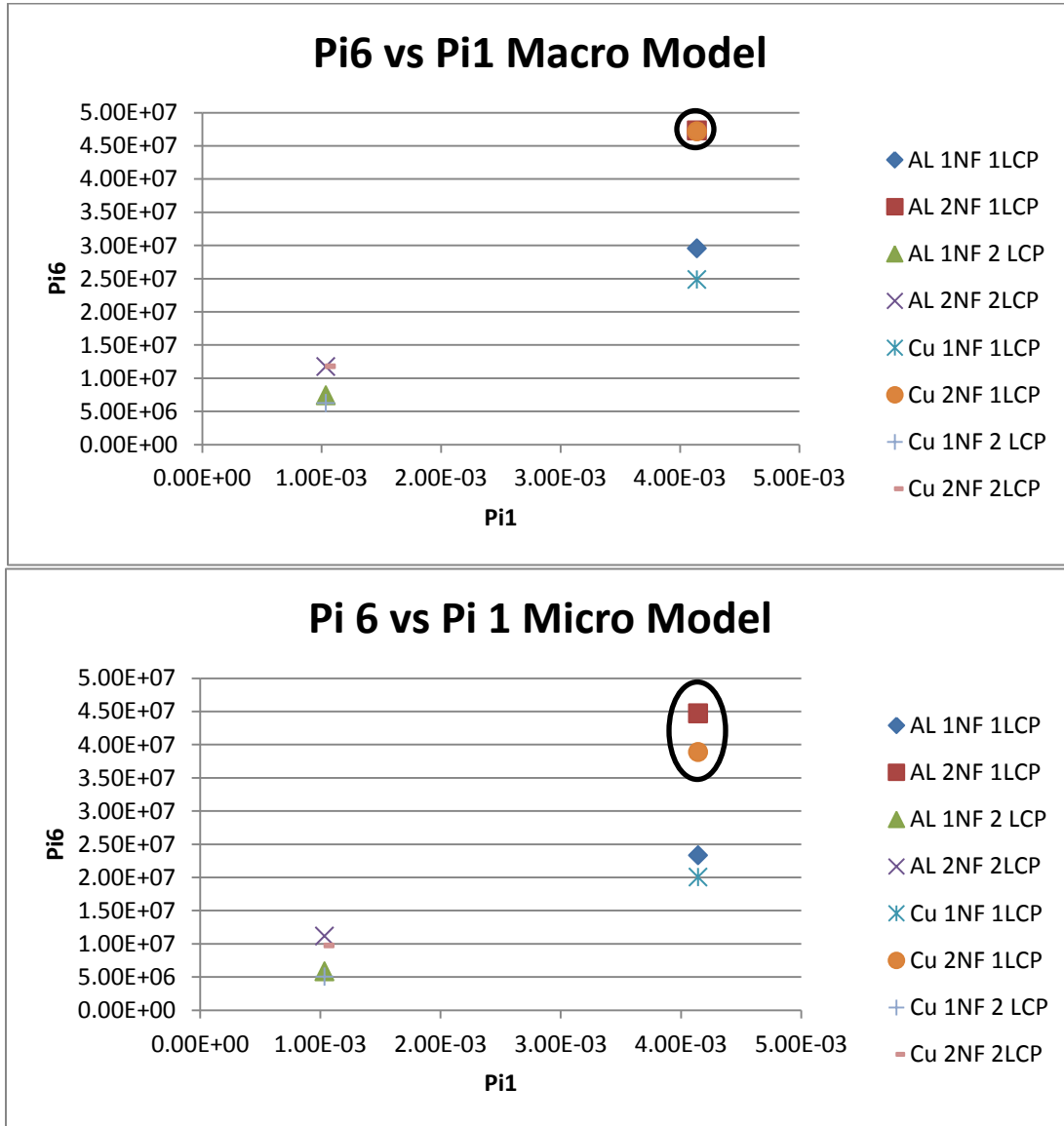


**Figure 76: Comparison of Macro-Model and Micro-Model with Pi 6**

Figure 76 above is an example of the difference between the macro and micro models.

The numbers and relationships are relatively the same as seen above except for the relationship with the two, 2 Nanofoil 2 LCP models. The Aluminum model actually has a higher temperature this is because the geometry was scaled geometrically and does not scale perfectly. The Pi

numbers are different but the relationships are nearly the same. Altering the inputs so that the same  $P_i$  values are obtained in the microscale should give similar joining results when compared to the macro model and that was the exact reason for the dimensionless analysis.

#### **7.4 Discussion of Taco Method**

Using the Soldering iron to attempt to join LCP to itself was such a difficult task when applying heat to the outside of the LCP before the numerical models were completed it was decided to try and insert Nanofoil in between the two pieces of LCP. Heat spreaders were used as not to singe and burn the Nanoheater too much. The difficulty with the taco method is that it did not produce a large enough bond area and most of the actual strength in the bond was in the adhesion of the LCP to the aluminum heat spreader. The Aluminum sticks well to LCP and even when the aluminum was oxidized the aluminum could not be removed without compromising the LCP to LCP bond.

Problems with the flexibility of the Taco joining method also arose very quickly. Aluminum can bend but it cannot stretch like LCP so it makes it difficult to flex when joined to the LCP. Furthermore the LCP after ignition is still very rigid and glass like. At first it was postulated that by setting up the Nanofoil and taco in a certain way once everything was joined flexing the specimen could break free aluminum and Nanofoil without compromising the LCP to LCP bond. A setup was never found to be beneficial and now has been concluded to be impractical since the LCP to LCP bond is so small and weak when compared to the strong bond that was made between the aluminum and the LCP.

## **7.5 Discussion of Sandwich Method**

The sandwich method is much more promising and appears to be a method that could work since the method was able to produce strong bonds that given the proper set-up and automated assistance can create consistently desirable bonds. The Sandwich method and pull tests were also used to check the results of the simulations. A relationship was noticed between the heat affected zones of numerical and experimental results as shown in Table 5. The actual dimensions of the heat affected zones are not exactly the same but the differences between the heat affected zones of other specimens were similar.

### **7.5.1 Discussion of Inside Out Sandwich Method**

At first the concern with using the inside out sandwich method was that the heat needed to join 2 pieces of LCP to themselves using Nanofoil on the outside would require too much heat and by the time the LCP got hot enough in the center the LCP on the outside would be much too hot and the outside would begin to degrade and create an undesirable material that had degraded. The Nanofoil used has only a certain energy release rate and duration of time for heating and so in the physical testing the Nanofoil would not have been able to join different LCP thicknesses but by using the Pi groups other thicknesses can be used and by altering the duration of heating and the total amount of heating by using custom mixtures of Nanoheater powders virtually any size or thickness of joining area can be joined using nanoheaters.

## 7.6 Discussion of Leak Test and Battery

While the leak tests were not entirely successful most of the failure can be attested to the variation and error associated with doing everything by hand. At times the seals were of very good quality while the majority of the time there would be problems or holes.

The Taco method was able to seal the LCP only once. The amount of attempts was not recorded to make a hermetically sealed pouch but on 3 occasions a pouch that appeared to be sealed was made. Only one of these pouches did not leak for an extended amount of time but once the pouch was tested for flexibility the seal broke very easily.

The inside out sandwich method showed a lot of promise since preliminary tests found that the inside out sandwich method produced a large seal area and the copper heat spreaders could be removed with some careful attention. When positioning the grains of the LCP parallel to each other the LCP stayed very flexible but when positioning the grains perpendicular produced a rigid and less flexible bond that was more prone to breaking. For the experiments the two pieces of LCP were positioned parallel to each other, no 4 or 3 sided pouches were able to be made due to the difficulty in set up and execution of the joint. Two sides were successfully joined and a simple leak test was conducted by putting drops of dye in the pocket that the two joined sides made. These simple tests produced desirable results with no leaks but many times the simple tests produced leaks due to the nature of the LCP. The LCP is made up of grains and when the LCP was melted the material could become too thin and dye could leak through the grains. It is believed that this variation is due to the varied pressure that was applied when joining. When using Nanofoil, pressure is needed because the Nanoheater reaction has an explosive element to it not just a pure heat release element. The variation in pressure sometimes

produced joints that were, too thin and leaked, were just right and didn't leak or did not have enough pressure, did not bond fully and leaked.

. Some controls that will better facilitate more consistent results would be pre-formed nanoheater strips, manufacturing machines to manufacture consistent and accurate dimensions of the LCP and heat spreader material. Using very thin silicon wafer material would work much better as a heat spreader since it does not stick to LCP. Instrumentation should be used in a vacuum to reduce the variation of oxidation of the heat spreader material and reduce contamination of the nanofoil material. Machines that can perform the assembly of the tests can improve accuracy, consistency and time.

Cutting the LCP aluminum and copper to precise dimensions is not very difficult but requires a lot of care. When trying to make a hermetic seal stacking up 3 pieces of Nanofoil on top of each other than placing a piece of copper, 2 pieces of LCP another piece of copper, 3 more Nanofoils and then a silicon wafer on top of everything is very difficult with only hand tools, something nearly always gets bumped. Not very much of the experimentation was performed in the Microscale because it is just too difficult to do by hand that's why all of the tests were conducted with small macro specimens whom were still difficult to work with.

The LCP battery worked but had a few problems. The battery only worked for less than an hour presumably because the battery does not have that much energy do to the thin size and use of less energy dense commonly available items. The copper leads were too thick to join the area were the leads stuck out so liquid electrical tape was used and the liquid electrical tape was weak and leaked when the battery was bent. Overall using better materials, thinner leads and a more automated way to stack the Nanofoils and silicon heat spreaders and then press everything

together evenly and consistently will create much better results. I believe the Nanofoil has the potential to join flexible polymers and to make flexible batteries, especially micro sized and integrated batteries.

## **8 Conclusion**

In conclusion this research thesis focused on studying the feasibility of joining polymer materials using nanoheaters for microscale and macroscale applications (i.e., flexible batteries). Numerical simulations simulating the heat generation of the nanoheaters in a thermomechanical study were developed to identify operating conditions to achieve melting and joining. A series of experimental tests were performed to verify the numerical model. The results for numerical simulations and experimental runs were used in a dimensionless analysis and a design of experiments to generalize the results. The dimensionless analysis and numerical model were used to predict conditions for microscale joining of polymers for microelectronic applications. Sources of error include the uneven pressure on the joining interface, inconsistency with the sizing of the nanoheaters and the heat spreaders as well as uneven place placing of the nanoheaters and heat spreaders due to manual manufacture handling and assembly.

Human error was a very difficult problem for this research in nearly every aspect of the experimentation. Human error resulted in a lot of wasted time and wasted test specimens. With the tools given it was difficult to cut the brittle glass like Nanofoil to accurate widths without shards cracking off. The flatness and rigidity made the Nanofoil difficult to pick up with tweezers when it is lying flat on a hard flat surface. For the Nanofoil to work optimally the surfaces that the Nanofoil touched had to be cleaned or sometimes the Nanofoil would not ignite. There is also a suspicion but no conclusive evidence that the Nanofoil's energy output is reduced when the Nanofoil is scratched.

While the variation in these results can vary widely from many possible variables when creating things by hand, some controls that will better facilitate more consistent results for commercial use would be pre-formed nanoheater strips, manufacturing machines to manufacture consistent and accurate dimensions of the LCP and heat spreader material. Using very thin and flexible silicon wafer material would work much better as a heat spreader since it does not stick to LCP. Instrumentation should be used in a vacuum to reduce the variation of oxidation of the heat spreader material and reduce contamination of the nanofoil material. A machine that can perform the assembly such as placing the nanofoil strips, heat spreader and LCP in the correct place with very little variation and then apply a pressure that doesn't vary as well can improve accuracy, consistency and time.

The numerical simulation and the Pi groups provide a wealth of knowledge into how well nanoheaters, which produce such a large amount of heat over such a small amount of time, behave in a joining situation. In general the main concern with the nanoheaters is that because of the short duration, will there be a large enough heat affected zone and will the substrate melt enough to create a good quality bond and is the bond capable of hermetically sealing something. The 8 different studies which were conducted allowed for some insight on all of these questions. The design of experiments was instrumental in providing a reasonable amount of tests that could be run on the computer using finite element analysis and conducted in the lab carrying out actual experiments to understand numerically what is going on and verify the numerical model with the experimental models.

The data from the Pi groups along with the design of experiments can be used in other experiments to find out things like, if there is a substrate with a certain thickness and certain material properties how much nanofoil is needed and for how long to create a good heat affected

zone that will produce a good bond. The numerical and experimental results show a pattern in the Pi numbers that produce favorable results. There are two conditions that can produce good results and these two conditions have unique Pi1 through Pi5 combinations. The first condition is with a thick substrate a favorable joint would require a lot of heat through the thickness. The combination of favorable Pi values are, Pi1 values near  $1.04 \times 10^{-3}$  but not as high as  $4.14 \times 10^{-3}$  along with Pi2 values of  $1.11 \times 10^7$  but not as high as  $4.45 \times 10^7$  along with a Pi3 values of  $9.50 \times 10^{12}$  but not as low as  $4.45 \times 10^{12}$  along with a Pi4 value between  $2.54 \times 10^{-9}$  and  $2.84 \times 10^{-9}$  and lastly a Pi5 between 1.42 and 1.69. The second condition that can produce good results is with a thin substrate where a large heat affected zone is needed to produce good joining results. The combination of favorable Pi values are, Pi1 values near  $4.14 \times 10^{-3}$  but not as low as  $1.04 \times 10^{-3}$  along with Pi2 values of  $4.45 \times 10^7$  but not as low as  $1.11 \times 10^7$  along with a Pi3 value of  $3.04 \times 10^{12}$  but not as low as  $9.50 \times 10^{12}$  along with a Pi4 value between  $7.11 \times 10^{-10}$  and  $6.34 \times 10^{-9}$  and lastly a Pi5 between 5.67 and 6.77. Following these combinations can produce good quality joints when different materials with different geometries other than the ones used in this thesis are used.

Significant progress has been made in the development of using nanoheaters to join flexible polymer materials. The numerical model in conjunction with the Pi groups and the design of experiments created general information and understanding that can be used for many different joining applications. The physical experiments verified some of the numerical experiments predictions as well as brought to light difficulties in the physical set up and execution of using the nanoheaters to join flexible polymer materials in the real world.

## **9 Future Work**

Thinking ahead to make nanoheaters more commercially viable for flexible electronic devices more complex ignition methods and ways to apply pressure to the bond during ignition should be explored or a new method to not need pressure could be very beneficial. Using thin flexible silicon wafers for heat spreaders will help to increase consistency. Nanoheaters are a technology that can also be considered for entirely different technologies that are still in their nascent research stage.

## Appendix A

### Heat Capacity/Latent Heat of Fusion of LCP

Sample: Cebe\_LCP-iQLP

Size: 8.9800 mg

Method: Ramp

Comment: Cebe - running service work sample of LCP

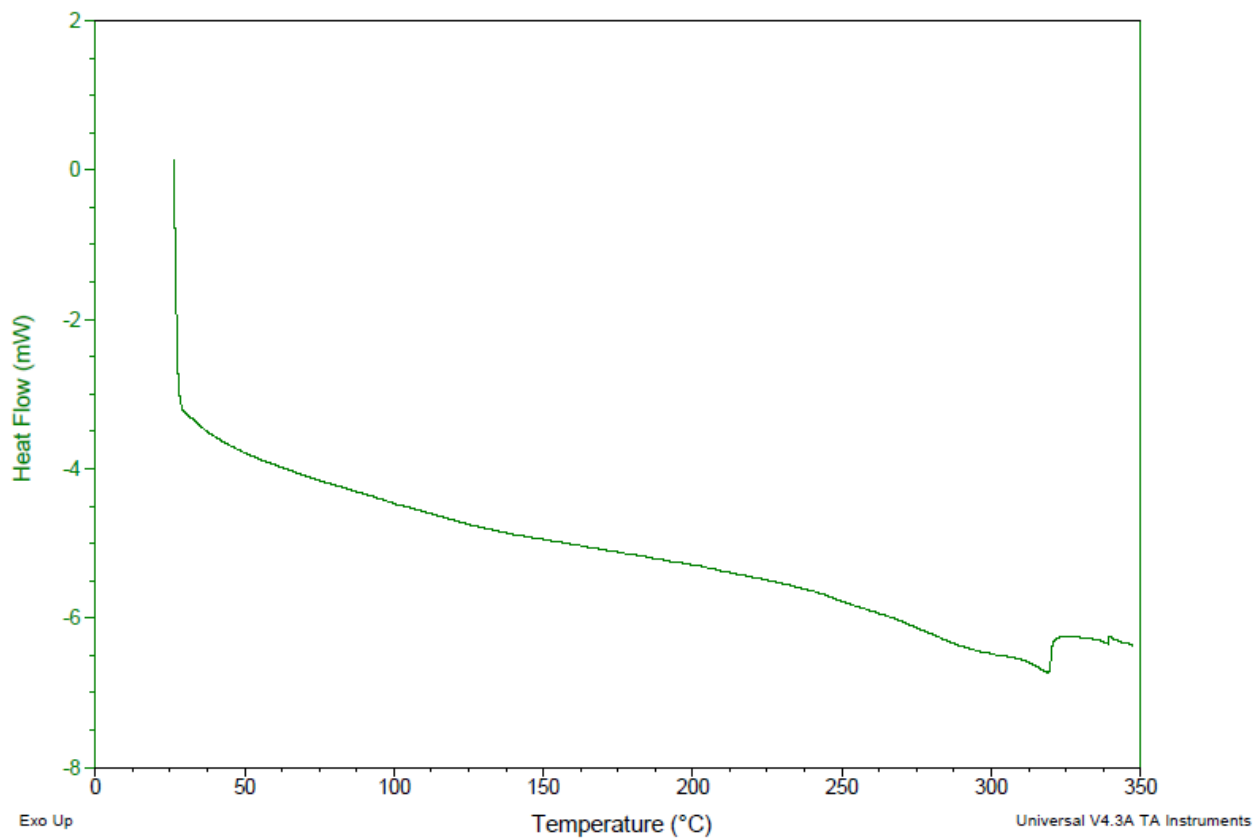
DSC

File: C:\TA\Data\DSC\Peggy\Cebe\_LCP-iQLP.001

Operator: Cebe

Run Date: 01-Aug-2013 09:28

Instrument: DSC Q100 V9.9 Build 303



## Works Cited

C. T. Ko, K.-N. Chen. “Wafer-level Bonding/Stacking Technology for 3D Integration”, *Microelectronics Reliability* **2009**, in press (doi:10.1016/j.microrel.2009.09.015).

J. Cecil, D. Powell, D. Vasquez. “Assembly and Manipulation of Micro-devices – A State of the Art Survey”, *Robotics and Computer –Integrated Manufacturing* **2007**, 23, 580-588.

C. L. Bauer, and G. G. Lessmann. “Metal-Joining Methods”, *Ann. Rev. Mater. Sci.* **1976**, 6, 361-387.

G. Cam, M. Kocak. “Progress in Joining of Advanced Materials”, *Int. Mater. Rev.*, **1998**, 43, 1-44.

G. Smolka, A. Gillner, L. Bosse and R. Lützel. “Micro Electron Beam Welding and Laser Machining– Potentials of Beam Welding Methods in the Micro-system Technology”, *Microsystem Technologies* **2004**, 10, 187-192.

Z. Sun, R. Karppi. “The Application of Electron Beam Welding for the Joining of Dissimilar Metals: An Overview”, *J. Mater. Processing Technology* **1996**, 59, 257-267.

A. P. Mackwood and R. C. Crafer. “Thermal Modelling of Laser Welding and Related Processes: A Literature Review”, *Optics & Laser Technology* **2005**, 37, 99-115.

R. M. do Nascimento, A. E. Martinelli, A. J. A. Buschinelli. “Recent Advances in Metal-Ceramic Brazing”, *Cerâmica* **2003**, 49, no.312 (doi: 10.1590/S0366-69132003000400002).

H. H. Manko. *Solders and Soldering: Materials, Design, Production, and Analysis for Reliable Bonding*, 2nd Edition, McGraw-Hill, New York, **1979**.

J. S. Hwang. *Solder Paste in Electronics Packaging*, Kluwer Academic, **1989**.

W. H. Kearns. *Welding Handbook*, 7th Ed., Vol. 3, American Welding Society, **1980**, Chapter 10.

G. Harman. *Wire Bonding in Microelectronics Materials, Processes, Reliability, and Yield*, second edition, McGraw-Hill, New York, 1997.

R.R. Tummala, *Fundamentals of Microsystems Packaging*, McGraw-Hill, New York, 2001, Chapter 9.

S. Nakada, “Joining Processes for Microelectronics”, *Seimitsu Kikai* **1984**, 50, 62-64.

H. H. Manko. *Soldering Handbook for Printed Circuits and Surface Mounting (Electrical Engineering)*, Springer, **1995**.

J. S. Hwang. *Modern Solder Technology for Competitive Electronics Manufacturing*, McGraw-Hill, New York, **1996**.

Q. Cui, F. Gao, S. Mukherjee, Z. Gu. “Joining and Interconnect Formation of Nanowires and Carbon Nanotubes for Nanoelectronics and Nanosystems”, *Small* **2009**, 5, 1246-1257.

Z. Gu, H. Ye, D. H. Gracias. “The Bonding of Nanowire Assemblies Using Adhesive and Solder”, *J. Miner., Metals Mater. Soc. (JOM)* **2005**, 57, 60-64.

Z. Gu, H. Ye, D. Smirnova, D. Small, D. H. Gracias. “Reflow and Electrical Characteristics of Nanoscale Solder”, *Small* **2006**, 2, 225-229.

F. Gao, Z. Gu. “Nano-soldering of Magnetically-aligned Three-dimensional Nanowire Networks”, *Nanotechnology* **2010**, in press.

S. Bohm, K. Dilger, J. Hesselbach, J. Wrege, S. Rathmann, W. Ma, E. Stamman, G. Hemken. “Micro Bonding with Viscous Adhesives”, *Microsyst Technol*, **2006**, 12, 676-679.

S. Bou, D. Fratila, A. Boglea, D. Andrijasevic, A. Almansa, W. Palfinger, W. Mann, A. Olowinsky, W. Brenner, R. Most, Z. Rozynek. “Technologies for Microassembly: Selected Methods”, *4M 2007 - Third International Conference on Multi-material Micro Manufacture – Proceedings*, **2007**.

N. Ilic, M. T. Jovanovic, M. Todorovic, M. Trtanj and P. Saponji. “Microstructural and Mechanical Characterization of Postweld Heat-Treated Thermite Weld in Rails”, *Materials Characterization* **1999**, 43, 243-250.

C. Meric, E. Atik, S. Sahin. “Mechanical and Metallurgical Properties of Welding Zone in Rail Welded via Thermite Process”, *Science and Technology of Welding & Joining* **2002**, 7, 172-176.

J. Wang, E. Besnoin, O. M. Knio, T. P. Weihs. “Effects of Physical Properties of Components on Reactive Nanolayer Joining”, *J. Appl. Phys.* **2005**, 97, 114307.

J. C. Trenkle, J. Wang, T. P. Weihs, T. C. Hufnagel. “Microstructural Study of an Oscillatory Formation Reaction in Nanostructured Reactive Multilayer Foils”, *App. Phy. Lett.* **2005**, 87, 153108.

J. C. Trenkle, L. J. Koerner, M. W. Tate, S. M. Gruner, T. P. Weihs, T. C. Hufnagel. “Phase Transformations during Rapid Heating of Al/Ni Multilayer Foils”, *App. Phy. Lett.* **2008**, 92, 081903.

A. P. Alivisatos. “Semiconductor Clusters, Nanocrystals, and Quantum Dots”, *Science* **1996**, 271, 933-937.

C. J. Murphy, T. K. Sau, A. M. Gole, C. J. Orendorff, J. Gao, L. Gou, S. E. Hunyadi, T. Li.  
“Anisotropic Metal Nanoparticles: Synthesis, Assembly, and Optical Applications”, *J. Phys. Chem. B* **2005**, *109*, 13857-13870.

C. Lieber. “Nanoscale Science and Technology: Building a Big Future from Small Things”, *MRS Bull.* **2003**, 486-491.

S. Iijima. “Helical Microtubules of Graphitic Carbon”, *Nature* **1991**, *354*, 56-58.

P. M. Ajayan. “Nanotubes from Carbon”, *Chem. Rev.* **1999**, *99*, 1787-1799.

F. Mafune, J.-Y. Kohno, Y. Takeda, T. Kondow. “Nanoscale Soldering of Metal Nanoparticles for Construction of Higher-Order Structures”, *J. Am. Chem. Soc.* **2003**, *125*, 1686-1687.

R. Klajn, K. J. M. Bishop, M. Fialkowski, M. Paszewski, C. J. Campbell, T. P. Gray, B. A. Grzybowski. “Plastic and Moldable Metals by Self-assembly of Sticky Nanoparticle Aggregates”, *Science* **2007**, *316*, 261-264.

M. Wang, J. Wang, Q. Chen, L. M. Peng. “Fabrication and Electrical and Mechanical Properties of Carbon Nanotube Interconnections”, *Adv. Funct. Mater.* **2005**, *15*, 1825-1831.

D. N. Madsen, K. Mølhave, R. Mateiu, A. M. Rasmussen, M. Brorson, C. J. H. Jacobsen, P. Bøggild. “Soldering of Nanotubes onto Microelectrodes”, *Nano Lett.* **2003**, *3*, 47-49.

F. Banhart. "The Formation of a Connection between Carbon Nanotubes in an Electron Beam", *Nano Lett.* **2001**, *1*, 329-332.

Y. Lu, J. Y. Huang, C. Wang, S. Sun & J. Lou. "Cold Welding of Ultrathin Gold Nanowires", *Nature Nanotech.* **2010**, in press (doi:10.1038/nnano.2010.4).

"NanoFoil®." Indium Corporation NanoFoil®. N.p., n.d. Web. 15 May 2013.

Indium Corporation. Product Data Sheet. N.p.: Indium Corporation, n.d. NanoFoil® Technical Documents. Web. 6 Apr. 2013. <http://www.indium.com/nanofoil/#whitepapers>

Comsol Multiphysics Reference Guide Version 4.3. May 2012. Reference Guide.

J. D. Hoffman. "*Numerical Methods for Engineers and Scientists*". 2nd ed. Boca Raton: CRC, 2001. Print.

J. Fish, and T. Belytschko. *A First Course in Finite Elements*. West Sussex: John Wiley & Sons, 2007. Print.

P. J. Pritchard and J. C. Leylegian. *Fox and McDonald's Introduction to Fluid Mechanics*. 8th ed. Hoboken: John Wiley & Sons, 2011. Print.

"How to Perform a Design of Experiments." Knoware. QI Macros, n.d. Web. 12 May 2013.  
<<http://www.qimacros.com/lean-six-sigma-articles/how-to-perform-a-design-of-experiments/>>.

|